

U. S. Army Communications-
Electronics Command

AD-A286 605

2



Night Vision & Electronic Sensors Directorate

Title: Optical Power Limiting Liquid Crystal Composites

Author(s): Michael A. Lee, P. Palffy-Muhoray, J. W. West,
L. C. Chien, J. W. Doane

Address: Liquid Crystal Institute
Kent State University
Kent, Ohio 44242

Type of Report (Final, Interim, etc.): Final

DTIC
ELECTE
NOV 21 1994
S B D

Date: November 10, 1994

DISTRIBUTION STATEMENT A

Approved for public release;
Distribution Unlimited

Contract Number

DAAB07-88-C-F421

Report Number

NV-94-C11



Fort Belvoir, Virginia 22060-5806

94-35599



1368

94

11

16

11

9

REPORT DOCUMENTATION PAGE

Form Approved
OMB No. 0704-0188

1a. REPORT SECURITY CLASSIFICATION Unclassified			1b. RESTRICTIVE MARKINGS None		
2a. SECURITY CLASSIFICATION AUTHORITY N/A			3. DISTRIBUTION / AVAILABILITY OF REPORT Approved for Public Release Distribution Unlimited		
2b. DECLASSIFICATION / DOWNGRADING SCHEDULE N/A					
4. PERFORMING ORGANIZATION REPORT NUMBER(S)			5. MONITORING ORGANIZATION REPORT NUMBER(S) NV-94-C11		
6a. NAME OF PERFORMING ORGANIZATION Kent State University		6b. OFFICE SYMBOL (if applicable)	7a. NAME OF MONITORING ORGANIZATION U.S. Army CECOM NVESD		
6c. ADDRESS (City, State, and ZIP Code) Office of Research and Graduate Studies Kent State University Kent, Ohio 44242-0001			7b. ADDRESS (City, State, and ZIP Code) 10221 Burbeck Road, Suite 430 Ft. Belvoir, VA 22060-5806		
8a. NAME OF FUNDING / SPONSORING ORGANIZATION ARPA		8b. OFFICE SYMBOL (if applicable)	9. PROCUREMENT INSTRUMENT IDENTIFICATION NUMBER F421 DAAB07-88-C-F412		
8c. ADDRESS (City, State, and ZIP Code) 3701 N. Fairfax Drive Arlington, VA 22230-1714			10. SOURCE OF FUNDING NUMBERS		
			PROGRAM ELEMENT NO. 62 301 E	PROJECT NO.	TASK NO. DO
11. TITLE (Include Security Classification) Optical Power Limiting Liquid Crystal Composites (U)					
12. PERSONAL AUTHOR(S) Michael A. Lee					
13a. TYPE OF REPORT Final		13b. TIME COVERED FROM 6/88 TO 6/93		14. DATE OF REPORT (Year, Month, Day) 1994/11/10	
15. PAGE COUNT 135					
16. SUPPLEMENTARY NOTATION					
17. COSATI CODES			18. SUBJECT TERMS (Continue on reverse if necessary and identify by block number)		
FIELD	GROUP	SUB-GROUP			
20	5				
20	6				
19. ABSTRACT (Continue on reverse if necessary and identify by block number) <p>This final report covers the experimental and theoretical investigations of optical power limiting in liquid crystal systems. Both pure and composite systems were investigated. Evaluation of a variety of liquid crystal materials for optical power limiting applications is reported. Under this project, optical power limiting of several pure materials was demonstrated in the nanosecond regime, with the cyanobiphenyls being found most effective for passive OPL applications. For CW lasers, polymer dispersed liquid crystals in a polymer matrix were shown to be effective optical power limiters when used in an active configuration. Extensive research on the mechanisms causing optical nonlinear response in liquid crystals is reported.</p> <p>Additional work on a separate subproject to evaluate and develop the shuttering capability of polymer dispersed liquid crystals in the IR is reported. Work on a variety of polymer/liquid crystal materials is reported. Successful shuttering of IR radiation was shown.</p>					
20. DISTRIBUTION / AVAILABILITY OF ABSTRACT <input checked="" type="checkbox"/> UNCLASSIFIED/UNLIMITED <input type="checkbox"/> SAME AS RPT. <input type="checkbox"/> DTIC USERS			21. ABSTRACT SECURITY CLASSIFICATION U		
22a. NAME OF RESPONSIBLE INDIVIDUAL Byong H. Ahn			22b. TELEPHONE (Include Area Code) (703) 704-2031		22c. OFFICE SYMBOL AMSEL-RD-NV-LPD

1 Executive Summary

This project was initiated as a response to an RFP soliciting novel and innovative approaches to optical power limiting. The central thrust of the original contract was the investigation of liquid crystal systems, including pure and composites, as potential sources for novel nonlinear optical effects that could be utilized in optical power limiting applications.

The initial phase of our activities investigated polymer dispersed liquid crystal systems in active and passive OPL configurations. Polymer dispersed liquid crystals, (PDLCs) had previously been shown to be effective optical shutters with essentially no insertion loss due to absorption and thus "water clear" optical properties in the transmitting state. PDLCs can be switched, through electro-optic mechanisms, to essentially opaque (milky white) states in the scattering mode. We assessed our findings as exceptionally effective for OPL with the active electro-optic configuration and promising for passive operation.

The later effort of the contract followed the directions of interest indicated by DARPA and the COTR, seeking results for OPL using liquid crystals in the nanosecond regime. A smaller effort continued in the CW and picosecond regime. With interrupted funding and a reduced rate of funding, the effort continued from June 1988 until June 1993.

A broad selections of liquid crystals were synthesized or purchased as part of a screening program in nonlinear materials properties. The nonlinear optical properties were measured using the Z-scan technique to determine the nonlinear indices of refraction and the nonlinear absorption coefficients. These properties were determined for CW, nanosecond and picosecond lasers. Materials were also tested for optical power limiting performance. Several good candidates were found with large nonlinearities and good limiting characteristics.

Our group was the first to discover 5CB as a nonlinear liquid crystal with OPL potential. 5CB (4-cyano-4'-n-pentylbiphenyl), 8CB (4-cyano-4'-n-octylbiphenyl) and a few selected few compounds were investigated in detail, while approximately 30 other compounds were evaluated. We carried out an effort to identify the nonlinear mechanisms as well as screen promising materials. The presence of two-photon absorption and fifth order nonlinearities were determined present as important mechanisms in the best materials.

In addition to the nonlinear studies, a separate subproject involving *linear* properties of polymer dispersed liquid crystals in the infrared region was performed. The modulation properties of these materials were found promising, but difficulties were identified involving insertion loss and response time.

<input checked="checked" type="checkbox"/>	
<input type="checkbox"/>	
<input type="checkbox"/>	
By _____	
Distribution _____	
Availability Codes	
Dist	Avail and/or Special
A-1	

Contents

1	Executive Summary	1
2	Introduction	5
3	CW Regime	6
3.1	Active Linear Feedback Optical Power Limiting for CW Ar ⁺ laser	6
3.2	Passive OPL Study of PDLs	8
3.3	Nonlinear Materials Parameters in the CW regime	13
3.3.1	Thermal Behavior in the CW Regime	15
4	Nanosecond Nd YAG Nonlinear Optical Response	17
4.1	Time Dependence of Nonlinear Response: Two-Pulse Measurements	19
4.2	Temperature Dependence of Nanosecond Nonlinear Response	21
4.3	Higher Order Nonlinearities	23
4.4	Photoacoustic Measurements	25
4.5	Nanosecond Optical Power Limiting	26
4.5.1	ARDEO DVO Test Bed	26
5	Picosecond Nonlinear Optical Response	30
5.1	Mechanism Analysis	32
5.1.1	Millisecond Mechanisms	32
5.1.2	Nanosecond Mechanisms	36

5.1.3	Picosecond Mechanisms	37
5.1.4	Overall Mechanism Discussion	38
6	Damage Studies	39
6.1	CW Damage Studies	39
6.2	Nanosecond Laser Damage	40
7	Theory and Modeling	42
7.1	Electronic Structure Modeling	42
7.1.1	Small Molecule Comparisons	43
7.1.2	Large Molecule Calculations	44
7.1.3	Discussion of Electronic Nonlinearities	47
7.2	Modeling Molecular Orientational Relaxation and the Thermal Nonlinear Refraction of Nematic Liquid Crystals	50
7.2.1	Time Scale of Thermal Nonlinearities	50
7.2.2	Thermal Properties of Nematic Liquid Crystals	53
7.2.3	Orientational Relaxation	58
7.2.4	Analysis of Thermal and Relaxation	64
7.3	Nonlinear Optical Propagation Modeling	65
7.3.1	Experiments Being Modeled	66
7.3.2	Pulse Propagation	68
7.3.3	Calculated Results	70
7.3.4	Interpretations	77

8	Materials Synthesis, Acquisition and Preparation	80
8.1	Materials Preparation	80
8.2	Nonlinear Materials Selection	81
9	IR Shutter	87
9.1	Concept Testing	88
9.2	Contrast Enhancement	90
9.3	Angular Transmission	94
10	IR Camera	96
10.1	Temporal Response	98
10.2	Transmission Enhancement	99
10.3	Angular Distribution of Scattering	100
11	Summary, Conclusions and Recommendations	102
11.1	Summary	102
11.2	Conclusions	102
11.3	Recommendations	104
A	Appendix: Materials Survey	108
A	Appendix: Data Sheets and Results Tabulation	119

2 Introduction

This research effort carried out a wide range of investigations of both linear and nonlinear optical phenomena in liquid crystals in order to evaluate their effectiveness in certain optical power limiting and optical modulation applications. The areas of investigation included:

- 1. CW Ar⁺ power limiting by liquid crystal composites**
- 2. Nanosecond Nd YAG laser pulse limiting by pure liquid crystal**
- 3. Picosecond Nd YAG laser pulse limiting by pure liquid crystal**
- 4. IR shuttering capabilities of polymer liquid crystal composites.**

These activities were supported by efforts in three areas:

- Experimental laser measurements**
- Materials preparation and synthesis**
- Theoretical analysis.**

The body of this report outlines the specific research efforts and summarizes the results. Additional details may be found in the Quarterly Scientific and Technical Reports which were filed with the COTR during the course of investigation.

3 CW Regime

The main thrust of the first stage of the experimental effort was the investigation of the possibilities for power limiting of the polymer dispersed liquid crystal (PDLC) films with continuous wave (CW) lasers. This proceeded in accordance with the proposed work by investigating both passive and active electronic feedback configurations. The effort resulted in an active feedback system meeting the requirements for an Optical Power Limiting (OPL) device in the CW regime, i.e. transparent at low intensity and blocking high intensity transmission.

3.1 Active Linear Feedback Optical Power Limiting for CW Ar^+ laser

The active feedback investigations studied a combined device design with an electronic sensor that controlled a light shutter using liquid crystals. The light shutter technology is based on the polymer dispersed liquid crystal (PDLC) technology established in liquid crystal display (LCD) applications.

The use of PDLCs in display applications is a mature technology. It is based on scattering of light by liquid crystal inclusions in a transparent polymer. While the materials and geometry of a PDLC may vary greatly, there is a common basic structure from which all applications derive. This basic structure is a clear polymer which has impregnated (by a variety of processes) spherical inclusions of liquid crystals. (Figure 3 shows this geometry for example.) The liquid crystal inclusions are essentially nonabsorbing, so when the index of refraction of the liquid crystal is the same as the polymer, then the medium is "water clear". Because all liquid crystal materials are birefringent, they have two different indices of refraction depending on the orientation of the liquid crystal relative to the direction and polarization of light. This direction of orientation is electrically controlled. This control forms the basis of the active feedback mechanism investigated.

The PDLC films studied consisted of the liquid crystal E7 dispersed in the epoxy matrix made using Epon 282, MK107 and Capcure. The films can be switched from a scattering opaque state to a clear transparent state by the application of a voltage across the film. We constructed a feedback circuit so that the voltage applied across the film was a function of the intensity of light transmitted by the film. The optical power transmitted by the sample was measured by a photodiode; the output voltage of the photodiode amplifier circuit was used as the input of a linear feedback circuit. The amplitude of the 1kHz sinusoidal voltage applied to the film was therefore a linear function of the transmitted

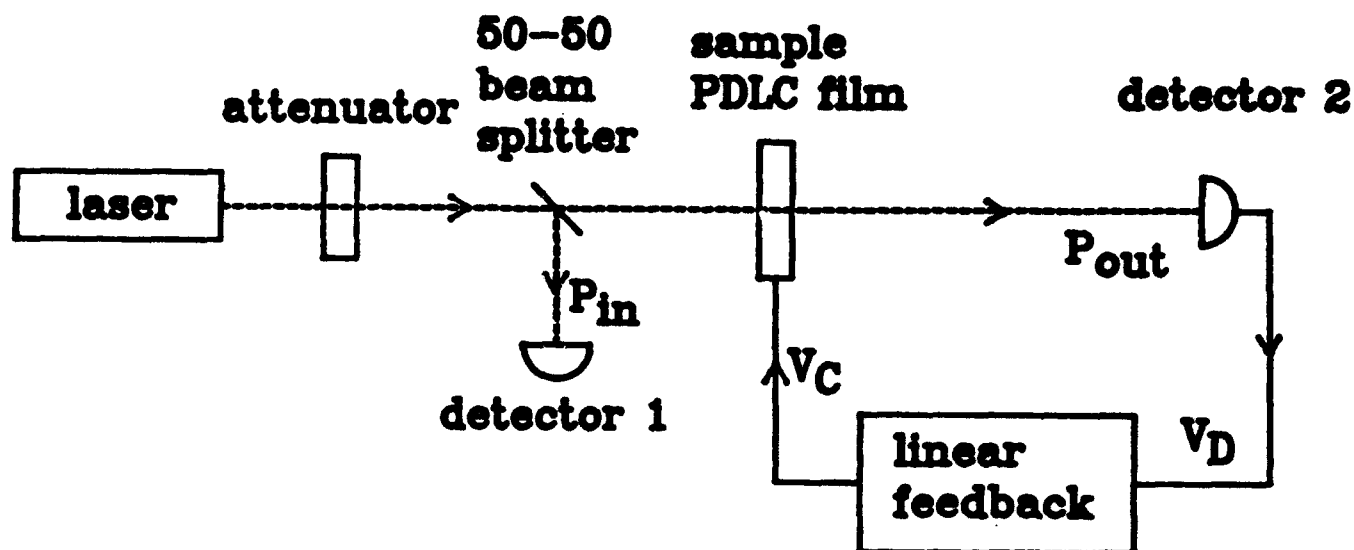


Figure 1: Schematic of experimental arrangement for active feedback OPL.

power. The schematic diagram of the experimental arrangement is shown in Fig. 1.

The transmittance of the film depends on the applied voltage, and, in the presence of feedback, becomes a function of incident power. The response of the sample in the case of negative feedback exhibits optical power limiting behavior as shown in Fig. 2 for different feedback parameters.

In the case of negative feedback, for some range of optical input power, the system has two stable and one unstable states for a given input. This optical bistability may be of interest for optical memory applications.

The OPL characteristics of this feedback arrangement are excellent and offer promise for use in CW protection applications. There is considerable latitude in the selection of electric circuit parameters, such as driving voltage and sensor sensitivity. Similarly, a variety of liquid crystal and polymer materials may be used and the liquid crystal droplets can be varied in size and concentration. Because of this flexibility, the system parameters may be optimized for a variety of applications.

The work on this aspect of the project was designed to provide a demonstration of a

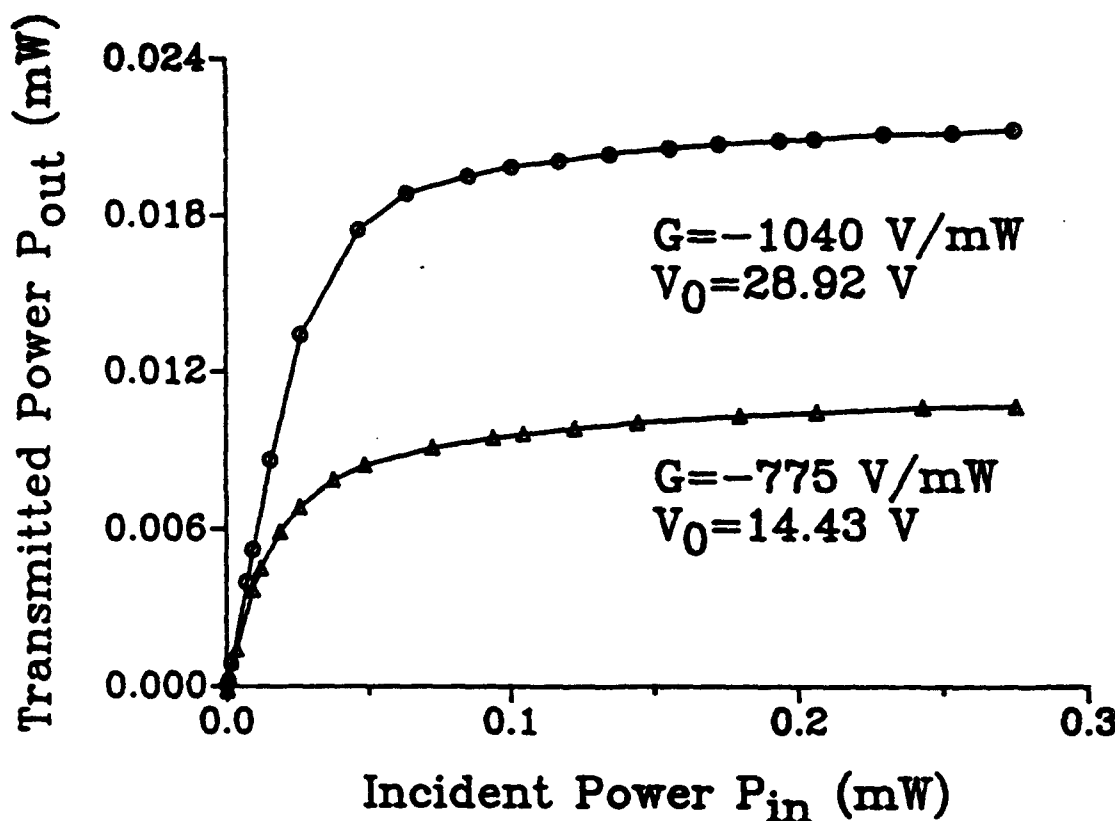


Figure 2: Optical power limiting response for different feedback parameters.

CW OPL device concept. A prototype of this device was delivered to the COTR. Work was completed on this phase of the project. Further efforts could be directed toward meeting specific device requirements if such requirements are provided. In particular, response times and dynamic range could be tested and optimized in the future.

3.2 Passive OPL Study of PDLs

One of the contract requirements was to investigate passive OPL properties of liquid crystal over a wide range of time scales. Passive OPL has inherent advantages, such as not relying on electronic circuits, but developing materials properties and geometries is inherently more difficult. For CW laser beams, active feedback devices such as that described in the previous section may be expected to be superior. Nonetheless, passive OPL behavior was studied and characterized in PDLs as required. Two sets of experiments were carried out to study passive optical switching in PDLs. The mechanisms available

for CW switching included heating effects and optical field induced reorientation of the liquid crystal molecules in the droplets.

The first experiments studied these two switching mechanisms and the geometry used in the study was an initially transparent PDLc film. The observation of switching is then observed as induced scattering by the liquid crystal droplets as illustrated schematically in Fig. 3.

The geometry for optical switching starts from the "on" or transparent state described above with a quasi-static field applied perpendicular to the plane of the film. The optical field of an argon-ion laser is then incident normally on the film and the electric field of the light is perpendicular to the quasi-static field maintaining the transparent "on" orientation of the droplets. In theory, when the electric field of the light becomes comparable to the quasi-static field, the competition will cause the loss of orientation or possibly reorientation of the droplets. We found that the intensity of our 10 watt Argon ion laser was adequate to this purpose.

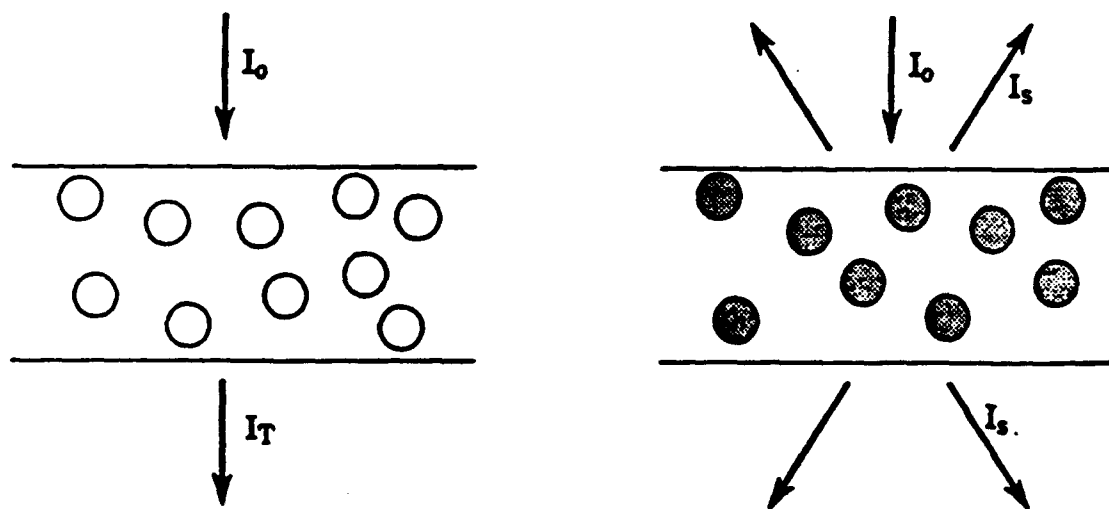


Figure 3: Light scattering results when the optical field induces a change in the dielectric properties of the inclusions producing optical index mismatch.

We set up this experiment with a chopped Argon ion beam incident on an initially transparent PDLC. The transmittance of the PDLC was monitored by a small He-Neon laser. The layout of the apparatus is shown in Fig. 4.

At low intensity of the Argon ion laser, the probe beam is essentially unattenuated (90% transmittance). At high intensity, we found that transmission was strongly attenuated. Fig. 5 shows transmittance measured by the probe beam as function of the Ar pump beam intensity.

The maximum decrease in probe beam intensity is about 80% and is dependent on the relative orientation of polarization of the pump and probe beams. This difference in the polarization indicates that both optical reorientation and thermal effects are present.

A second set of experiments on laser inducing scattering in PDLCs was performed to

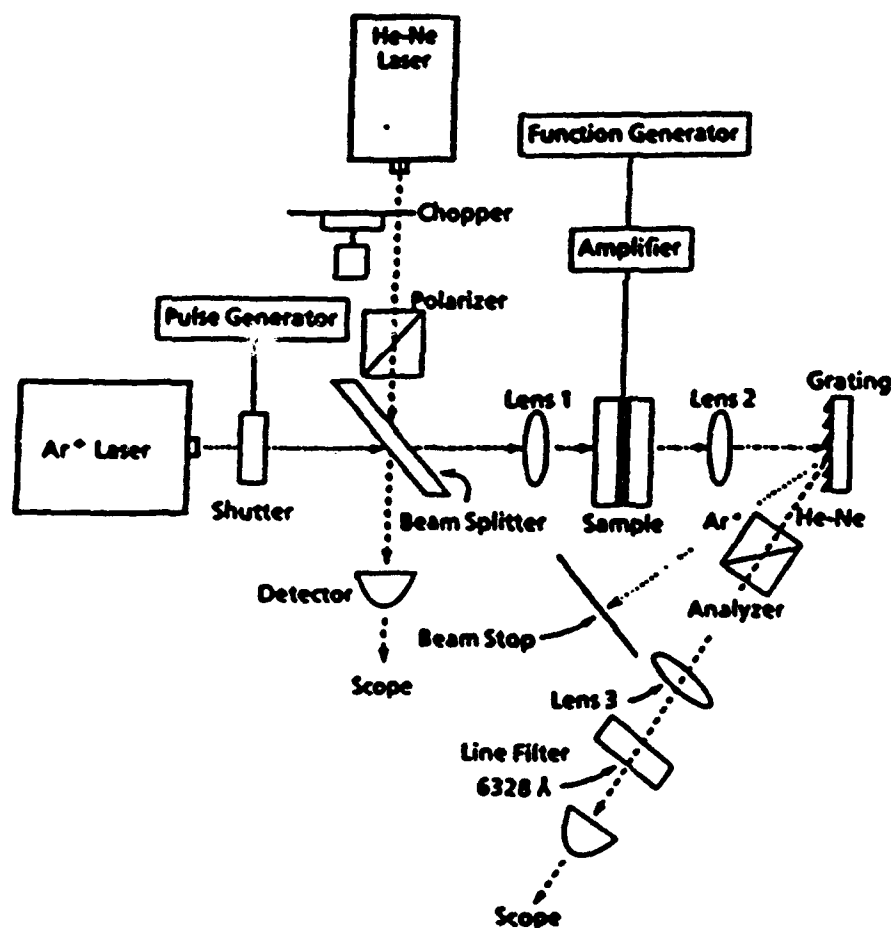


Figure 4: Experimental set up for passive switching measurements

further elucidate the competition between the optical field reorientation and the heating effect in the switching experiments on PDLCs. There are two essential differences between the data taken in the second set of experiments. Firstly, PDLCs were artificially heated to temperatures approaching the nematic-isotropic transition. Secondly, we performed experiments on samples with no stabilizing static field applied to the droplets initially. We were therefore trying to switch from a scattering state to a transmitting state in these experiments.

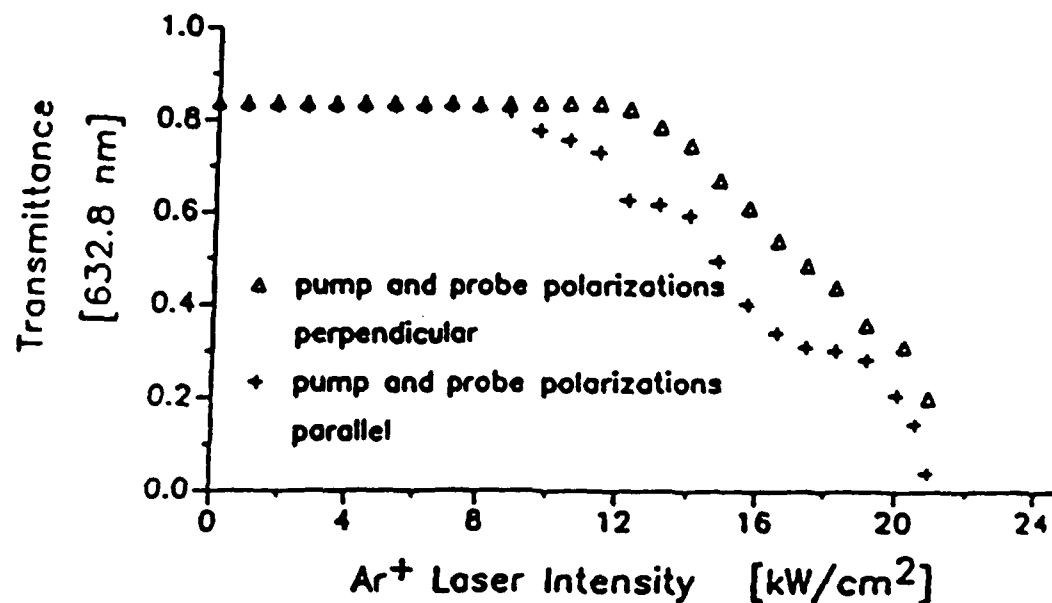


Figure 5: Minimum transmittance as a function of pump beam intensity.

As expected, there is no effect whatever at room temperature. At higher temperatures, the elastic and viscous forces in the liquid crystal droplets weaken and we expect an optical field to be more effective in reorienting liquid crystal molecules into a transmitting geometry. This is indeed what was observed as is shown in Fig. 6.

The particular importance of these results lies not in the size of the effect (although it is not small) but rather in the demonstrated optical orientability of a random PDLC. To our knowledge, this was the first such demonstration although we have had informal reports of attempts by researchers at Hughes, University of California at Berkeley[1], and Celanese in similar systems.

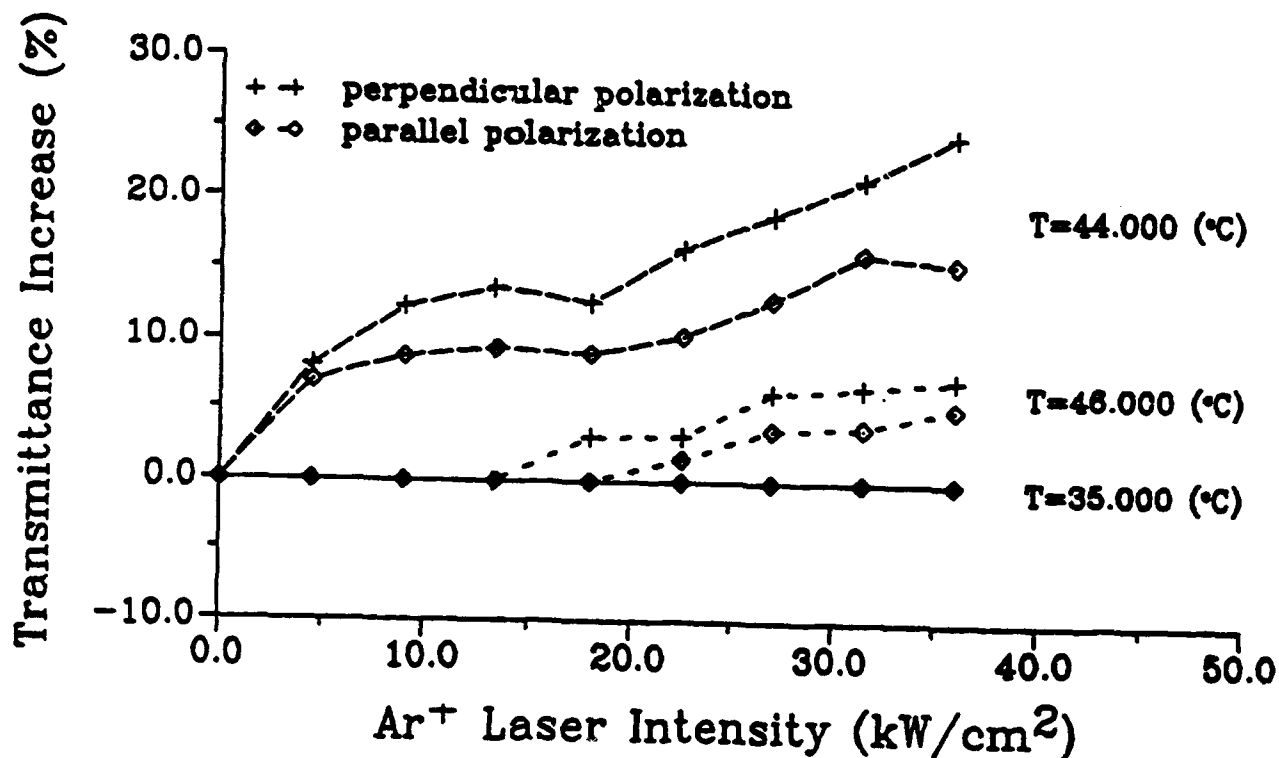


Figure 6: Optical field induced transmission.

3.3 Nonlinear Materials Parameters in the CW regime

Pure liquid crystal materials were studied extensively in addition to the PDLC systems. Results tabulating CW and pulsed materials characteristics are contained in Appendix A and Sec. 5.1. Here we report the experiments on selected compounds.

We carried out systematic measurements of the nonlinear refractive indices n_2 of pure liquid crystal materials. The method of measurement is the z-scan technique, developed by E. van Stryland et al. at CREOL. This is essentially a measurement of self-focusing by the sample; the nonlinear refractive index of the sample can be readily determined from intensity of the transmitted radiation in the far field. Since liquid crystals are birefringent, we can measure two nonlinear refractive indices (and the nonlinear birefringence).

During the z-scan measurements, the samples are translated along the direction of beam propagation across the focal point of a beam focusing lens. The samples are homogeneously aligned (parallel) monodomain samples of the liquid crystal 5CB, between parallel glass plates. The sample thickness varied from 25 μm to 120 μm . The Ar^+ beam was chopped by an electromechanical shutter to produce pulses with a width of approximately 10 ms. The far-field transmittance was measured with the laser polarization both parallel and perpendicular to the nematic director. (The nematic director is the direction the molecules point, and hence the direction along which the polarization of the light experiences the greatest linear index of refraction.)

Typical results for the z-scan measurements of transmission intensity versus position of the sample are shown in figures 7 and 8. The figure shows the results of two measurements, one with the polarization parallel to the director (Fig. 8) and one with the polarization perpendicular to the director (Fig. 7). The sample, 5CB, has a very typical structure of a liquid crystal (see structures in Appendix A).

A sophisticated fitting procedure was employed to determine the nonlinear optical parameters of the sample material from the z-scan measurements. Even without such analysis, it can be seen from the above figure that the nonlinear response of the liquid crystal is extremely large. First, observe that the sign of the nonlinear index of refraction is opposite for the two polarization. As the sample is translated the perpendicular polarization intensity first decreases then increases. The opposite is true for the parallel polarization. Secondly, notice that the decrease in intensity reaches a minimum of around 10% of the unaltered intensity. This sample is exhibiting optical power limiting and it is quite a large effect. The effect is similar in other liquid crystals with similar molecular structures.

The quantitative analysis of our results with the Ar^+ laser, at $\lambda = 514\text{nm}$, with 10ms

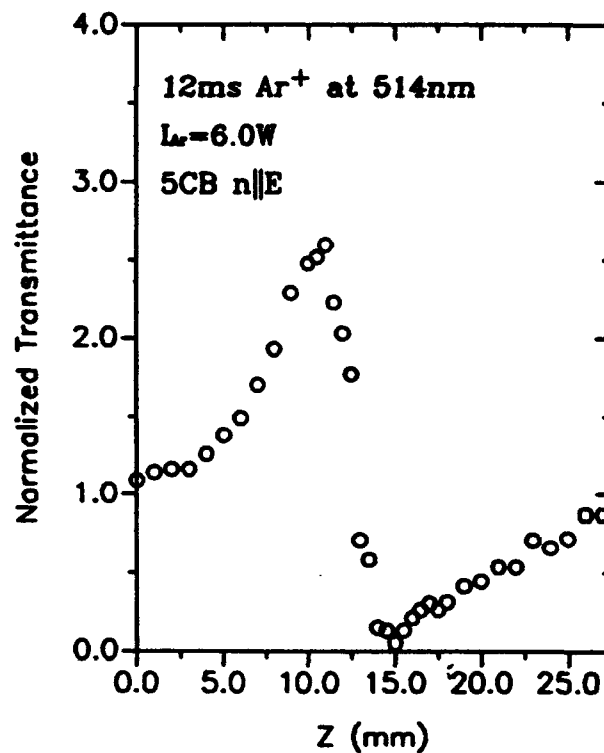
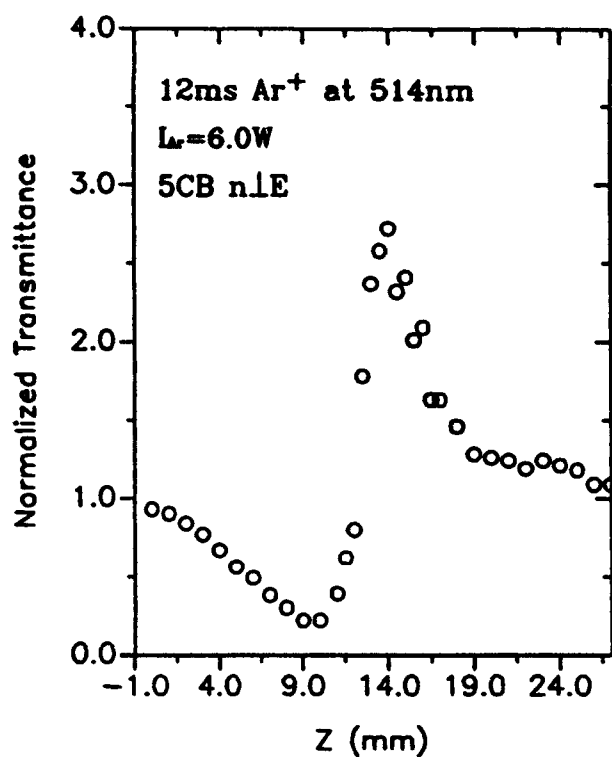


Figure 7: (left). Z-scan of 25 μm thickness sample of 5CB with polarization perpendicular to director, CW Ar⁺ laser at 514 nm.

Figure 8: (right). Z-scan of 25 μm thickness sample of 5CB with polarization parallel to director using CW Ar⁺ laser at 514 nm.

pulses, yielded the following values for the nonlinear index of refraction of 5CB:

- for polarization parallel to the director $n_2 \approx -10^{-2}$ esu,
- for polarization perpendicular to the director $n_2 \approx 10^{-2}$ esu.

We see then that the nonlinearity is large, but of the opposite sign than is expected from optical field reorientation. In particular, the negative n_2 means the material is *self defocusing* for polarization parallel to the director. This is suggestive of large thermal effects which were also investigated and are described in Sec. 3.3.1.

3.3.1 Thermal Behavior in the CW Regime

The negative value of the nonlinear index in the direction of molecular ordering suggests that heating may be the operative mechanism. In such an event, the increase in temperature would decrease the order parameter, and the parallel index of refraction would decrease as well. The opposite would be true for the index of refraction when the polarization is perpendicular to the direction of orientation.

The physical properties of liquid crystals change dramatically as they are heated toward the isotropic (normal liquid) phase. The above results are for a temperature a few degrees below the melting temperature. To determine the change of the nonlinearity as a function of temperature, the temperature dependence of these quantities was also determined. A divergence of the nonlinear index as the isotropic transition approached is shown in Fig. 9.

The temperature dependence in Fig. 9 is for the nematic liquid crystal 5CB using 10ms Ar^+ laser pulses at $\lambda = 514\text{nm}$. The nonlinear birefringence diverges as temperature approaches the nematic-isotropic transition temperature. The extremely small nonlinearity above the transition temperature shows that it is the properties of the liquid crystal nematic phase which is the origin of the nonlinearity and not a property inherent in the individual molecules. More accurately, the molecules are not able to contribute to the optical nonlinearity effectively unless they are in the liquid crystal phase.

This is compelling evidence for a strong thermal component in the nonlinear response in the CW regime. Nonetheless, there is also clear evidence for optical reorientation in the PDL results of Sec 3.2. (See Sec. 7.2 for a related theoretical discussion.)

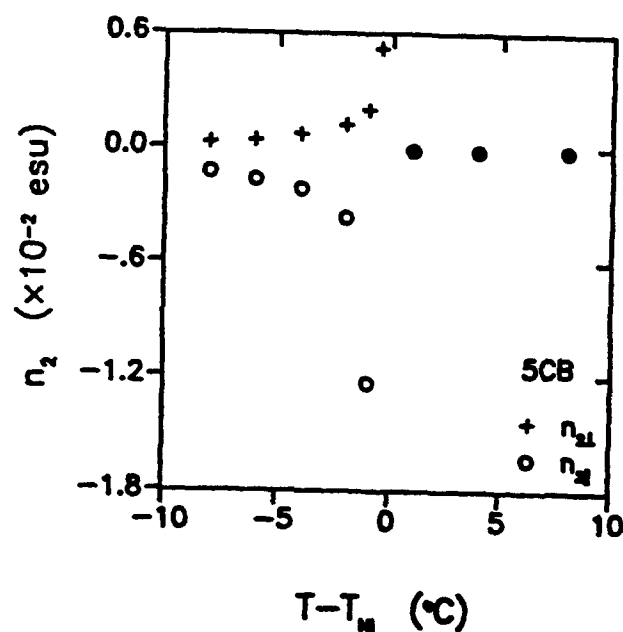


Figure 9: The temperature dependence of $n_{2||}$ and $n_{2\perp}$

4 Nanosecond Nd YAG Nonlinear Optical Response

A systematic study of nonlinear parameters of a variety of liquid crystals was carried out using our Q-switched Nd:YAG laser, with nanosecond pulses. Typical results for 5CB for polarizations parallel and perpendicular to the director are shown in Figs. 10 and 11. The effect for the parallel polarization is large, for the perpendicular polarization is quite small. The third-order hyperpolarizability in the nanosecond regime is $\chi^{(3)} \approx 10^{-9}$ esu, some two orders of magnitude greater than that of CS₂. Results for 8CB, which exhibits a smectic phase, are considerably greater. Theoretical work provided models for the mechanisms for these effects and is discussed in Sec. 7. Additional work on measurements of other liquid crystalline materials, and on molecular structure/physical property relationships is tabulated in Appendix A and in Sec. 5.1 where we discuss the mechanisms involved in the nanosecond nonlinearities.

The measurements on the 5CB were used to determine the nonlinear index of refraction and nonlinear absorption coefficient at $\lambda = 532\text{nm}$. We obtained the values:

- $n_2 = -54 \times 10^{-11}$ esu for polarization parallel to director.
- $n_2 = +8.3 \times 10^{-11}$ esu for polarization perpendicular to director.
- $n_2 = -24 \times 10^{-11}$ esu for the isotropic phase .

The nonlinear absorption coefficient β has also been measured with the results:

- $\beta = 265 \text{ cm/GW}$ for polarization parallel to director.
- $\beta = 36 \text{ cm/GW}$ for polarization perpendicular to director.
- $\beta = 114 \text{ cm/GW}$ for for the isotropic phase.

The key result is that n_2 for 5CB in the nematic phase in the nanosecond regime for the wavelength $\lambda = 532\text{nm}$ is nearly two orders of magnitude greater than CS₂. We have verified the accuracy of our measurements by measuring n_2 for CS₂, and have obtained values in agreement with those in the literature.

We have also attempted to measure the nonlinear response at the fundamental wavelength $\lambda = 1.06\mu\text{m}$ of the Q-switched Nd:YAG laser. Our experimental results for 5CB show very weak nonlinearities at this wavelength, up to the damage threshold of the sample cell (not the liquid crystal). (For a discussion of damage, see Sec. 6.) The nonlinear

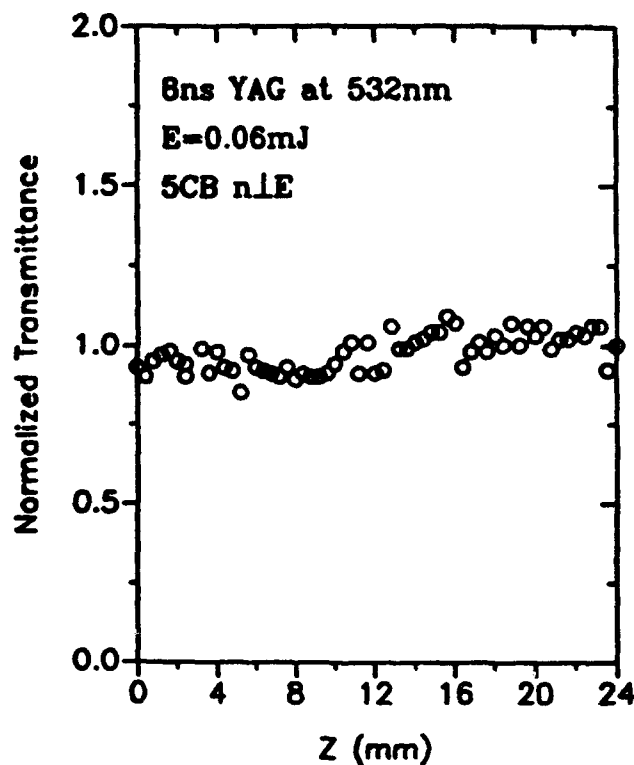
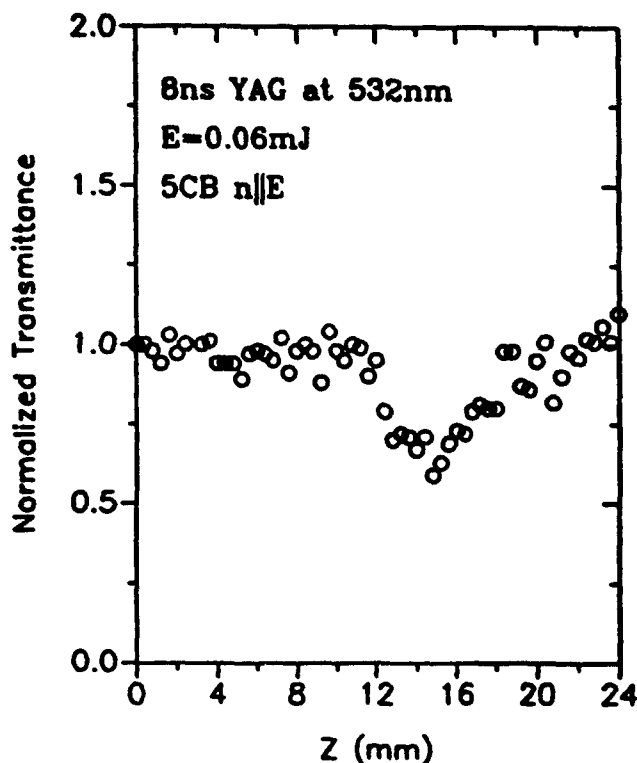


Figure 10: (left). Z-scan of $120\ \mu\text{m}$ thickness sample of 5CB with polarization parallel to director using 8ns pulses at 532 nm.

Figure 11: (right). Z-scan of $120\ \mu\text{m}$ thickness sample of 5CB with polarization perpendicular to director using 8ns pulses at 532 nm.

contribution to the transmittance could not be effectively separated from noise because of its small magnitude.

As in the CW case, we see then that the nonlinearity is large, but of the opposite sign than is expected from optical field reorientation. In particular, the negative n_2 means the material is *self defocusing* for polarization parallel to the director. In the CW measurements, we interpreted the negative value of n_2 for parallel polarizations to be due to heating. In the nanosecond regime this would be a very peculiar result because conventional wisdom would suggest that thermal effects are too slow to be operative in the nanosecond regime. The temporal characteristics of the nonlinear response were therefore experimentally investigated and are reported in Sec. 4.1. (The possible role of thermal

effects were also investigated theoretically and are discussed in Sec. 7.2.)

4.1 Time Dependence of Nonlinear Response: Two-Pulse Measurements

In order to identify the dominant mechanism responsible for the observed large nonlinearities in nanosecond regime, it is useful to have an estimate of the characteristic time of the contributing process. To estimate this time, we have devised a time resolved double pulse Z-scan scheme. The experiment setup is shown in Fig. 12.

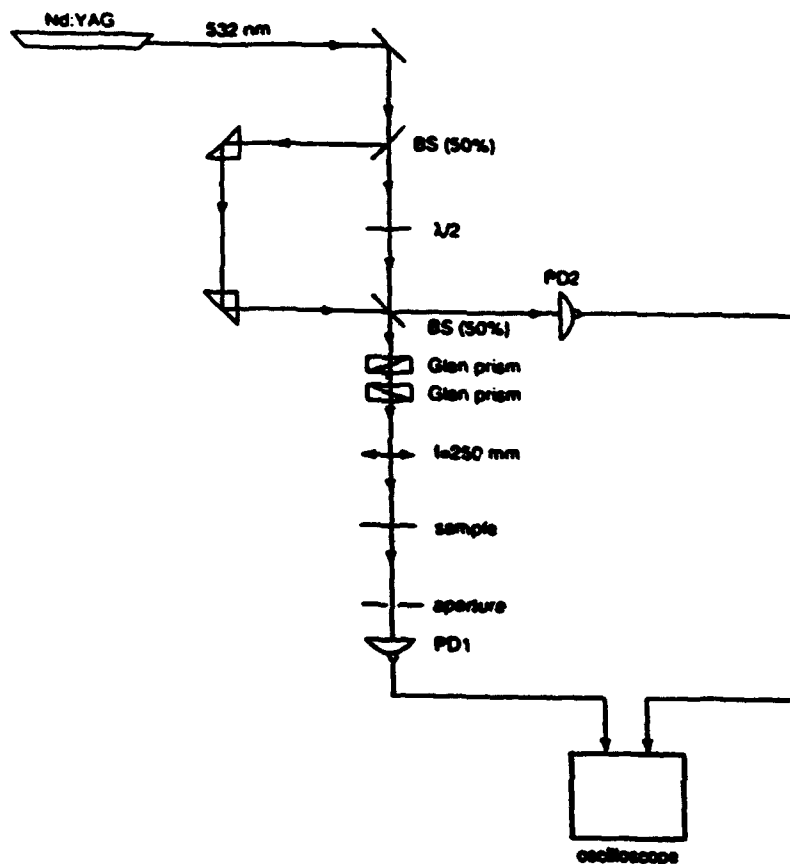


Figure 12: Experimental set up for two-pulse measurements

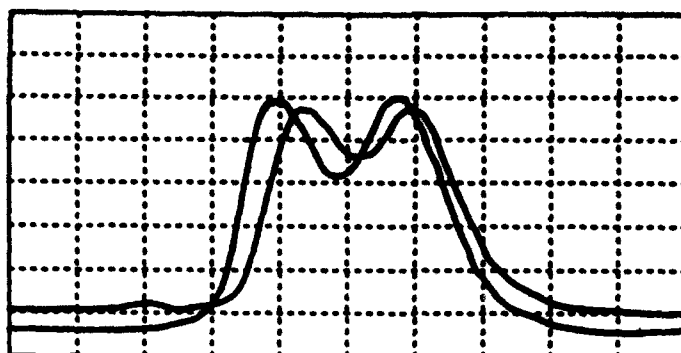


Figure 13: Transmitted pulses when the sample was placed far from the focal point

In this experiment, a portion of the beam from the laser is first delayed and then recombined with the original beam, resulting in two pulses of nearly identical amplitude separated in time. By performing Z-scan measurements using these two pulses, it is possible to determine if the first pulse affects the response to the second. If it does, then the decay time of the process can not be less than the temporal separation of the pulses. For this scheme to work, it is essential that at the sample the two beams be parallel and that both pulses pass through the same region of the sample, a nontrivial task.

The time delay between the two pulses can be varied by changing the length of the delay line. The energy of each pulse can be adjusted independently by changing the angles between the half wave plate and the Glan prisms. In our experiment, the two pulses had nearly the same energy and a time delay down to 11ns. The incident and transmitted intensities were recorded on the oscilloscope. The sample was 5CB at 24 degrees C. The incident polarization of both pulses was parallel to the director. Figs. 13 and 14 show the oscilloscope record when a small aperture was placed in front of the photodetector PD1. In this geometry, a nonlinear response removes energy from the beam.

Fig. 13 shows the transmitted pulses when the sample was placed far from the focal point. In this geometry, the intensity in the sample is low and hence no nonlinear response is expected. As expected, Fig. 13 shows that the two transmitted pulses have almost the same height. This confirms that the intensity is low and nonlinear effects are negligible. However, when the sample is moved close to the focal point, at a particular sample position, the first pulse is suppressed due to nonlinear absorption and nonlinear refraction, while the second one is increased rather than decreased. Such an example is shown in Fig. 14.

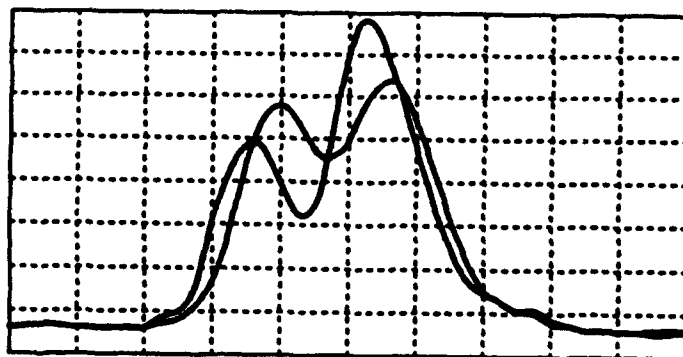


Figure 14: Transmitted pulses when the sample was placed near the focal point

The increase in the amplitude of the second transmitted pulse is clearly due to the effect of the first pulse, since when the first pulse is blocked, the second pulse decreases also. This behavior implies that, regarding nonlinear refraction, the second pulse "sees" the effect of the first pulse. However, if the total transmittance is measured without an aperture in front of the detector, i.e. all transmitted light is detected, the two transmitted pulses have the same response regardless of the sample position relative to the focal point. This implies that, regarding nonlinear absorption, the second pulse does not see the effect of the first.

These observations raised significant questions about the role of orientational order in nonlinear response. If the first pulse changed the orientational character of medium, and the nonlinear absorption were anisotropic, then the absorption should change for the second pulse as well. One of the ways to change orientational order in liquid crystals is to change the temperature, since they become more ordered at low temperature. Experiments on the temperature dependence of nanosecond nonlinearities were accordingly performed and are described in Sec. 4.2.

4.2 Temperature Dependence of Nanosecond Nonlinear Response

We have also carried out measurements of the temperature dependence of the nonlinear response of 5CB on the nanosecond scale at 532nm wavelength. We found, as in millisec-

ond case, that $n_{2\parallel}$ and $n_{2\perp}$ in the nematic phase have opposite signs, and that there is an abrupt change in these values across the nematic-isotropic transition. However, unlike in the millisecond case, the values of $n_{2\parallel}$ and $n_{2\perp}$ do not change appreciably with temperature in the nematic phase, and remain nearly constant up to the nematic-isotropic transition temperature.

Figs. 15 and 16 show the temperature dependence of the parallel component of n_2 and β . We note, as shown in Fig. 15, that $n_{2\parallel}$ is constant to within 5% from 0 to 10 degrees C below the transition; the transition was approached to within less than 400mK. Similar behavior holds for β_{\parallel} in Fig. 16. However, there is an abrupt jump at the transition temperature both for $n_{2\parallel}$ and β_{\parallel} .

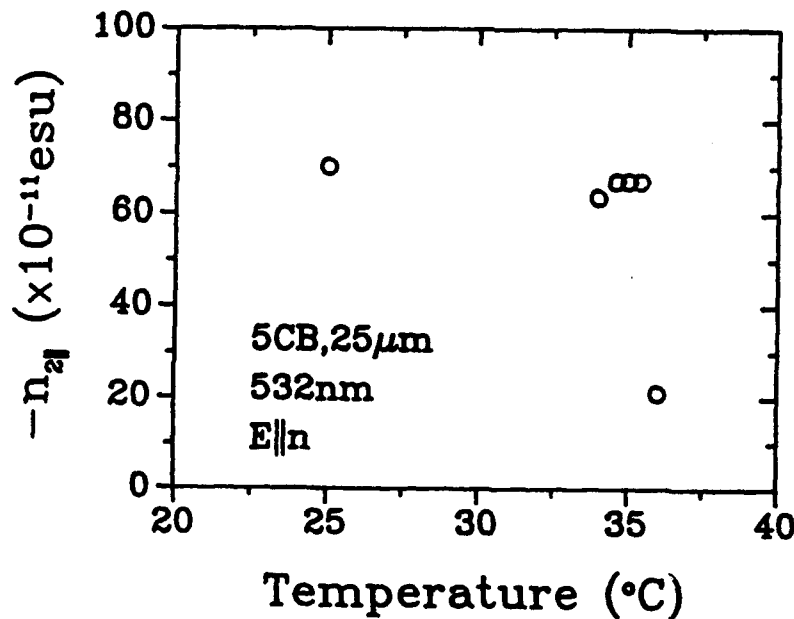


Figure 15: Temperature dependence of the parallel component of n_2 .

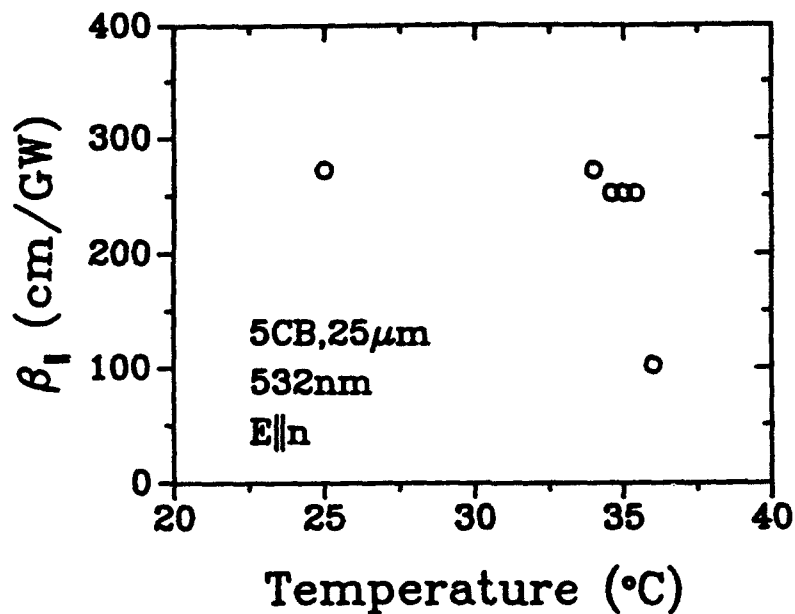


Figure 16: Temperature dependence of the parallel component of β

4.3 Higher Order Nonlinearities

We have also measured the intensity dependence of the nonlinear absorption coefficient β_{\parallel} and refractive index $n_{2\parallel}$ for 5CB at 532nm using ns pulses. The sample has a thickness of 25 μm and the sample temperature is 24 degrees C. In this set of measurements, for each incident energy, we performed a Z-scan measurement and obtained the nonlinear refraction and absorption coefficients. In this way, n_2 and β were determined as function of incident intensity. Fig. 18 shows the result for the geometry where the incident polarization is parallel to the director. The horizontal axis represents on-axis laser intensity I_0 , defined as $I_0 = 2P/(\pi\omega_0^2)$, where P is the power and ω_0 is the beam waist.

As can be seen in Fig. 17, the nonlinear refractive index $n_{2\parallel}$ remains essentially constant within our experimental error, as expected for a third-order process. Interestingly, however, the effective nonlinear absorption increases linearly with the intensity. This has implications for the mechanisms operating to produce the nonlinearity. We discuss these mechanisms further in Secs. 5.1 and 7.3, but we note that the increase in nonlinear absorption or refractive index with intensity serves to enhance the OPL behavior.

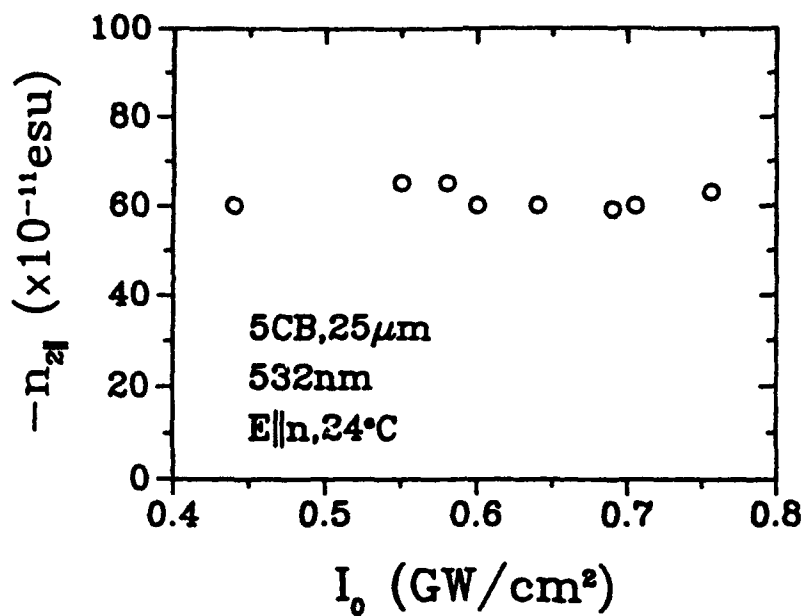


Figure 17: Intensity dependence of the nonlinear refractive index $n_{2||}$ for 5CB at 532nm using 7 ns pulses

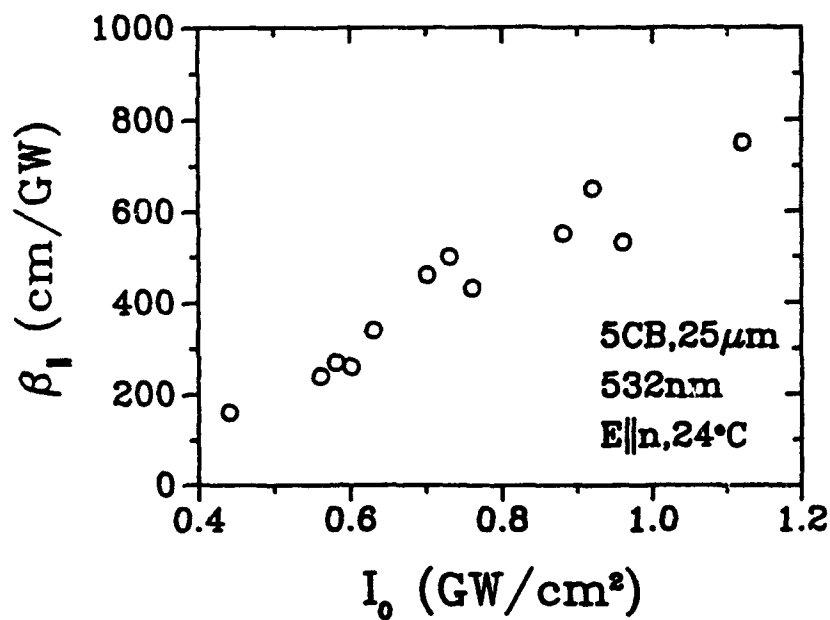


Figure 18: Intensity dependence of the nonlinear absorption coefficient $\beta_{||}$ for 5CB at 532nm using 7 ns pulses

4.4 Photoacoustic Measurements

We also attempted photoacoustic measurements where an attempt was made to detect an acoustic wave generated by a nonlinear pulse under conditions of strong nonlinear absorption. We did not have an unambiguous answer to the question of where the energy went which was removed from the beam during OPL circumstances, thus we sought to investigate sound generation as a process for dissipation of the absorbed energy. A sensitive accelerometer, consisting of a piezoelectric element, was attached to one glass plate of a 120 μm thick 5CB sample. The sample was then exposed to 532nm pulses. The incident polarization was parallel to the director and the pulse energy was 64 μJ . With the sample positioned near the focal point of the lens, the transmittance was about 0.5. At this intensity, a signal was detected by the accelerometer, indicating that acoustic excitations play do play some role in the dissipation process. Unfortunately, during the duration of this effort, we were unable to refine these measurements to obtain a quantitative measure of the amount of energy dissipated.

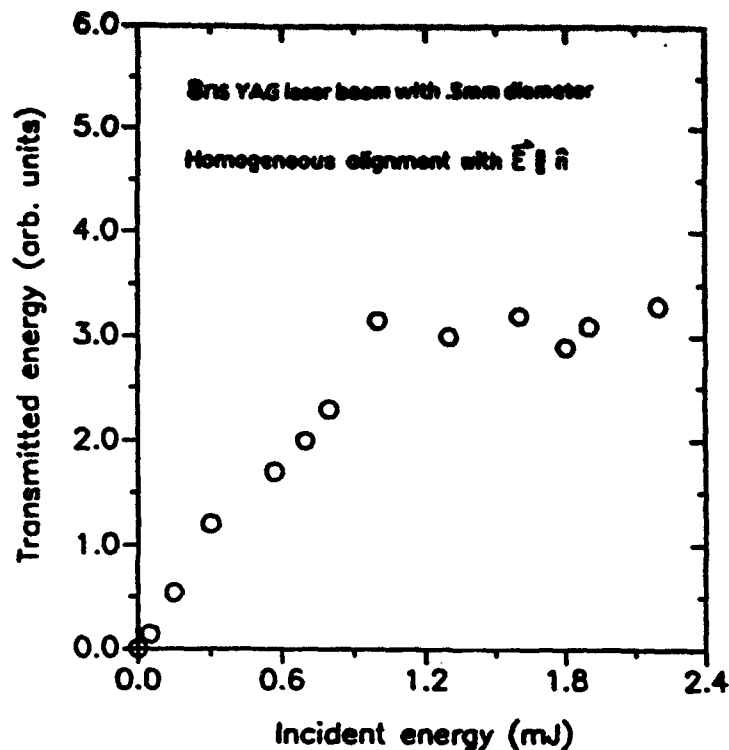


Figure 19: Optical power limiting behavior of 25 μm sample of 5CB.

4.5 Nanosecond Optical Power Limiting

Optical power limiting behavior in these materials on the nanosecond time regime has also been observed. In Fig. 19 we show the OPL response of a 25 μm thick sample of nematic 5CB (homogeneous alignment) to 8ns pulses at 532nm.

Notice that the shape of the curve in Fig. 19 shows a nearly ideal OPL behavior. The energy threshold here is $\approx 1\text{mJ}$ with a $500\mu\text{m}$ spot size. This threshold is greatly reduced in geometries appropriate to devices used in the field. (See Sec. 4.5.1.) With a faster lens to give a $10\mu\text{m}$ spot size, this threshold would be reduced to $0.4\mu\text{J}$. We produce this particular plot here because believe this was the first demonstration among any of the contractors of effective OPL by nematic liquid crystals in the nanosecond regime.

4.5.1 ARDEO DVO Test Bed

Under this contract we provided two "best samples" for evaluation with the ARDEO DVO test bed. These samples were of 8CB and differed in thickness and "doping" with

dye (anthraquinone dye d_{27} from BDH is itself a liquid crystal). Sample 1 is 240 mm thick and has a dye concentration of 0.05%. Sample 2 is 120 mm thick with dye concentration 0.02%. These are very thick samples for optimum effect of the nonlinear response. The nominal transmission of our "best sample" was 80%, in keeping with the transmission standards required.

Prior to delivery, we replicated the required optics and performed our own measurements of OPL. These samples were also characterized for nonlinear absorption and nonlinear refraction.

Our measurements were performed with a "top hat" beam profile as specified for use in the test bed. Fig. 20 shows the beam profile. It is "dirty" as required, showing significant spikes across the profile. This is a characteristic expected under field conditions.

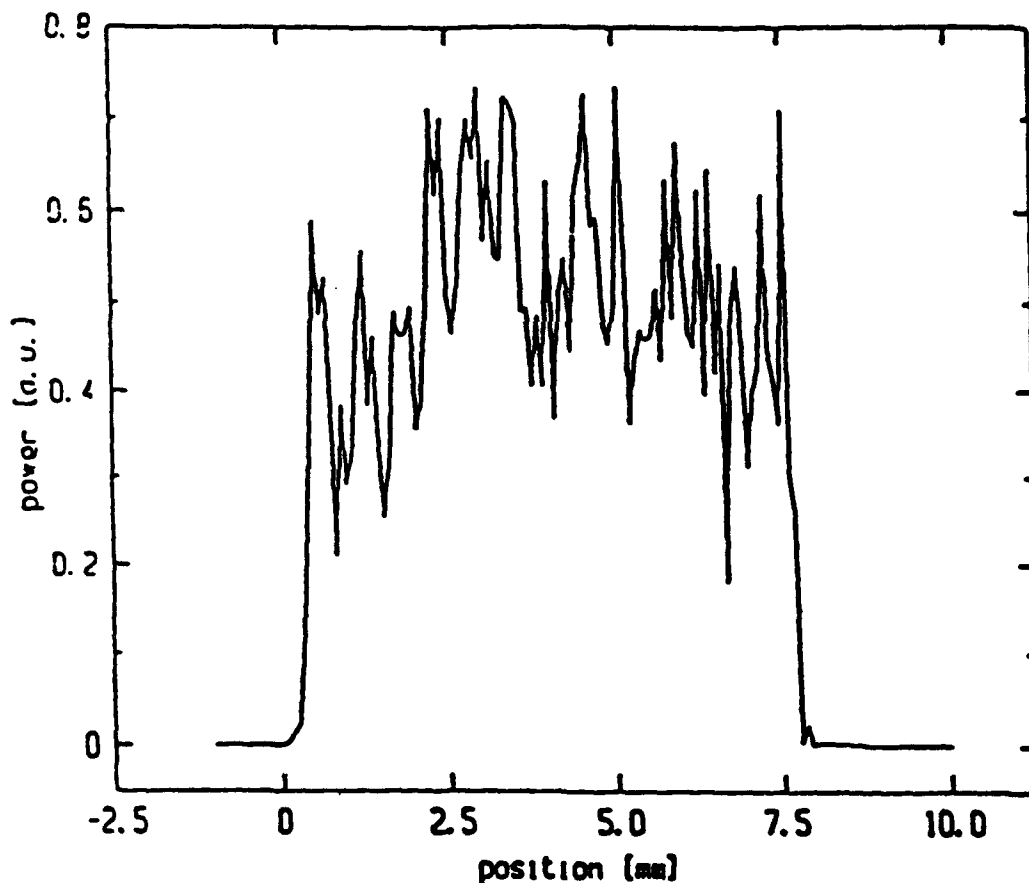


Figure 20: Beam profile used in measuring samples provided for test bed

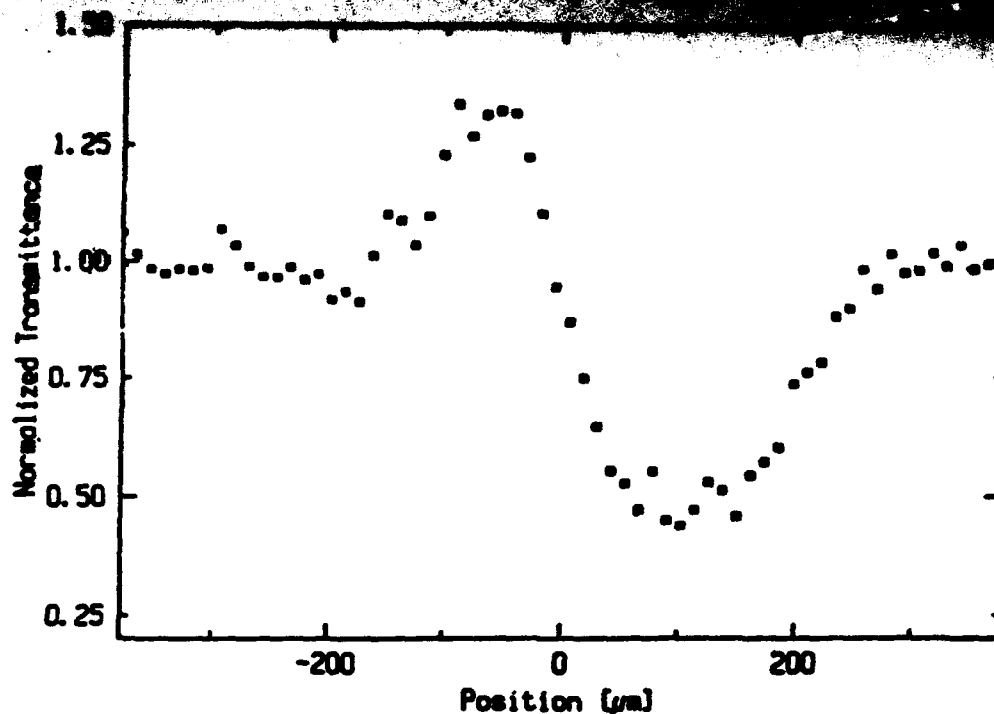


Figure 21: Z-scan to determine nonlinear refractive index using top hat beam

Samples were characterized using the Z-scan technique for nonlinear index and nonlinear absorption as shown in Figs. 21 and 22 respectively.

Doped samples of 8CB give the largest nonlinear index of refraction and the largest nonlinear index of refraction of any materials we have tested. As stated above, 80% transmission was maintained with a doping of less than 0.05% by weight. The values

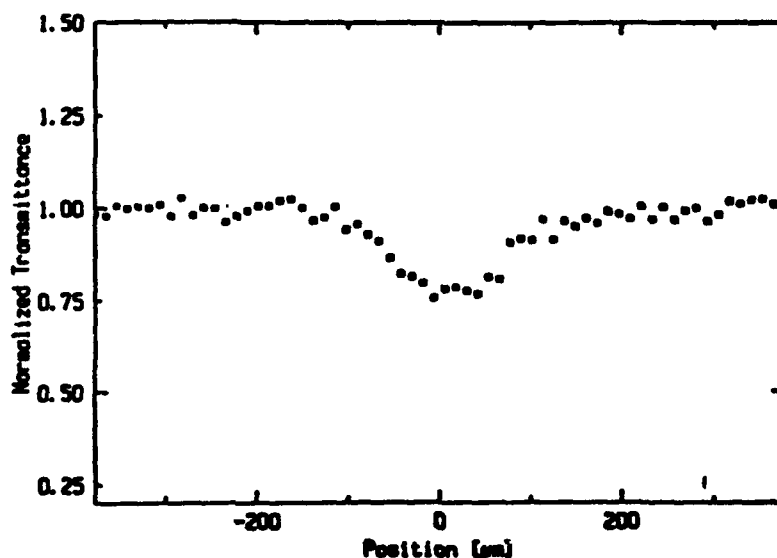


Figure 22: Z-scan to determine nonlinear absorption using top hat beam

$n_{2\parallel} = -152 \times 10^{-11} \text{ esu}$ and $n_{2\perp} = +10.5 \times 10^{-11} \text{ esu}$ were obtained for polarisations parallel and perpendicular to the director. In the isotropic phase, the nonlinear index, $n_{2i} = -48 \times 10^{-11} \text{ esu}$ was obtained. Compared to the pure material, the doping increased the largest nonlinearity by a factor of six.

Large values of the nonlinear absorption were also obtained. The values $\beta_{\parallel} = 380 \text{ cm/GW}$ and $\beta_{\perp} = 30 \text{ cm/GW}$ were obtained for polarisations parallel and perpendicular to the director. In the isotropic phase, the nonlinear absorption value, $\beta_i = 193 \text{ cm/GW}$ was obtained. Compared to the pure material, the doping increased the largest nonlinearity by a factor of six.

We measured the OPL characteristics of the two samples under simulated test bed conditions. Both performed well. Figs. 23 and 24 show the power limiting curves for these samples.

Increasing the thickness of the sample and increasing the amount of dye decreased the transmission to 80% of the undyed level. A relatively small improvement is accordingly observed in the power limiting characteristics of sample 2. Notice that the horizontal axis is much enlarged over the vertical so that the turn over of the transmission curve is

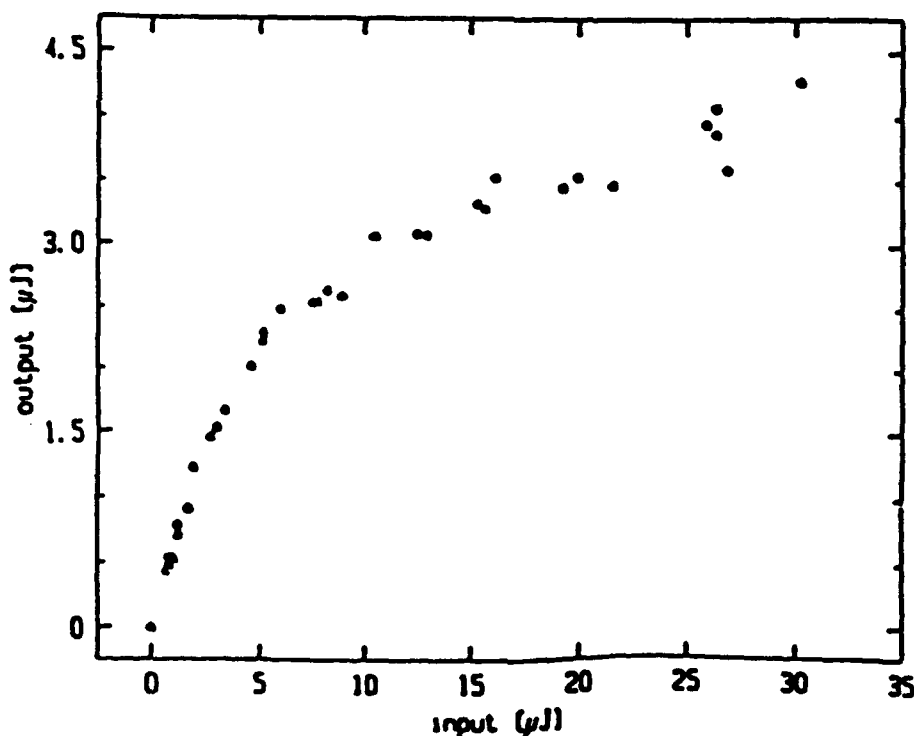


Figure 23: Optical Power Limiting curve for Sample 1

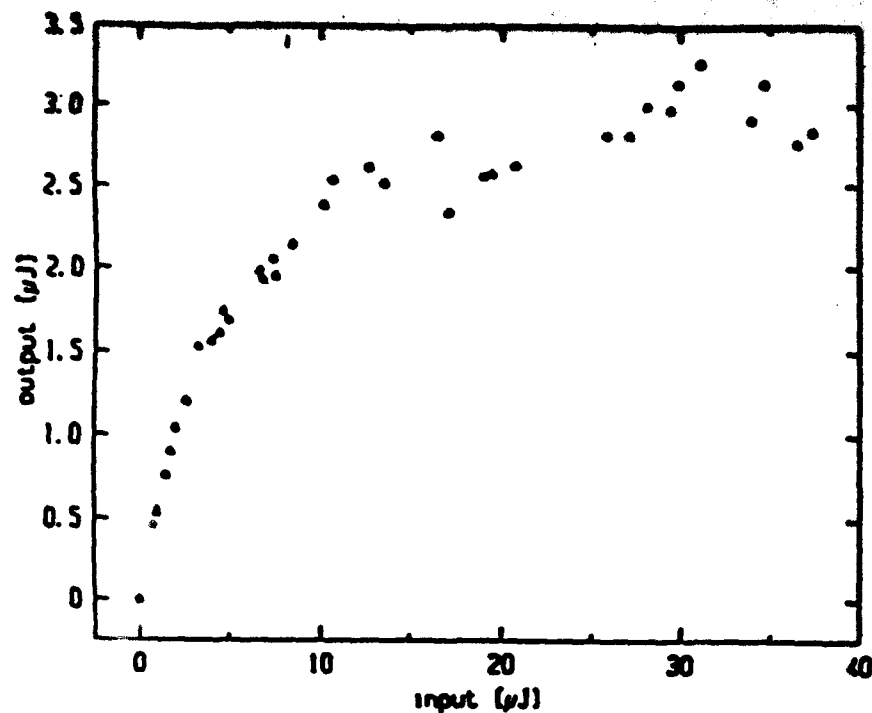


Figure 24: Optical Power Limiting curve for Sample 2

magnified. From this curve one sees an onset of power limiting at approximately 3 μJ and the maximum transmission is accordingly approximately 3 μJ . This is almost ideal OPL behavior. It further illustrates the extent to which improvements have progressed towards operational devices. When the project started, very few materials looked like they would within an order of magnitude of this degree of performance.

Damage in these samples occurred at 40 μJ and was caused by the polyimide alignment layer.

5 Picosecond Nonlinear Optical Response

The third time scale investigated for optical nonlinearities in liquid crystals was the picosecond regime. Using the Nd YAG with a 33 picosecond pulse, z-scan measurements were carried out to determine the nonlinear index of refraction and nonlinear absorption of liquid crystal materials. Tabulated results covering all three time scales are contained in Appendix A. Here we report on one compound, 5CB, which was studied most extensively.

We were able to obtain very good data in the picosecond regime. We attach a z-scan produced at the CREOL facility. This is a small aperture scan and shows a much smaller variation in intensity (4%) than the nanosecond scans (40%). Still, as can be seen, the scatter in the data is very small and hence we are confident in our measured values of nonlinear index.

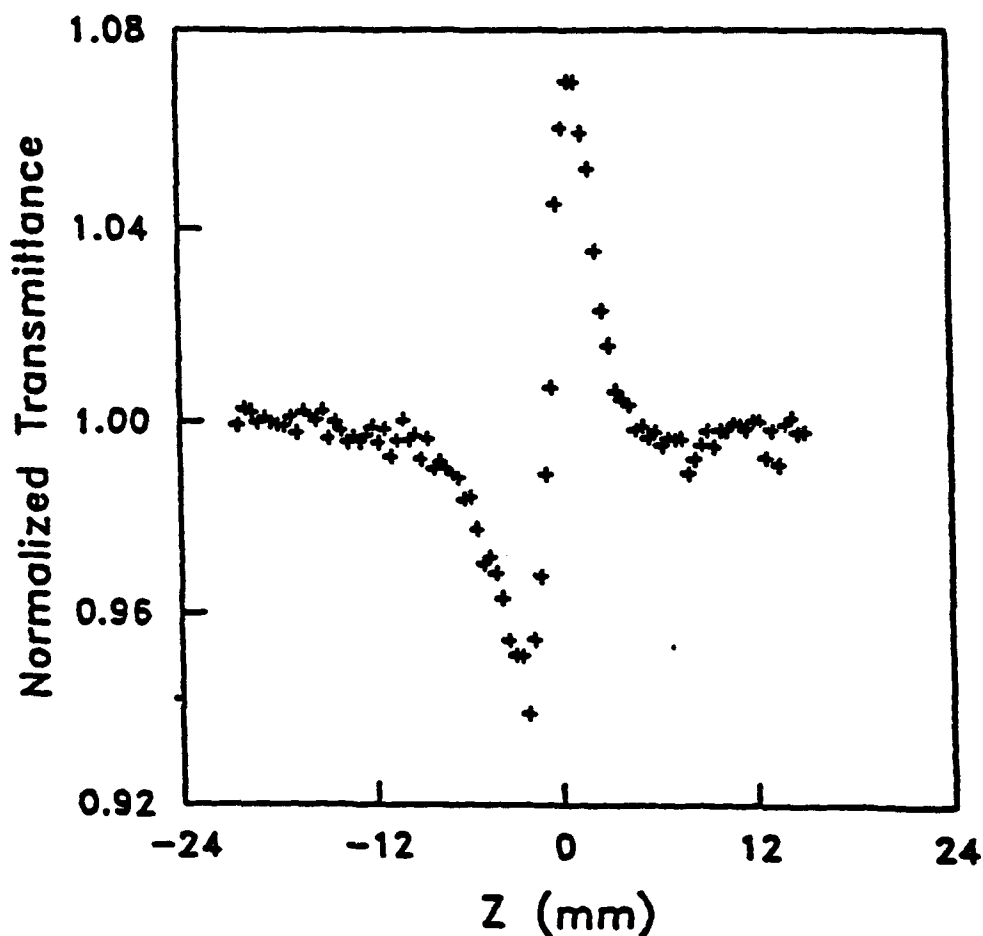


Figure 25: Z-scan of sample with $2.3 \mu\text{J}$ pulses of 33 picosecond duration.

5.1 Mechanism Analysis

In this section, we bring together the results of our measurements on 8 different liquid crystals and discuss the conclusions we have reached about mechanisms. Five of these materials are commercially available; however, OPL-7-1, OPL-10-1 and OPL-10-2, were synthesized by the group of L.C. Chien at the Liquid Crystal Institute at Kent State University. In addition to pure liquid crystals, a dyed sample (anthraquinone dye d_{27} from BDH) of 8CB was also studied. The experimental results for these materials is provided in Appendix A, but we extract those relevant to the current discussion and present them here also.

The molecular structures are also shown along with the wavelength, λ , at which the measurements were carried out, δ the laser pulse width, and T the sample of temperature. The subscripts \parallel and \perp indicate polarisation parallel and perpendicular to the director, and i denotes the isotropic phase. The uncertainty in the figures is approximately 10 %. Also, in Tables 1, 2 and 3 the previous results on 5CB, 8CB, E7 are included for the purpose of comparison.

Of all the pure materials studied on the nanosecond time scale, 5CB shows the largest nonlinearities. To interpret the nanosecond measurements, it is useful to briefly summarize the results of millisecond measurements given in Table 2.

5.1.1 Millisecond Mechanisms

In our geometry, where reorientation is not expected to take place, the nonlinearity on the millisecond time scale originates from laser heating due to linear absorption. The resulting temperature increase causes a decrease in the degree of orientational order and in the density, with the result that, in most materials, the extraordinary index decreases while the ordinary index increases. This gives rise to $n_{2\parallel} < 0$ and $n_{2\perp} > 0$, as observed in the case of 5CB. Furthermore, $-n_{2\parallel}$, $n_{2\perp}$ and the nonlinear birefringence, $n_{2\perp} - n_{2\parallel}$ all increase dramatically as the nematic-isotropic temperature is approached from below. At the intensities used in these measurements, no nonlinear absorption is observed. The signs of the two nonlinear refractive indices measured for 5CB and ZLI-2303 are in accordance with the above trend. However, for ZLI-1538 and T15 both nonlinear refractive indices are negative. ZLI-1538 is the only material studied whose core consists of cyclohexane rather than benzene rings, and hence is without conjugation. Due to the lack of conjugation, the linear polarisability and the refractive indices are small, and hence order parameter changes are not effective in changing the index of refraction. Thus, the effect of thermal expansion or other smaller nonlinearity may be dominant. T15 on the other hand has

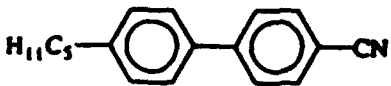
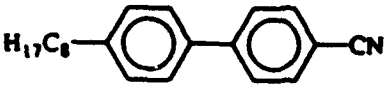
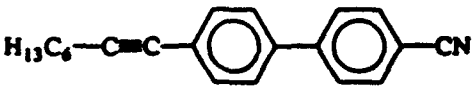
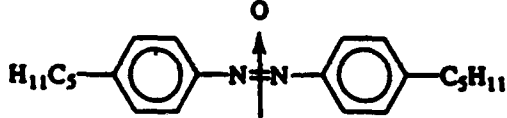
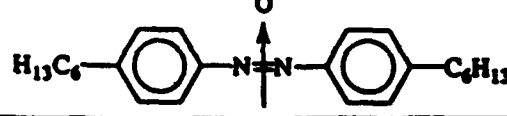
Material	$n_2(\text{esu})$	$\rho(\text{cm/GW})$	T(°C)
5CB 4-cyano-4'-n-pentylbiphenyl	$\parallel: -54 \times 10^{-11}$ $\perp: +8.3 \times 10^{-11}$ $i: -24 \times 10^{-11}$	$\parallel: 265$ $\perp: 36$ $i: 114$	24 24 40
			
8CB 4-cyano-4'-n-octylbiphenyl	$\parallel: -26 \times 10^{-11}$ $\perp: +3.7 \times 10^{-11}$	$\parallel: 246$ $\perp: 20$	22 24
			
d ₂₇ doped(<0.2%) 8CB	$\parallel: -152 \times 10^{-11}$ $\perp: +10.5 \times 10^{-11}$ $i: -48 \times 10^{-11}$	$\parallel: 380$ $\perp: 30$ $i: 193$	22 22 40
OPL-7-1 4-(1-octynyl)-4'-cyanobiphenyl	$\parallel: -27 \times 10^{-11}$ $\perp: +7.0 \times 10^{-11}$ $i: -5.5 \times 10^{-11}$	$\parallel: 112$ $\perp: 19$ $i: 33$	37 37 60
			
OPL-10-1 4-4'-dipentylazoxybenzene	$\parallel: -9.9 \times 10^{-11}$ $\perp: +4.5 \times 10^{-11}$ $i: -2.4 \times 10^{-11}$	$\parallel: 55$ $\perp: 3.7$ $i: 11$	40 40 80
			
OPL-10-2 4-4'-dihexylazoxybenzene	$\parallel: -15 \times 10^{-11}$ $\perp: +2.0 \times 10^{-11}$ $i: +5.0 \times 10^{-11}$	$\parallel: 38$ $\perp: 4.2$ $i: 21$	50 50 66
			

Table 1: Summary of measurements of nanosecond nonlinearities at 532 nm

Table I (continued)

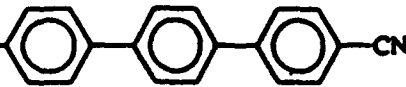
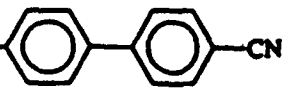
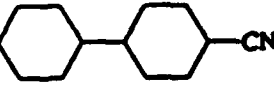
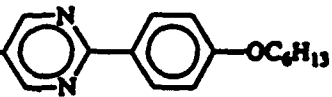
Material	$n_2(\text{esu})$	$\beta(\text{cm/GW})$	T(°C)
T15 4-cyano-4'-n-alkyl-p-terphenyl	$\parallel: -52 \times 10^{-11}$	$\parallel: 270$	180
H_{11}C_5 -  -CN	$\perp: +21 \times 10^{-11}$	$\perp: 18$	180
E7	$\parallel: -38 \times 10^{-11}$	$\parallel: 284$	24
	$\perp: +3.3 \times 10^{-11}$	$\perp: 40$	24
CB15	$i: +7.4 \times 10^{-11}$	$i: 38$	24
$\text{H}_3\text{C}_2\text{HCH}_2\text{C}$ -  -CN			
ZLI-1538 Cyclohexylcyclohexane	$\parallel: \sim 0$	$\parallel: \sim 0$	70
H_9C_4 -  -CN	$\perp: \sim 0$	$\perp: \sim 0$	70
	$i: \sim 0$	$i: \sim 0$	90
ZLI-2303 Phenylpyrimidine	$\parallel: -20 \times 10^{-11}$	$\parallel: 67$	45
H_{13}C_6 -  -OC ₆ H ₁₃	$\perp: +3.0 \times 10^{-11}$	$\perp: 8.2$	45
	$i: -3.8 \times 10^{-11}$	$i: 19$	85

Table 1: Continued. Measurements of nanosecond nonlinearities at 532 nm

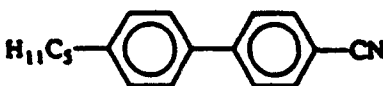
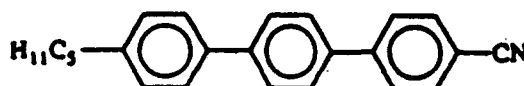
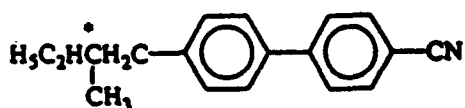
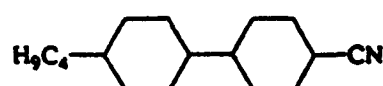
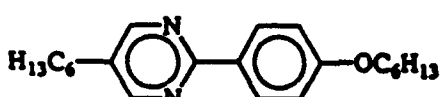
Material	$n_2(\text{esu})$	$\beta(\text{cm/GW})$	T(°C)
5CB 4-cyano-4'-n-pentylbiphenyl	$\parallel: -10 \times 10^{-4}$	$\parallel: 0$	24
	$\perp: +2.0 \times 10^{-4}$	$\perp: 0$	24
	$i: -2.0 \times 10^{-4}$	$i: 0$	40
T15 4-cyano-4'-n-alkyl-p-terphenyl	$\parallel: -0.68 \times 10^{-4}$	$\parallel: 0$	180
	$\perp: -0.092 \times 10^{-4}$	$\perp: 0$	180
CB15	$i: -0.25 \times 10^{-4}$	$i: 0$	22
			
ZLI - 1538 Cyclohexylcyclohexane	$\parallel: -0.43 \times 10^{-4}$	$\parallel: 0$	70
	$\perp: -0.13 \times 10^{-4}$	$\perp: 0$	70
	$i: -0.35 \times 10^{-4}$	$i: 0$	97
ZLI - 2303 Phenylpyrimidine	$\parallel: -0.97 \times 10^{-4}$	$\parallel: 0$	45
	$\perp: +0.082 \times 10^{-4}$	$\perp: 0$	45
	$i: -0.3 \times 10^{-4}$	$i: 0$	85

Table 2: Summary of measurements of nonlinearities at 514 nm, 10 ms pulse

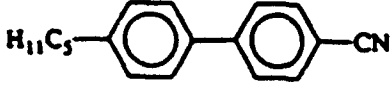
Material	n_2 (esu)	β (cm/GW)	T(°C)
5CB			
4-cyano-4'-n-pentylbiphenyl	\parallel : $+1.04 \times 10^{-11}$	\parallel : 2.26	24
	\perp : $+0.69 \times 10^{-11}$	\perp : 0.78	24

Table 3: Summary of measurements of picosecond nonlinearities at 532 nm

three benzene rings instead of two, and thus the reason why both nonlinear indices are negative is not clear. The observed nonlinearities seem to be relatively insensitive to structural changes other than the presence of benzene rings. For example, the addition of a chiral branched alkyl chain in CB15 does not change the nonlinear index in the isotropic phase appreciably.

5.1.2 Nanosecond Mechanisms

Next, we consider possible mechanisms responsible for the nonlinearities on the nanosecond time scale. Strong nonlinear refraction, nonlinear birefringence and nonlinear absorption is observed in these materials. By noting that the temperature dependence of the nonlinear indices on the nanosecond time scale is fundamentally different from that on the millisecond scale, we conclude that the dominant mechanism is not laser heating due to linear absorption. This is further substantiated by the observations that n_1 for CB15 and n_1 for T15 change sign as the pulse width is reduced from ms to ns.

Although many other mechanisms, such as direct optical field induced orientational effects, electrostrictive effects, electrostrictive effects combined with shear alignment, may contribute to the observed nonlinearities, order of magnitude calculations based on simple theoretical models indicate that they can not be the primary cause. The intensity dependent measurements on 5CB indicate that n_2 is independent of intensity, and therefore it is a third order process. Analysis of the measured peak and valley positions on the Z-scan

curves are consistent with this. Two-pulse measurements indicate that the mechanism is slow, that is, the response time can not be less than about 5ns. One possibility is that the nonlinear refraction originates from an excited state associated with the linear one-photon absorption. On the other hand, for 5CB, intensity dependence measurements show that the nonlinear absorption coefficient, β , is nearly proportional to the intensity. This is a signature of the 5th-order process; two pulse measurements furthermore show that the associated response time is less than about 5ns. It appears likely therefore, that at least in the case of 5CB, two different processes are operating simultaneously, a slow third-order process which contributes primarily to the nonlinear refraction, and a faster 5th-order process which contributes primarily to the nonlinear absorption.

The nonlinear behavior is linked to the presence of the benzene rings in the molecules. For example, for ZLI-1538 no observable nonlinearities (either nonlinear refraction or absorption) have been detected; this material does not have a benzene ring. Conversely, the addition of the anthraquinone dye d_{27} to 8CB significantly enhances the observed nonlinearity, without changing its character (i.e. signs of n_2 are unchanged from that of the pure material; both nonlinear refraction and nonlinear absorption increase).

Several other features of molecular structure of our selection of liquid crystals did not play an important role in determining the size of the nonlinearity. As can be seen in Table 1, the addition of the acetylene group (OPL-7-1) does not significantly contribute to the nonlinearity. Similarly, varying the linkage by adding small conjugated structures (azoxy group) also has little effect on the nanosecond response.

Our key findings on nanosecond time scale experiment are the following: the nonlinear refraction in a number of liquid crystals is anomalously large, the nonlinear refraction is accompanied by large nonlinear absorption, and the magnitude of the nonlinearity is closely linked to the number of benzene rings in the molecules, and appears insensitive to the presence of other conjugated units. Our results indicate that in 5CB a slow third-order process is responsible for the nonlinear refraction, while a faster fifth-order process is responsible for the nonlinear absorption.

5.1.3 Picosecond Mechanisms

If the measured β was due to three photon absorption, then picosecond measurements should show very large values of β , since the intensities are more than one order of magnitude higher. However, β measured with 33ps is smaller; values are given in Table 3. It is likely therefore that the response time of the absorption process is long compared to picoseconds (but short compared to 10ns) and this accounts for the decrease of β

seen in the picosecond measurements. Such a process could be excited state absorption from a two-photon excited state. Since the nonlinear refraction which dominates on the nanosecond time scale is slow, it will be attenuated by more than two orders of magnitude in the picosecond measurements. The picosecond n_2 values thus originate from another mechanism, such as nonresonant electronic hyperpolarizability. The result that both n_2 and β are very small at $\lambda = 1.06\mu m$ is not consistent with this model. The contribution of the excited state at this wavelength to the molecular polarizability could be much smaller than that at 532 nm, and the multiphoton absorption cross-section is certain to be very different.

5.1.4 Overall Mechanism Discussion

There are a variety of other possible origins to nonlinear response in liquid crystals in the nanosecond regime. We have considered above those most likely to be large and those which are clearly evident from the experimental measurements. Still, we are convinced that other nonlinearities are present and their understanding and quantification are necessary to actually predict theoretically the nonlinear behavior over a wide range of time scales, wavelengths and device geometries.

In particular, in the nanosecond regime, it is possible that electrostriction, short-axis reorientation, photostimulated conformational changes and complex intramolecular energy transfers play a role, but more study is needed to understand this behavior. It seems to be true that while the nanosecond OPL properties of several liquid crystals are large and operative over many wavelengths on the nanosecond regime, this cannot be attributed to a single third order nonlinear process and we do not understand the factors that make the materials work well.

Even in the millisecond regime where the mechanisms involving thermally induced disorder and optical field reorientation seem to be relatively clear, specifics for each molecule are however not quantified.

Only the picosecond regime seems to be simple to understand, but it remains difficult to predict for any given molecule. We feel secure that the picosecond nonlinearities are almost entirely electronic but, while we have a rule of thumb ability to predict, there remains an inability to predict accurately and there remains a number of molecules which have not been measured.

6 Damage Studies

In both the CW and nanosecond OPL studies, damage to the samples was observed at high intensity. Studies were undertaken to identify the damage thresholds and mechanisms.

6.1 CW Damage Studies

The damage threshold studies were motivated by the idea that there may be some focusing of the laser beam by the liquid crystal droplets causing a damage threshold in the PDLC to be lower than that inherent for either the polymer host or liquid crystal materials separately. Controlled experiments were thus performed on the three types of sample, each 10 μm thick, sandwiched between ITO coated glass plates.

The sample types were:

- Type I PDLC (Polymer with 33% liquid crystal by weight)
- Type II Pure Polymer (Epon plus Capcure in equal parts)
- Type III Pure liquid crystal (E7, commercial mixture)

The following thresholds were observed:

- Type I: $26 \pm 1 \text{ kW/cm}^2$ (10ms pulse, 95 μm beam diameter)
- Type I: $18 \pm 1 \text{ kW/cm}^2$ (20ms pulse, 95 μm beam diameter)
- Type II: $32 \pm 1 \text{ kW/cm}^2$ (10ms pulse, 95 μm beam diameter)
- Type III: $> 40 \text{ kW/cm}^2$ (10ms pulse, 95 μm beam diameter)

It is clear that the liquid crystal material is not the damaged material, but the fact that PDLC damages at a lower threshold than the polymer suggests that some mechanism such as focusing is operational. The reduction in threshold with the addition of the liquid crystal is a small effect, 20%, but the mechanism is not completely understood. The criterion applied to determine damage was discoloration (brown). Both PDLC and pure polymer samples showed the same type of damage.

Following an informal report on results of measurements by David Pepper at Hughes, we investigated the role played by the ITO coating. Similar samples (thickness $20\mu\text{m}$) of the three types were studied between uncoated glass. The results were:

- Type I: $> 41\text{kW}/\text{cm}^2$ (10ms pulse, $95\mu\text{m}$ beam diameter)
- Type II: $> 41\text{kW}/\text{cm}^2$ (10ms pulse, $95\mu\text{m}$ beam diameter)
- Type III: $> 41\text{kW}/\text{cm}^2$ (10ms pulse, $95\mu\text{m}$ beam diameter)

The 6% optical absorption by the ITO is apparently large enough to contribute the primary effect in damaging the polymer material. This absorption is essentially unnoticeable in normal electro-optic applications involving liquid crystals.

These experiments show that the ITO is the vehicle whereby damage is inflicted, but the difference between PDL threshold and polymer threshold remains unexplained, but is likely due to the difference in heat diffusion away from the surface.

6.2 Nanosecond Laser Damage

We have studied laser damage in homeotropically (parallel) aligned samples of 5CB. We found that the cells are damaged by nanosecond laser pulses at relatively low fluence ($\approx 1\text{ J}/\text{cm}^2$) due to self-defocusing of the beam by the liquid crystal sample. The damage is produced on the interior surface of the glass; there is no apparent damage to the liquid crystal. This effect may be utilized as a sacrificial optical fuse.

With the materials deliver for the ARDEO DVO test bed, we found that damage in these samples occurred at $40\mu\text{J}$ and was caused by the polyimide alignment layer.

We can not confirm our final evaluation of the damage mechanisms, but we have several thoughts. It appears that in the nanosecond regime, the damage condition is simply that the intensity at the interface of the sample cell must reach the damage threshold of the material of the surface. In the case when there is an alignment layer such as polyimide, the polyimide is damaged. If the interface is simply a liquid crystal/glass interface, then the glass is damaged. We have no independent determination of the damage threshold of polyimide, but for glass, it appears that the damage intensity is simply the usual damage level of a glass surface and has nothing to do with the liquid crystal. The only effect of the liquid crystal seems to be that the focal point or location of the beam waist is

modified as a function of intensity due to the presence of the liquid crystal. If the beam waist is defocused from the center of the sample to the surface, then the surface damage results sooner than it does in a thicker sample or a sample without liquid crystal. This can obviously be incorporated in the design of a device by adjusting the device geometry (thickness) and choosing high threshold materials for the sample holder.

7 Theory and Modeling

The modeling and theory effort under this project undertook to provide predictive support for materials selection and theoretical modeling to explain the mechanisms involved in the nonlinear response of liquid crystals materials. Three separate areas of activities were involved, electronic structure modeling, optical fields induced order modeling, and nonlinear optical propagation modeling.

7.1 Electronic Structure Modeling

While there is no set of rules which specify which molecules will actually exhibit liquid crystalline phases, there are strong chemical trends which are well known and extensively studied. Molecular polarizability is an essential quality of most liquid crystals. All but a few liquid crystalline molecules have an aromatic core usually composed of one or more benzene rings. In addition, it is well known that the liquid crystalline properties are strongly influenced by substituent groups attached to this core.

Molecular polarizability strongly correlates with electronic nonlinear optical properties of organics. That is why one should expect liquid crystals to exhibit strong nonlinear optical properties. Given the variety of liquid crystals, one should also expect a variety, and some of them large, nonlinear optical characteristics. These qualitative considerations are reasons to study nonlinear optical properties of liquid crystals, but they do not provide an explanation of those properties. Ultimately, as we have discovered, there are properties of the liquid crystal phases which affect the nonlinear properties and there are a number of mechanisms for optical nonlinearities that interact in a complex manner.

While molecular polarizability correlates with nonlinear properties, it is not the origin of the nonlinearity. It is the electronic *hyperpolarizability* that is the origin of molecular electronic nonlinearities. This requires a quantum mechanical theory of molecular electronic structure. As our first theoretical effort was to investigate electronic nonlinearities, we adapted a fairly direct method of electronic structure calculation to use to determine trends in and origins of electronic nonlinearities in liquid crystals. The theoretical approach was to isolate the electronic structure of the aromatic core of the liquid crystal molecule, since past experience has shown us that this molecular segment contribute dominantly to the linear and nonlinear molecular polarizability. We employed the Hückel and PPP models to describe the electronic structure of the core. This models includes only the so-called pi electrons, i.e. those involves in the conjugation of double and triple bonds in the molecule. Substituent groups and heteroatoms are treated as perturbation of the

basic Hamiltonian.

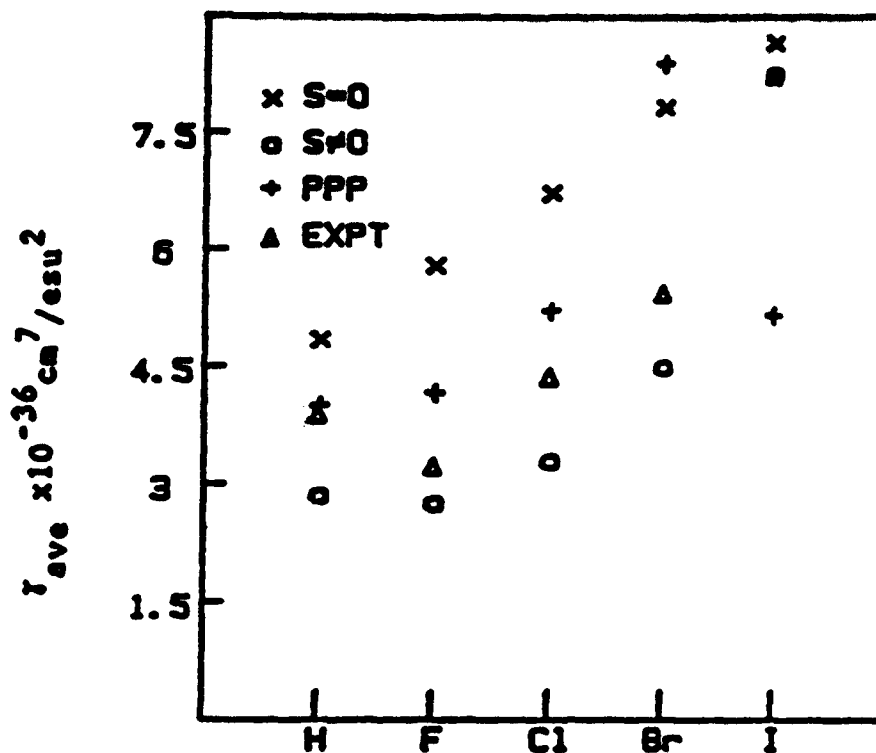
Additional background on the specifics of the quantum mechanical calculation for this portion of the theoretical effort can be found in the Quarterly Scientific and Technical Reports. Also in the Report are extensive listings of the many molecules calculated and discussions of trends found. Here, we will summarize a few aspects that were used in guiding materials selection and synthesis.

7.1.1 Small Molecule Comparisons

We will first discuss our efforts at verification of the electronic structure work. We did this by comparing the results of calculations of the two different Hamiltonians. The Hückel Hamiltonian is quite simple and amenable to calculation, even for large molecules. Its simplicity makes it suspect however. The PPP Hamiltonian is more complex and includes electron-electron interactions. It is computationally difficult because the cost of a calculation increases as the factorial of the number of electrons. We reasoned that if the complicated Hamiltonian predict the same trends in nonlinear properties as does the simple Hamiltonian, then we could rely on the predictions of the Hückel Hamiltonian in developing materials selection criteria.

The largest molecules where we could use both Hamiltonians were substituted benzene molecules and straight chain alkenes. Fig. 26 shows the results of a series of calculations of the molecular hyperpolarizability of substituted benzenes. Included are both sets of theoretical results and the experimental results taken from the literature.

The agreement in Fig. 26 is quite gratifying. Not only do the two theoretical predictions have the same trend as each other and the experimental results, the quantitative agreement is reasonably good among all three. The extend to which there is disagreement can be understood semiquantitatively in terms of the hyperpolarizability of the S electrons and sigma bonds that are not included in the theories. Such a discussion has been published[20], but since we are interested in trends and large changes in hyperpolarizability, we will not include that discussion here. These considerations were discussed extensively in the Quarterly Scientific and Technical Reports.



Halogen substitution

Figure 26: Hyperpolarizability of substituted benzenes

7.1.2 Large Molecule Calculations

We calculated the linear (first order) polarizabilities and the second and third order electronic hyperpolarizabilities for a number of liquid crystal molecules. Calculations were performed for a good many small molecules as well, as part of the verification process.

Fig. 27 shows the chemical structure of the aromatic cores for a number of liquid crystal molecules that we considered. We provide this as a guide for the tables which follow.


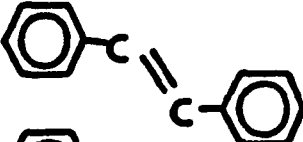
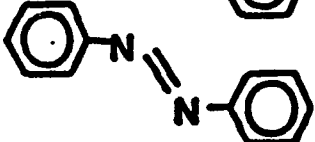

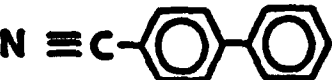

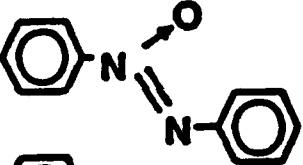
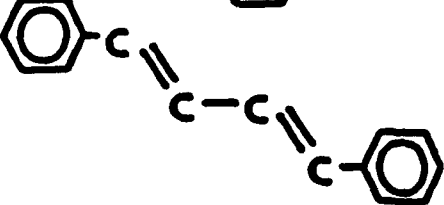
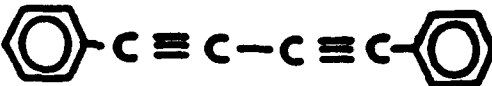
- | | | |
|----|---|----------------------------|
| 1. |  | biphenyl |
| 2. |  | stilbene |
| 3. |  | azobenzene |
| 4. |  | diphenylacetylene |
| 5. |  | cyanobiphenyl |
| 6. |  | terphenyl |
| 7. |  | azoxybenzene |
| 8. |  | 1,4 diphenyl-1,3 butadiene |
| 9. |  | 1,4 diphenyl-1,3 butadiyne |

Figure 27: Structure and names of molecules used in tables

Molecule	α_{xx}	α_{yy}	α_{ave}
biphenyl	3.5098	2.3707	1.9601
stilbene	5.6223	2.9519	2.8581
azobenzene	5.5200	2.9767	2.8322
diphenylacetylene	7.2849	2.3804	3.2220
cyanobiphenyl	8.8123	2.3609	3.7245
terphenyl	6.3734	3.5560	3.3097
azoxybenzene	6.5519	3.9954	3.5160
diphenyl-butadiene	8.5798	4.3319	4.2672
diphenyl-butadiyne	12.985	2.3812	5.1221

Table 4: Molecular linear polarisabilities

As indicated in the introductory discussion, linear polarisability is expected to follow nonlinear properties for several reasons. The nonlinear properties in the picosecond regime are expected to be electronic and largely caused by the hyperpolarisability of the aromatic core. As we will see, the size of the core is a major factor in both the linear and hyper polarisabilities, hence the correlations. We refer here to *nonresonant* nonlinearities. The presence of fortuitously located excited states can cause enormous nonlinearities over a very narrow wavelength range. Our charge was to seek materials suitable for "frequency agile" lasers, thus resonant phenomena were not emphasised. The polarisabilities reported here are static, hence we believe more appropriate for predicting trends in materials over a wide wavelength regime.

Table 4 shows the linear polarisabilities calculated for the molecules under discussion. It is followed by Table 5 showing the third order hyperpolarisabilities calculated.

The table on molecular linear polarisabilities gives the values of the nonzero components of the molecular polarisability tensor α . These values are due only to the conjugated (aromatic) portion of the molecule. The long-axis polarisabilities track with the nematic polarization in the direction of the molecules and the short axis polarisability tracks with the perpendicular direction in the molecule. We will ignore mixing of long axis polarisation with short axis polarisation in the nematic phase caused by thermal averaging, but in the isotropic phase this averaging is complete and it is the average that tracks with the


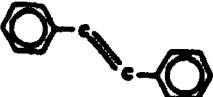

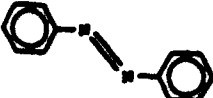


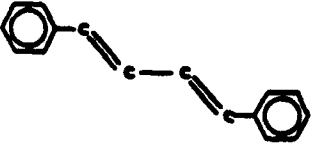
	γ_{max}	γ_{ave}
	0.72	0.14
	2.39	0.47
	6.91	1.32
	2.51	0.50
	4.33	0.83
	3.12	0.62
	6.90	1.45

Table 5: Molecular hyperpolarisabilities

isotropic phase polarisability (i.e. index of refraction).

The Table on molecular hyperpolarisabilities gives the values of the nonzero components of the molecular hyperpolarisability tensor γ . The hyperpolarisability is a more complex entity than the linear polarisability since it is a rank four tensor (rather than rank two). These values are also due only to the conjugated (aromatic) portion of the molecule. The long-axis hyperpolarisabilities track with the nematic hyperpolarisation in the direction of the molecules and the short axis hyperpolarisability tracks with the perpendicular direction in the molecule. We will ignore mixing of long axis hyperpolarisation with short axis polarisation in the nematic phase caused by thermal averaging, but in the isotropic phase this averaging is again needed but is more complex than the linear case. The entry for the average has been calculated and it tracks with the isotropic phase hyperpolarisability (i.e. nonlinear index of refraction).

7.1.3 Discussion of Electronic Nonlinearities

One can see the origin of our selection rules in the tabulated results. The experiments in the millisecond regime (CW) will be most influenced by the linear polarisability. This is because the induced dipole is directly proportional to the optical torque, and that portion of the dipole which is effective in optical reorientation is directly proportional to

the anisotropy of the linear polarizability tensor, $\Delta\alpha$. The net effective nonlinear index resulting from optical reorientation should then track with the anisotropy.

Simply by looking at the molecules, it can be seen that the anisotropy in polarizability tracks with the anisotropy in the shape of the molecular core. This rule of thumb is easily implemented as a synthesis guide. This particular rule has advantages and disadvantages. On the positive side, the tendency of a molecule to form a liquid crystal is well known to increase as the anisotropy in the core increases. On the negative side, there is also generally an increase in the temperature at which the nematic forms, sometime getting well above room temperature, and there is an increase in viscosity making it less liquid and more difficult to reorient.

Fortunately, much of the above discussion applies to the general trends observed for hyperpolarizability. Indeed, hyperpolarizability increased even more rapidly than linear polarizability when compared to the the geometric anisotropy of the aromatic core. The more complex nature of the hyperpolarizability make such rules of thumb less clearly applicable. In particular, the off diagonal elements of the hyperpolarizability are often large and of opposite sign to the long axis hyperpolarizability. The assumption of ignoring thermal averaging in the nematic phase is thus compromising. While it is not difficult to carry out thermal averaging (and we have done this), it is not reliable because the absolute magnitudes of the components of the hyperpolarizability tensors are not reliable. As we stated in the beginning, we are seeking *trends* from the Hückel model, not absolute prediction, when we use it for large molecules. In particular, we believe that the Hückel model significantly over estimates γ_{zzzz} and it enters in a crucial way in the averaging scheme.

Rather than use the averages that we can extract from the hyperpolarizability tensors, we adopted a more qualitative approach. One can see, for example, that the addition of double bonds between benzene rings increases some hyperpolarizability components. It does not however increase the dominant component as much as the addition of another benzene ring. This, simply looking at the shape of the molecule is not nearly as adequate in predicting hyperpolarizability as looking at the actual calculations. These ideas were to be testing experimentally, and that was part of the reason for choosing to synthesize some materials with double bonds connecting or appended to benzene ring systems.

These calculations told us that by varying structure of the core and varying linkages between cores and by varying substituent groups, we could expect to see variations in the nonlinear properties of the liquid crystals. While our discussion here is not complete, and it was supplemented with heuristic expectations of molecular origins of nonlinear response, it did help us to choose to select materials for evaluation. We extract here a portion of the discussion on Appendix A where we state the essential elements of our

selection rules.

- Varying sizes of conjugated cores
- Varying linkages between benzene rings
- Varying substituent groups
- Ease of synthesis or even possible commercial availability.
- Simple and small conjugation structures to facilitate theoretical calculations

In Sec. 8.2 we list the molecules chosen for study. Many of these were synthesized in house. To obtain a representative sample covering a reasonable portion of the above list we had to synthesize some even though they represented simpler structures than some commercially available compounds. In the end, we had more compounds than we had time to measure and we had identified dozens more (Appendix A) that were not acquired. The extension of a survey involving these compounds would be desirable.

Of the compounds selected for study, one can see the application of the above rules and the theoretical calculations. For instance, the addition of a double bond between two benzene rings had a much smaller predicted effect than the addition of a cyano group on the end. Indeed, before we ever measure the nonlinear response of 5CB, our calculations (See Table 5) predicted the the core of 5CB would have the largest hyperpolarisability. Only with the addition of three intermediate carbons (and two double bonds) does the molecular anisotropy increase enough to yield a predicted nematic hyperpolarisability as large as that of 5CB.

We do not want to make too much out of this agreement between the measure nonlinear response and the theoretical predictions of hyperpolarizability. There are, as we have repeated stated, other nonlinear mechanisms involved. Still, we found these calculations useful in determining the compounds we would synthesize and purchase.

Finally, we emphasize that we have discussed here molecular properties. Modeling these systems on the macroscopic scale was a valuable additional activity to determine how the various nonlinear mechanisms would manifest themselves experimentally. Secs. 7.2 and 7.3 describe our theoretical efforts in those areas.

7.2 Modeling Molecular Orientational Relaxation and the Thermal Nonlinear Refraction of Nematic Liquid Crystals

Laser heating is known to make an important contribution to the nonlinear refraction of liquid crystals due to the large rate of change of the refractive index with temperature, dn/dT . There is a strong enhancement of dn/dT near the nematic-isotropic phase transition which is associated with the rapid variation of the nematic order parameter, S , with temperature. This has been seen to lead to a strong enhancement of the nonlinear refraction. However, if the nonlinear refraction is probed with laser pulses on the nanosecond time scale, incomplete relaxation of the order parameter during the pulse results in a reduction of the observed nonlinear refraction. The time scale for relaxation of the order parameter also shows a large peak near the phase transition temperature, so that for short laser pulses, the temperature dependence of the effective nonlinear refractive index, n_2 , will be strongly influenced by the relaxation dynamics of the order parameter. We have developed a simple model for the time evolution of the orientational order of a nematic liquid crystal subjected to heating by a gaussian laser pulse. By treating the orientational degrees of freedom with a phenomenological Landau-de Gennes theory, and assuming that the other degrees of freedom equilibrate quickly compared to the pulse duration, it is possible to solve for the time dependence of the order parameter, and thus the indices of refraction. By defining an intensity weighted average of the change in index of refraction, an effective nonlinear refractive index can be extracted, such as would be measured in an experiment of the z-scan type. Using parameters which have been measured for the material 5CB, it is found that the slow relaxation completely cancels the enhancement of dn/dT near the phase transition, resulting in an effective n_2 which is nearly independent of temperature, for pulse durations less than a few tens of nanoseconds.

7.2.1 Time Scale of Thermal Nonlinearities

The nonlinear optical response of liquid crystals has been the subject of much investigation recently.[2]-[9] In particular, as part of our effort, we have undertaken to measure the nonlinear optical properties of various liquid crystalline materials, under a variety of temperatures, optical pulse durations, and optical field intensities as described in Secs. 3, 4 and 5 and published works[4, 5]. These experiments made use of the z-scan technique [10, 11] which relies on the self-refraction of a single pulse. The results of the measurements allow the samples to be characterized by a nonlinear refractive index, n_2 , where the intensity dependent index of refraction is

$$n(E^2) = n + \frac{1}{2}n_2E^2 \quad (1)$$

and a nonlinear absorption coefficient, β , where the intensity dependent absorption is given by

$$\alpha(I) = \alpha + \beta I \quad (2)$$

One of the simplest mechanisms which can contribute to the nonlinear refraction is a thermal mechanism, wherein linear absorption of energy from the optical field leads to heating of the sample, thereby changing its index of refraction. This mechanism is expected to lead to large effects in liquid crystals due to the rapid variation of the index of refraction with the temperature in these materials. This is especially true near the nematic-isotropic phase transition, where the variation of n with T is most rapid. This effect has been found to contribute significantly to a number of measurements; more detailed references and brief reviews are published [2, 3].

An estimate of the effective value of n_2 due to the thermal effect, as measured with a pulsed laser, can easily be obtained. For a sample with a linear absorption coefficient α , and heat capacity per unit volume C , in a laser pulse of peak intensity I_0 and duration τ , the change in temperature is $\Delta T \approx \alpha I_0 \tau / C$. The effective value of n_2 is approximately

$$\begin{aligned} n_2^{eff} &\approx \Delta n / E_0^2 \\ &\approx \frac{dn}{dT} \Delta T c n / I_0 \\ &= \frac{dn}{dT} \frac{\alpha \tau c n}{C} \end{aligned} \quad (3)$$

where c is the speed of light and n is the linear index of refraction. All factors of order unity have been dropped for the purposes of this order of magnitude estimate. Eq. 3 ignores the diffusion of heat. In the experiments under consideration, the laser pulse duration is much shorter than the time scale for diffusion of heat across the beam, so that diffusion of heat will be neglected in all the follows. Note that the result of Eq. 3 depends explicitly on the pulse duration, τ , as well as on material properties. This is the reason for referring to the "effective" n_2 .

It was concluded in Sec. 3.3.1 and also published by Palffy [2, 4], that the observed nonlinear refraction for pulses of several millisecond duration was due to the thermal mechanism. This conclusion was based on comparison of the measurements with order of magnitude estimates from Eq. 3 and, most important, the fact that the measured n_2 has a pronounced dependence on the temperature as the nematic-isotropic transition is approached from below. This strong temperature dependence is expected, since dn/dT is strongly temperature dependent for liquid crystals near the transition temperature. On the other hand, it was found[5] that for pulses of 7 ns duration, the observed n_2 was essentially independent of temperature, right up to the transition. This was taken as an indication that the dominant effect on that time scale did not have a thermal origin.

It should be pointed out, however, that Eq. 3 is only appropriate if the heating is quasi-static, that is if the temperature changes slowly enough that the instantaneous change in index of refraction is related to the instantaneous change in temperature by the equilibrium coefficient, $\frac{dn}{dT}$. This will only be the case if the relaxation process which governs the change in index of refraction takes place on a time scale which is short compared to the pulse duration. If slow relaxation prevents the index of refraction from keeping pace with the instantaneous temperature during the optical pulse, then the observed n_2 will be reduced from the quasi-static prediction. For nematic liquid crystals, the variation of the index of refraction with temperature is primarily due to the change of the orientational order parameter, S , which is a measure of the degree of alignment of the long molecular axes, and is proportional to the dielectric anisotropy. It is the rapid variation of the order parameter with temperature near the transition which gives rise to the large value of dn/dT . In a sample subjected to rapid heating by a laser pulse, the order parameter may not maintain equilibrium with the instantaneous temperature as defined, for example, by the mean kinetic energy of the molecular centers of mass. In such a case, the observed nonlinear refraction will be reduced, to the extent that the order parameter, and thus the index of refraction, is unable to equilibrate during the pulse.

The free relaxation of the orientational order parameter has been observed directly [6, 21, 9] in the isotropic phase, and has been found to show a substantial pre-translational slowing down as the transition is approached from above. This is in accordance with a theory due to de Gennes.[12] The time scales involved are found to be on the order of hundreds of nanoseconds for temperatures close to the transition. On the basis of the theory of de Gennes [12], it is expected that a similar phenomenon will occur in the nematic phase, with a similar slowing down as the transition is approached from below. Thus, near the nematic-isotropic transition, the effective value of n_2 measured in the nanosecond regime will be determined by a competition between a large coefficient, dn/dT , and slow relaxation of the orientational order, leading to a long rise time for the thermal nonlinear refraction. In fact, this effect has already been seen experimentally by Armitage and Delwart,[8] who found that the rise time for a thermal diffraction grating showed a large increase as the nematic-isotropic transition was approached from below. They also attributed the effect to slow relaxation of S . Therefore, in order to predict the effective value of n_2 which will be observed with laser pulses in the nanosecond regime, and especially to account for the temperature dependence of n_2 near the phase transition, it will be necessary to include the appropriate relaxation dynamics in the description.

Here we will show our results which illustrate how the relaxation dynamics of the orientational order can be accounted for in describing the thermal nonlinear refraction of a nematic liquid crystal. In particular, emphasis is placed on the role of slowing down of the orientational relaxation near the nematic-isotropic transition in determining the observed nonlinear response.

In Sec. 7.2.2, some aspects of the theory of de Gennes [12] which underlie the subsequent treatment of both equilibrium and relaxation phenomena in nematic liquid crystals are reviewed. In Sec. 7.2.3 a simple model for the response of the orientational order of a liquid crystal subject to heating by an optical pulse with a Gaussian temporal profile is presented. This model is based on treating the non-orientational degrees of freedom as constituting a "bath" which is assumed to equilibrate quickly to a well-defined temperature. Energy taken up by the system from the optical pulse can exchange between the bath and the orientational degrees of freedom. The orientational order is taken to relax exponentially toward the equilibrium value associated with the instantaneous temperature of the bath. In this way, it is possible to obtain a closed system of equations for the time development of the order parameter and the bath temperature. By defining a suitable intensity weighted average of the change in index of refraction, one can obtain an effective n_2 which is appropriate for the types of measurements described in Secs. 3.3.1 and 4.2 by Palffy [4, 5]. This is illustrated numerically using parameters for the material 5CB. It is found that the effective n_2 is strongly peaked just below the transition temperature for pulse durations greater than $\sim 0.5\mu\text{s}$. However, for pulse durations in the nanosecond regime, slowing down of the orientational relaxation near the transition results in n_2 being nearly independent of temperature. Thus, the experimental observation[5] that the nonlinear refraction of 5CB, as measured with 7 ns pulses is independent of temperature is not inconsistent with the nonlinearity being thermal in origin.

7.2.2 Thermal Properties of Nematic Liquid Crystals

According to the theory due to de Gennes[12], the nematic phase is characterized by a symmetric, traceless tensor order parameter, Q_{ij} which is proportional to the anisotropic part of the dielectric tensor, ϵ_{ij} . In the cases of interest to us, the nematic order parameter tensor is found to be uniaxial in equilibrium, in which case, Q can be put in the form,

$$Q = \begin{pmatrix} -S/2 & 0 & 0 \\ 0 & -S/2 & 0 \\ 0 & 0 & S \end{pmatrix} \quad (4)$$

where S is the scalar order parameter. The temperature variation of S can be obtained from the free energy density,

$$\mathcal{F}(S, T) = \frac{1}{2}A(T)S^2 - \frac{1}{3}BS^3 + \frac{1}{4}CS^4 \quad (5)$$

by applying the condition

$$\frac{\partial \mathcal{F}}{\partial S} = 0. \quad (6)$$

where the temperature dependence of the coefficient, A , is given by

$$A(T) = a(T - T^*) \quad (7)$$

The free energy, \mathcal{F} , is that part of the total free energy which is singular at the nematic isotropic transition. \mathcal{F} is associated with the orientational degrees of freedom of the long molecular axes, and in the subsequent development it is assumed that the other degrees of freedom can be treated as having a constant specific heat over the temperature range of interest. The truncation of Eq. 5 at 4th order is somewhat arbitrary, but it has become conventional. This level of truncation provides a minimal description of the qualitative features of the nematic-isotropic transition. Applying the condition of Eq. 6 to Eq. reffreee gives rise to two solution branches which satisfy the local stability condition,

$$\frac{\partial^2 \mathcal{F}}{\partial S^2} > 0. \quad (8)$$

For $T > T^*$, there is an isotropic branch with $S = 0$. A nematic branch exists for $T < T^\dagger$, where

$$T^\dagger = T^* + \frac{1}{4} \frac{B^2}{aC} \quad (9)$$

with an order parameter given by,

$$S(T) = S^\dagger + \left(\frac{a}{C} (T^\dagger - T) \right)^{1/2} \quad (10)$$

where

$$S^\dagger = \frac{B}{2C}. \quad (11)$$

The actual nematic-isotropic phase transition occurs at a temperature, T_c between T^* and T^\dagger given by,

$$T_c = T^* + \frac{2}{9} \frac{B^2}{aC} \quad (12)$$

which is the temperature at which \mathcal{F} goes to zero for the nematic branch.

In addition to the order parameter, another quantity which can be obtained from \mathcal{F} , which will be needed later, is the part of the specific heat associated with the orientational degrees of freedom,

$$\begin{aligned} C_o &= -T \frac{d^2 \mathcal{F}}{dT^2} \\ &= \frac{aTS}{2} \left[\frac{C}{a} (T^\dagger - T) \right]^{1/2} \end{aligned} \quad (13)$$

where the total derivative notation has been used to indicate differentiation including the dependence of S on T .

The uniaxial order of the nematic phase gives rise to a uniaxial dielectric tensor with two eigenvalues, one for fields polarized parallel to the director and one for fields polarized perpendicular to the director, which can be written

$$\begin{aligned}\epsilon_{||} &= \epsilon_1 + \epsilon_2 S \\ \epsilon_{\perp} &= \epsilon_1 - \frac{1}{2}\epsilon_2 S\end{aligned}\quad (14)$$

These give rise to extraordinary and ordinary indices of refraction,

$$\begin{aligned}n_e &= \sqrt{\epsilon_{||}} \\ n_o &= \sqrt{\epsilon_{\perp}}\end{aligned}\quad (15)$$

In all the numerical calculations that follow, the following set of parameters, which have been obtained for 5CB,[9] are used.

$$\begin{aligned}a &= 0.13 \times 10^6 J/K m^3 \\ B &= 1.6 \times 10^6 J/m^3 \\ C &= 3.9 \times 10^6 J/m^3 \\ T^* &= 34^\circ C\end{aligned}\quad (16)$$

Using this set of parameters in Eqs. 10 and 14, and by determining the values of ϵ_1 and ϵ_2 at the reference point,[13]

$$\begin{aligned}T &= 34.9^\circ C \\ n_e &= 1.632 \\ n_o &= 1.532\end{aligned}\quad (17)$$

the temperature dependence of the indices of refraction shown in Fig. 28 is obtained. In these plots, it has been assumed that the only temperature dependence of $\epsilon_{||}$ and ϵ_{\perp} comes through the dependence of S on T . Actually, ϵ_1 ϵ_2 will also depend on the temperature through their dependence on the molecular density. However, the most important part of the temperature dependence of the indices of refraction, particularly near the phase transition is due to changes of S with T . Since the focus of this work is mainly on the behavior near the phase transition, and on the dynamics of the orientational order, the density will be treated as being constant throughout.

Before proceeding, some comment regarding the accuracy of the numerical results is in order. It was remarked earlier that the truncation of the free energy expansion, Eq. 5, at fourth order in S is somewhat arbitrary. This truncation has the result that the calculated behavior of S is not in very good agreement with direct observations[14] for temperatures more than a few degrees below the phase transition. The indices of refraction have a

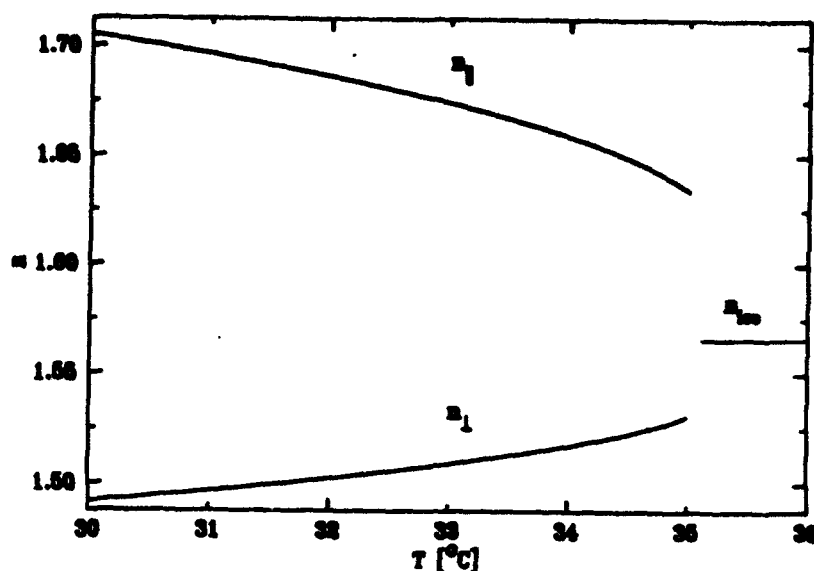


Figure 28: Predicted temperature dependence of indices of refraction

corresponding departure from measurements.[13] The value of S calculated from Eq. 10 does not saturate properly in the nematic phase, and so the resulting indices of refraction are changing more rapidly at low temperatures than the experimentally measured ones. It should be possible to correct this by using a higher order expansion for Eq. 5, but since there are not any widely agreed upon parameters for a higher order expansion, it seems preferable to live with the limitations of the fourth order expansion. The main focus here is on the behavior near the nematic-isotropic transition where Eq. 5 should be adequate, but it should be borne in mind that the numerical results are not quantitatively accurate more than a few degrees into the nematic phase. It is expected that in general, the qualitative conclusions will be valid.

Fig. 28 shows that the indices of refraction have a strong temperature dependence close to the nematic-isotropic transition. According to Eq. 3, this is expected to lead to a large effective n_2 . It has been argued that this can be counteracted for short pulse durations, by slow relaxation of the orientational order close to the transition. Following DeGennes[12], the free relaxation of the order parameter is governed by

$$\nu \dot{S} = -\frac{\partial \mathcal{F}}{\partial S} \quad (18)$$

where ν is a viscosity coefficient, which can be related to the Leslie coefficient γ_1 . [15] If Eq.

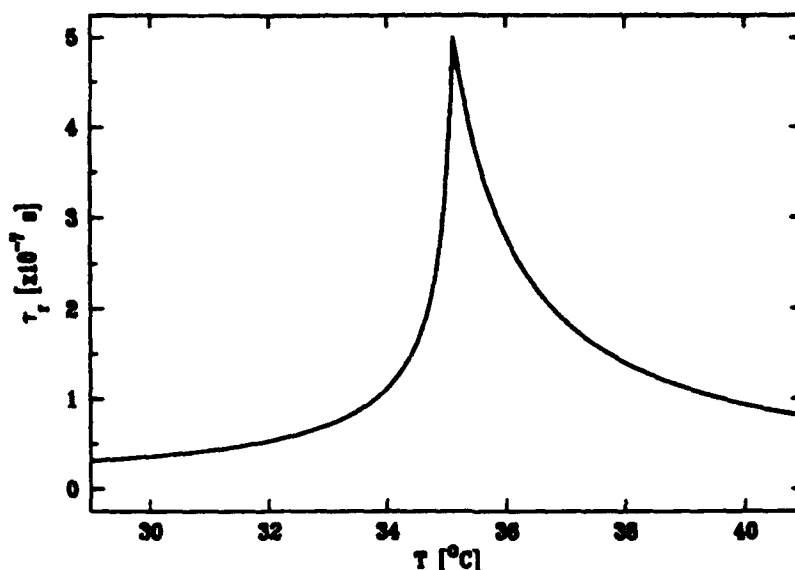


Figure 29: Predicted behavior of relaxation time with temperature

18 is linearized about the equilibrium state, assuming a fixed temperature, one obtains

$$\nu \dot{S} = -\frac{\partial^2 \mathcal{F}}{\partial S^2} (S - S_0) \quad (19)$$

where S_0 is the equilibrium value of S at the given temperature. This leads to exponential relaxation of the order parameter to the equilibrium value, with a time constant

$$\tau_r = \nu / \frac{\partial^2 \mathcal{F}}{\partial S^2} \quad (20)$$

which will be referred to as the isothermal relaxation time. This exponential relaxation behavior has been observed directly in the isotropic phase using the optical Kerr effect.[6, 21, 9] In the experiments, a strong optical pulse induces alignment of the molecules in an isotropic fluid. The subsequent decay of the orientational order is monitored by observing the induced birefringence with a weak probe beam. It is expected that the same description will hold in the nematic phase, although it will be more difficult to observe directly. Taking the value of ν from Coles[9], and using the free energy expansion given above, one obtains the behavior shown in Fig. 29 for the temperature dependence of τ_r . In the isotropic phase, τ_r is simply $\nu/a(T - T^*)$, as has been observed in experiments. In the nematic phase, the temperature dependence of τ_r is more complicated, but τ_r tends to diverge as $(T^* - T)^{1/2}$ on approaching the transition from below. The large value of τ_r near the nematic-isotropic transition is associated with the fact that the

transition temperature is very close to the critical temperatures, T^* and T' . It has been assumed here that ν is independent of temperature. There is some evidence that ν has some temperature dependence,[6] however this should be a weak correction to the rapid variation of τ_r near the phase transition.

7.2.3 Orientational Relaxation

In treating the time dependence of the orientational order, and hence the refractive indices, of a liquid crystal sample subjected to heating by an optical pulse, the simplification is adopted that all the non-orientational (vibrational, translational, etc.) degrees of freedom constitute a "bath" which equilibrates quickly to a well-defined temperature, T . This seems to be a reasonable assumption, since the time scales of interest here, tens to hundreds of nanoseconds, are long compared to the typical time scales for relaxation processes in liquids. This bath is assumed to be characterized by a specific heat, C_b , so that the balance of energy is given by,

$$\frac{du_o}{dS}\dot{S} + C_b\dot{T} = \alpha I \quad (21)$$

where α is the linear absorption coefficient and I is the intensity of the optical pulse. u_o is the internal energy of the orientational degrees of freedom. In addition, the orientational order is assumed to relax toward the equilibrium value associated with the instantaneous temperature, according to Eq. 18. It is assumed that the system is initially in an equilibrium state, characterized by $\partial\mathcal{F}/\partial S = 0$. By linearising with respect to the quantities ΔT and ΔS , which are assumed to be small, then Eq. 18 becomes,

$$\nu\dot{S} = -\frac{\partial^2\mathcal{F}}{\partial S^2} \left(\Delta S - \frac{dS}{dT}\Delta T \right) \quad (22)$$

where all coefficients, such as $\partial^2\mathcal{F}/\partial S^2$ should be understood as being evaluated at the initial state.

The first order system, Eqs. 21 and 22, can be solved straightforwardly, giving

$$\Delta S(t) = \frac{dS}{dT} \frac{\alpha}{C_b} \frac{1}{\tau_r} \int_{-\infty}^t dt' e^{-(t-t')/\tau_r} F(t') \quad (23)$$

where F is the fluence, the time integral of the intensity,

$$F(t') = \int_{-\infty}^{t'} dt'' I(t'') \quad (24)$$

and the time constant, τ' is related to the isothermal relaxation time, τ_r , by

$$\tau' = \tau_r \frac{C_b}{C_b + C_o} = \tau_r \frac{C_b}{C_t}. \quad (25)$$

Here C_t is the total specific heat, which is the sum of the part associated with the orientational degrees of freedom, which is calculated according to Eq. 13, and the part, C_b , associated with the other degrees of freedom, which is assumed to be temperature independent. The value used for C_b is 1.78×10^6 J/K m³, which is extracted from the data of Iannacchione and Finotello[16], as the value of the specific heat a few degrees above the transition where it is nearly constant, and by assuming a density of 1.0 gm/cm³.

In experiments with pulsed lasers, the optical intensity typically has a Gaussian temporal profile,

$$I(t) = I_0 e^{-(t/\tau)^2} \quad (26)$$

and this is assumed to be the case henceforth. With this assumption, the fluence is,

$$F(t) = \tau I_0 \frac{\sqrt{\pi}}{2} (1 + \text{erf}(t/\tau)). \quad (27)$$

If one defines

$$\Delta S_0 = \sqrt{\pi} \frac{dS}{dT} \frac{\alpha I_0 \tau}{C_t} \quad (28)$$

then the solution for ΔS can be written in the dimensionless form,

$$\Delta S(t) = \Delta S_0 g(t/\tau; \xi) \quad (29)$$

where $\xi = \tau'/\tau$ is the ratio of the time constant to the pulse duration, and the function g is defined to be

$$g(z; \xi) = \frac{1}{2\xi} \int_{-\infty}^z dx_1 e^{-(z-x_1)/\xi} (1 + \text{erf}(x_1)). \quad (30)$$

It is straightforward to verify that as $z \rightarrow \infty$,

$$g(z, \xi) \rightarrow 1 \quad (31)$$

so that as $t \rightarrow \infty$, $\Delta S(t) \rightarrow \Delta S_0$, independent of the value of the time constant. It is also easy to show that for $\xi \ll 1$, that is for small values of the time constant,

$$g(z, \xi) \rightarrow \frac{1}{2} (1 + \text{erf}(z)) \quad (32)$$

so that in this case $\Delta S(t)$ is simply proportional to $F(t)$, reproducing the quasi-static limit. Using Eq. 21 the time dependence of the temperature can also be expressed as

$$\frac{\Delta T(t)}{\Delta T_0} = \frac{1}{\tau} \left(\frac{F(t)}{F_0} - (1 - \tau) \frac{\Delta S(t)}{\Delta S_0} \right) \quad (33)$$

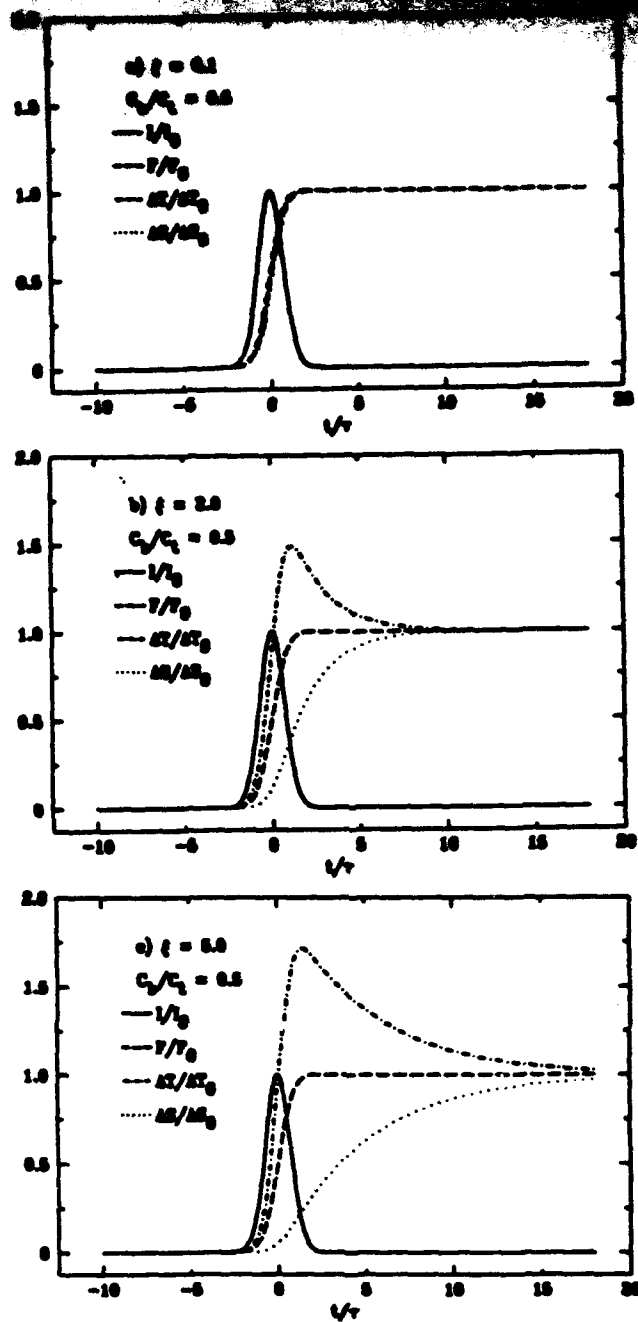


Figure 30: Time Dependence of order parameter and temperature.

where $\tau = C_b/C_i$ and

$$\begin{aligned} F_0 &= \sqrt{\pi} \alpha I_0 \tau \\ \Delta T_0 &= \sqrt{\pi} \frac{\alpha I_0 \tau}{C_i}. \end{aligned} \quad (34)$$

Eqs. 26, 27, 29 and 33 are illustrated numerically, for various values of ξ in Fig. 30. The value of $\tau = C_b/C_i$ is needed to define the temperature. The value $\tau = 0.5$ is a typical value, and is used in all the plots of Fig. 30 for illustrative purposes. In the plots, the fluence, temperature and order parameter are all normalised so that they approach 1 as

$t \rightarrow \infty$. In Fig. 30a, the value of $\xi = \tau'/\tau$ is 0.1, so that the time constant is shorter than the pulse duration. In this case both the temperature and the order parameter follow the fluence very closely, and the system is nearly in equilibrium at all times. Fig. 30b shows the case $\xi = 2.0$ so that the time constant is twice as long as the pulse duration. In this case there is a very noticeable departure from equilibrium. The order parameter is not able to keep pace with the fluence, and this means that the bath initially takes up more of the energy than would be the case in equilibrium, resulting in the bath overshooting its final temperature. The change in order parameter, and hence the refractive index, during the pulse is substantially reduced from the equilibrium response. The order parameter does not equilibrate until after the pulse has passed. Fig. 30c shows the case $\xi = 5.0$. This is qualitatively similar to Fig. 30b but there is an even greater overshoot of the bath temperature and further suppression of the change in S during the pulse.

In an experiment, such as those described in Sec. 4, in which the self-refraction of a pulse is used to probe the nonlinear refraction, only the change of n which occurs during the pulse will effectively contribute to the measurement. Since in the z -scan measurements the signal is proportional to Δn , and the weight with which it is detected is proportional to I , it is reasonable to define the intensity averaged quantities

$$\begin{aligned}\overline{\Delta S} &= \frac{\int dt I(t) \Delta S(t)}{\int dt I(t)} \\ &= \frac{1}{\sqrt{\pi}\tau} \int dt e^{-(t/\tau)^2} \Delta S(t)\end{aligned}\quad (35)$$

and

$$\overline{\Delta n} = \frac{dn}{dS} \overline{\Delta S}. \quad (36)$$

Using Eq. 29, $\overline{\Delta S}$ can be put in the form

$$\overline{\Delta S} = \Delta S_0 h(\xi) \quad (37)$$

where the function h is defined as

$$h(\xi) = \frac{1}{\sqrt{\pi}} \int_{-\infty}^{\infty} dz g(z; \xi) e^{-z^2} \quad (38)$$

By comparing the intensity averaged change in index of refraction with that obtained from an instantaneous nonlinear refraction, it is possible to define an effective n_2 . For an instantaneous nonlinearity, for which

$$\Delta n(t) = \frac{1}{2} n_2 E^2(t) \quad (39)$$

the intensity averaged change in index of refraction is

$$\overline{\Delta n} = \frac{2\pi I_0}{\sqrt{2}cn} n_2 \quad (40)$$

a^a	$0.13 \times 10^6 \text{ J/K m}^3$
B	$1.6 \times 10^6 \text{ J/m}^3$
C	$3.9 \times 10^6 \text{ J/m}^3$
T^a	$34 \text{ }^\circ\text{C}$
ν	$7.3 \times 10^{-2} \text{ kg/m s}$
n_e^b	1.632
n_o	1.532
C_b^c	$1.78 \times 10^6 \text{ J/K m}^3$

Table 6: Phenomenological parameters used in calculations

where c is the speed of light and n is the linear index of refraction. Using this relation, the effective nonlinear refractive index is defined in terms of the intensity averaged Δn as

$$n_2^{eff} = \frac{\sqrt{2}cn}{2\pi I_0} \overline{\Delta n} \quad (41)$$

Together with Eqs. 37 and 36, this leads to

$$n_2^{eff} = \frac{\sqrt{2}cn}{2\pi I_0} \frac{dn}{dS} \Delta S_0 h(\xi) \quad (42)$$

Using the definition 28 and the relation 15, one obtains

$$n_{2||}^{eff} = 2n_{2||}^0 h(\xi) \quad (43)$$

and

$$n_{2\perp}^{eff} = -\frac{1}{2}n_{2||}^{eff} \quad (44)$$

where

$$n_{2||}^0 = \frac{ce_2}{4\sqrt{2\pi}} \frac{dS}{dT} \frac{\alpha\tau}{C_i} \quad (45)$$

which is just the value of $n_{2||}$ in the quasi-static limit.

For convenience, the phenomenological parameters used in the calculations are summarized in Table 6. Fig. 31 shows the calculated results for n_2^{eff} along with n_2^0 for several values of the pulse duration. The value of the linear absorption coefficient, α , is taken

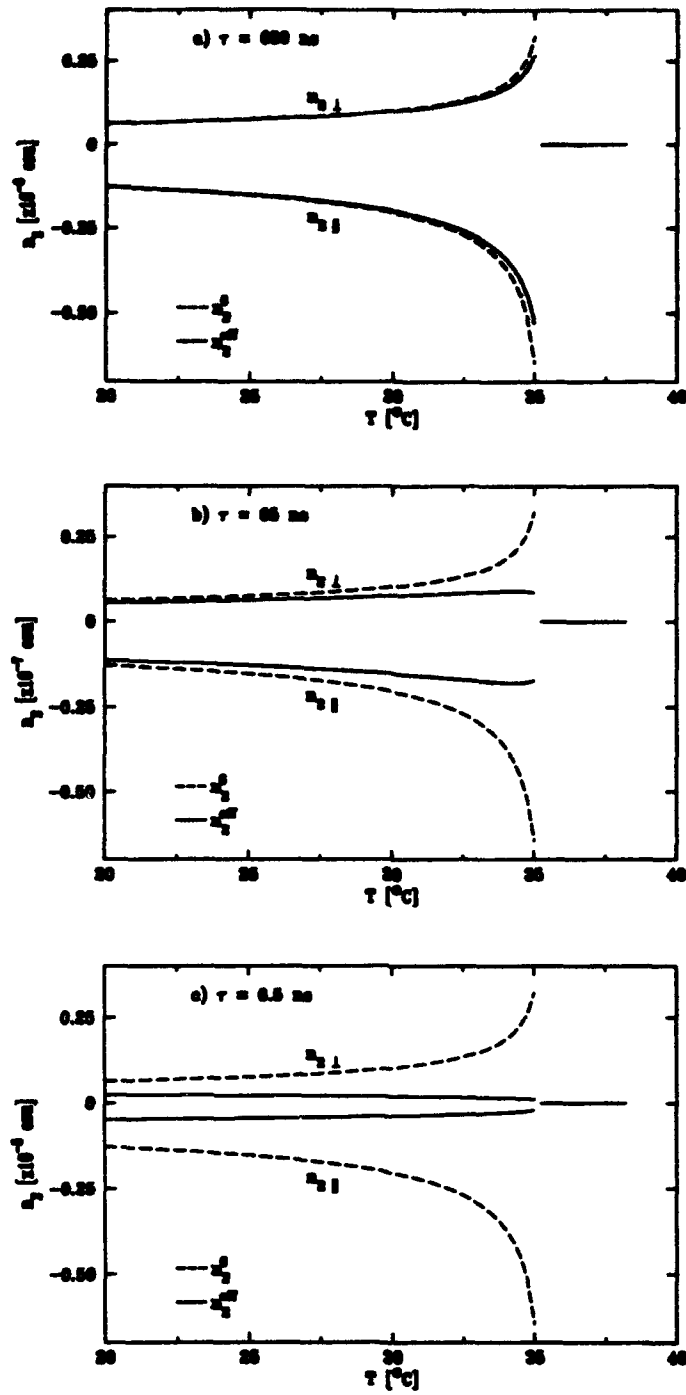


Figure 31: Calculated temperature dependence of n_2 for three pulse durations, $\tau = 650, 65, 6.5 \text{ ns}$. Dashed curves are the same in each figure and show quasi-static n_2^0 . Solid curves are n_2^{eff} .

to be 10 m^{-1} . The actual value of α for 5CB is not well known, so this value of α is chosen to approximately agree with measurements for related materials.[17] The value of α enters into the plots as an overall factor, through $n_{2||}^0$ as given in Eq. 45. Otherwise, the behavior shown in the plots is completely determined by independent measurements.

Fig. 31a shows the temperature dependence of n_2^{eff} and n_2^0 for polarisation parallel to and perpendicular to the director for a pulse duration of 650 ns. At this time scale the behavior is practically quasi-static, and there is very little departure of n_2^{eff} from n_2^0 . Fig. 31b shows the same result for a pulse duration of 65 ns. In this case, the slow relaxation of the orientational order near the phase transition has mostly canceled the enhancement of n_2 due to the large value of dn/dT . Fig. 31c shows the same thing again for $\tau = 6.5 \text{ ns}$, which is the time scale probed in the experiments of Sec. 4. In this case, there are significant effects of the finite relaxation time over the whole range of temperatures shown. The n_2^{eff} is nearly independent of temperature, and decreasing slightly, rather than increasing in magnitude on approaching the transition temperature. The order of magnitude of the calculated n_2 is consistent with the measurements of Sec. 4, although, given the uncertainty of linear absorption, α , more detailed comparisons with the measured magnitude of n_2 are not meaningful.

7.2.4 Analysis of Thermal and Relaxation

Our simple formulation accounts for the relaxation dynamics of the orientational order of a nematic liquid crystal subjected to heating by linear absorption of energy from an optical pulse. This enables the calculation of the time dependence of the order parameter and thus the refractive indices. By defining a suitable intensity weighted average of the change in index of refraction, an effective nonlinear refractive index, n_2^{eff} , is extracted, which is comparable to what would be obtained from a measurement in a z-scan experiment of the type described in Sec. 4 which we have also published, [4, 5].

Our main conclusion is that n_2^{eff} is essentially independent of temperature for pulses of several nanosecond duration. This is due to the fact that the relaxation time of the orientational order shows strong enhancement as the nematic-isotropic transition is approached from below, and for short pulses, this effect counteracts the strong increase of dn/dT near the transition.

With this result, it seems possible to explain many of the features of the observed nonlinear refraction in the nanosecond regime in terms of a thermal mechanism. For example, it was stated in Sec. 5.1 that for all the materials studied, $n_{2||} < 0$ and $n_{2\perp} > 0$, as would be expected if the main effect were reduction of orientational order due

to heating. In addition, experiments of Sec. 4.1 with two pulses separated by several nanoseconds showed a clear influence of the first pulse on the second, which is consistent with the accumulation of heat in the sample. The same type of temporal behavior was seen in the numerical simulation of pulse propagation in Sec. 7.3 which assumed a thermal mechanism. The magnitude of the observed nonlinearity seems to be consistent with heating, up to the uncertainty in the linear absorption coefficient.

However, a complete description of the thermal nonlinear refraction requires some extensions of this work. The thermal variation of the density has been neglected, which has the effect that the calculated n_2 is zero in the isotropic phase. In the measurements, n_2 is found to be smaller, but still significant in the isotropic phase, indicated that the density variations make a non-negligible contribution. The present calculations satisfy

$$n_{2\perp}^{eff} = -\frac{1}{2}n_{2\parallel}^{eff} \quad (46)$$

strictly, whereas the experimental measurements satisfy this only approximately. This is partly due to the density variations, which will make a negative contribution to n_2 for both polarizations. It is also likely that anisotropy of the optical absorption coefficient α contributes to departures from Eq. 46. Certain simplifications have been made here in order to focus attention on a specific point, and in order to avoid the introduction of a large number of adjustable parameters. The main result is expected to be independent of these simplifications.

7.3 Nonlinear Optical Propagation Modeling

We carried out a theoretical analysis of the z-scan experiments used to measure the nonlinear optical properties of liquid crystals, with the aim of clarifying the mechanism responsible for the observed nonlinearity in the nanosecond regime. We considered various orders of nonlinear absorption and nonlinear refraction in order to examine their effects on the resulting z-scan curve. The shape of the z-scan curve in principle contains information about the order of the nonlinearity. We found that qualitative features of the experimental z-scan curves are consistent with a fifth order absorption and a third order refraction. However, given the level of disagreement between the calculated and experimental curves, it is not possible to make quantitative statements about the coefficients of the various orders. The magnitude of the refractive part of the nonlinearity is consistent with laser heating due to linear absorption. The temporal profile of a two pulse experiment is also consistent with this mechanism. We suggest that the temperature dependence of the nonlinear refraction might be explained in terms of a thermal mechanism by accounting for the temperature dependence of the rate of relaxation of the orientational order.

7.3.1 Experiments Being Modeled

The experimental effort provides data on nonlinear parameters for pulse durations in the millisecond, nanosecond and picosecond regimes. We have also experimentally studied the dependence of these nonlinear susceptibilities on temperature and on the intensity of the probing beam. We carried out these experiments in geometries in which reorientation of the macroscopic director field is not expected to occur. In this section we present a theoretical analysis of the experiments, focusing attention on measurements of 5CB (4-cyano-4'-n-pentylbiphenyl) in the nanosecond regime where the mechanism underlying the observed nonlinear refraction is not known.

The *z*-scan technique is designed to measure the nonlinear refractive index, n_2 , which is proportional to the third order polarizability, χ_3 . However, in many cases, due to the temporally and spatially nonlocal character of the response function, χ_3 , the measured value of n_2 depends strongly on the geometrical and temporal properties of the measuring laser beam as well as intrinsic material properties. For example, if the measured response is due to laser heating of the sample, we expect

$$\begin{aligned} n_2 &\propto \Delta n/I \\ &\approx \frac{\alpha \tau}{dT} \frac{dT}{C} \end{aligned} \quad (47)$$

where α is the linear absorption coefficient, C is the specific heat per unit volume, I is the beam intensity and τ is the pulse duration. In Eq.47, we have assumed that the main source of heat is linear absorption of energy from the laser beam, and that the change in index of refraction, n , follows the equilibrium rate of change with temperature, dn/dT . Eq. 47 also assumes that the pulse duration, τ , is short compared with the time scale for diffusion of heat across the beam profile, which is given by

$$\tau_D = w_0^2/D \quad (48)$$

where w_0 is the beam waist, and D is the thermal diffusion constant. For values of D typical of liquid crystals, and for a beam waist of the order $10 \mu\text{m}$, one obtains, $\tau_D \approx 1$ ms, which is very long on the scale of the measurements we consider here, for which $\tau = 7$ ns.

The present analysis is concerned with addressing the mechanism behind the observed nonlinear index of refraction for pulses on the nanosecond time scale. In particular, we focus on laser heating as a possible mechanism. Our consideration of laser heating is motivated by certain experimental facts. First, the signs of the observed n_2 's are consistent with what is expected from laser heating. In particular, it has been observed[5] that in a large number of samples, n_2 is negative for polarization of the beam parallel to

the nematic director, while n_2 is positive for polarization perpendicular to the director. This is what one would expect from a picture in which the main effect is due to a reduction of nematic ordering, and thus optical anisotropy, by heating of the sample. We also note that other potential mechanisms, namely field induced orientational order and electrostriction, predict a positive n_2 regardless of polarization. Non-resonant electronic hyperpolarizability effects tend to produce a positive n_2 for polarization parallel to the director and variable sign for the perpendicular polarization.[20]

Second, the size of the observed nonlinear refraction is consistent with what would be predicted given reasonable values of material parameters. This is shown more clearly in the following section where we show comparisons of calculated and experimental z-scan curves. The reported nonlinear refractive index (Sec. 4) of -54×10^{-11} esu for 5CB measured with a 7 ns pulse is very large, and is more than an order of magnitude larger than the value obtained with a 33 ps pulse. Third, we note that Eq. 47 implies that if laser heating is the important mechanism, then the observed n_2 should scale in proportion to the pulse duration.

In Secs. 4 and 3 we described the measurement of n_2 for several nematic liquid crystals with pulses of both 10 ms and 7 ns of duration. From our experimental work, it was concluded that the observed n_2 in the 10 ms case was due to laser heating. If Eq. 47 holds, then the observed n_2 in the 7 ns case should be $\sim 10^{-6}$ times smaller than that in the 10 ms case. In fact, the observed n_2 in the 7 ns case for 5CB and for ZLI-2303 are of order 10 times larger than this prediction. We note, however, that 10 ms pulses are too long for Eq. 47 to hold. The response over 10 ms is expected to be reduced from the prediction of Eq. 47 by a factor $\sim \tau_D/\tau \sim 1/10$, and it is possible that the discrepancy could be explained by accounting for diffusion of heat in the 10 ms case.

Given these indications in favor of a thermal interpretation, we must note that in the case of the nanosecond pulses there is a shortcoming of this mechanism, which is that it apparently does not give the experimentally observed temperature dependence of n_2 . Specifically, the strong temperature dependence of dn/dT near the nematic-isotropic transition is expected to lead to a corresponding temperature dependence of n_2 . This is observed for 10 ms pulses, but in the case of the 7 ns pulses, n_2 is found to be essentially independent of temperature right up to the phase transition temperature. However, we point out that the equilibrium value of dn/dT gives an upper bound on the variation of n with T measured in a dynamical experiment. The temperature dependence of the index of refraction, n , is mainly due to the temperature dependence of the order parameter, S , with $dn/dT \propto dS/dT$. If the relaxation time for variations of the order parameter, τ_r , exceeds the duration of the pulse, then it is expected[2] that the observed n_2 will be reduced by roughly τ/τ_r . According to a theory of de Gennes,[12] the orientational order

relaxes according to

$$\gamma dS/dt = -\frac{\partial^2 F}{\partial S^2}(S - S_0) \quad (49)$$

where γ is a viscosity coefficient. This gives $\tau_r = \gamma/\frac{\partial^2 F}{\partial S^2}$. As one approaches the nematic-isotropic transition from below, $\frac{\partial^2 F}{\partial S^2}$ approaches zero as $(T^\dagger - T)^{1/2}$, where T^\dagger is the maximum superheating temperature, typically a fraction of a degree above the nematic-isotropic transition temperature. This leads to very large values of the relaxation time near the transition. At the same time $dS/dT \sim (T^\dagger - T)^{-1/2}$, so that for pulses that are short compared to τ_r , the effects of orientational relaxation may cancel the effects of rapid variation of S near the transition. Slowing down of the orientational relaxation has been observed directly[6, 21] in the isotropic phase using the optical Kerr effect, in which case $\tau_r \sim (T - T^*)^{-1}$. Relaxation times of the order of hundreds of nanoseconds have been seen in these experiments. In the calculations that follow, we will consider the measurements on 5CB at 25 °C, which is 10 °C below the nematic-isotropic transition, so that these slowing down effects may not be important. However, any attempt to describe the temperature dependence of the thermal nonlinearity near the transition must include these effects if it is to be valid in the nanosecond regime.

7.3.2 Pulse Propagation

In this section we present the theory behind our detailed simulations of z-scan experiments. The z-scan method is a single beam technique for measuring the nonlinear absorption and nonlinear refractive index of a sample.[10, 11] In this technique, the sample is moved along the axis of a focused beam, and the pulse energy transmitted through the sample is measured as a function of sample position. With an aperture in front of the detector, the measurement is sensitive to both nonlinear refraction and nonlinear absorption. Without an aperture, or with a large aperture, the total transmitted energy is measured, sensing only the nonlinear absorption. Usually, both types of measurements are performed, the large aperture scan giving an independent measurement of the nonlinear absorption. In our calculations, we assume that the incident pulse is represented by the fundamental gaussian beam,[22]

$$E_{in}(r, z_s, t) = E_0 \frac{w_0}{w(z_s)} \exp(-t^2/2\tau^2) \exp(i(kz_s - \Phi) - r^2(1/w(z_s)^2 - ik/2R(z_s))) \quad (50)$$

where w_0 is the beam waist, and

$$\phi(z_s) = \arctan(z_s/z_0) \quad (51)$$

$$w^2(z_s) = w_0^2 \left[1 + \left(\frac{z_s}{z_0} \right)^2 \right] \quad (52)$$

$$R(z_s) = z_s \left[1 + \left(\frac{z_0}{z_s} \right)^2 \right] \quad (53)$$

where z_0 , the diffraction length, is given by

$$z_0 = kw_0^2/2 \quad (54)$$

and k is the vacuum wavenumber for the beam. We use the symbol z_s to denote the position of the sample along the beam axis, relative to the focus.

Given the field at the incoming surface of the sample, the effect of propagation through the nonlinear medium is to attenuate the beam and distort the wave fronts through nonlinear refraction. In the limit of a thin sample, $L \ll z_0$, these effects are represented by the equations,

$$dI/dz = -(\alpha + \beta I + \mu I^2)I \quad (55)$$

$$d\Delta n/dz = k\Delta n \quad (56)$$

where α, β and μ are the linear, third order (two photon) and fifth order (three photon) absorption coefficients. Δn is the change in index of refraction due to nonlinear effects, and in the present calculation, Δn is modeled by,

$$\Delta n(r, z, t) = \gamma I(r, z, t) + dn/dT \frac{1}{C} \int_{-\infty}^t dt' [f_\alpha \alpha I(r, z, t') + f_\beta \beta I^2(r, z, t') + f_\mu \mu I^3(r, z, t')] \quad (57)$$

The first term in Eq. 57 represents a third order refractive effect which is instantaneous on the time scale of the pulse. The second term represents the effect of a change in temperature of the sample, due to the deposition of energy by the beam through the various absorption processes. The factors f_α, f_β and f_μ are included as adjustable constants, $0 \leq f \leq 1$, to account for the fact that only a fraction of the absorbed energy may be converted to heat in the duration of the pulse.

Having solved Eqs. 55-57, the field at the exit surface of the sample is given by

$$E(r, z_s + L, t) = E_{in}(r, z_s, t) \sqrt{I(r, z_s + L, t)/I_{in}(r, z_s, t)} \exp(i\Delta\phi(r, z_s, t)) \quad (58)$$

where L is the sample thickness. To propagate the field from the sample to the detector, we make use of Kirchoff's integral in the Fresnel diffraction limit.[23] In our simulated z -scans we vary the sample position, z_s , and calculate the pulse energy through the detector by integrating the intensity at the detector over the detector aperture and over time. We note that the theory presented here is not essentially different from that elsewhere[10, 11], except that we do not make use of the gaussian decomposition[24] to propagate the

field from the sample to the detector. We chose the present method over the gaussian decomposition, since the gaussian decomposition makes use of an expansion of $\exp(i\Delta\phi)$ in powers of $\Delta\phi$, which in our case is of order unity. Our method is convenient in practice, since the propagation from sample to detector is independent of any assumption about the propagation through the sample, enabling a great deal of flexibility with regard to the modeling of nonlinear effects.

7.3.3 Calculated Results

All of the subsequent results were calculated with the following parameters for the laser beam, chosen to correspond to the experiments which we also performed.

Pulse Energy:	24 μJ
Pulse Duration (fwhm):	6.5 ns
Beam Waist:	7.5 μm
Vacuum Wavelength:	532 nm .

We assume a sample thickness of 25 μm throughout, and all of the following results are calculated for polarization of the beam parallel to the director.

Figs. 32 and 33 show the results of a simulated z-scan. The small aperture scan was calculated with $A = 0.01$, meaning that in the absence of nonlinear absorption, 1% of the incident light passes through the aperture into the detector. In the large aperture case, we integrate all of the intensity at the exit surface of the sample, so that the large aperture scan is sensitive only to nonlinear absorption. The calculations are compared to the experimental results for the material 5CB, which shows some of the largest nonlinearities of the materials studied. The curves in Figs. 32 and 33 were calculated with the following material parameters, thought to be typical[2] for the materials under study:

$$\begin{aligned}
 dn/dT &= -3 \times 10^{-3} K^{-1} \\
 C &= 2 \times 10^6 J/m^3 K \\
 \alpha &= 35.0 m^{-1} \\
 f_\alpha &= 1.0 \\
 f_\beta &= 0.0 \\
 f_\mu &= 0.0 \\
 \gamma &= 0.0.
 \end{aligned}
 \tag{59}$$

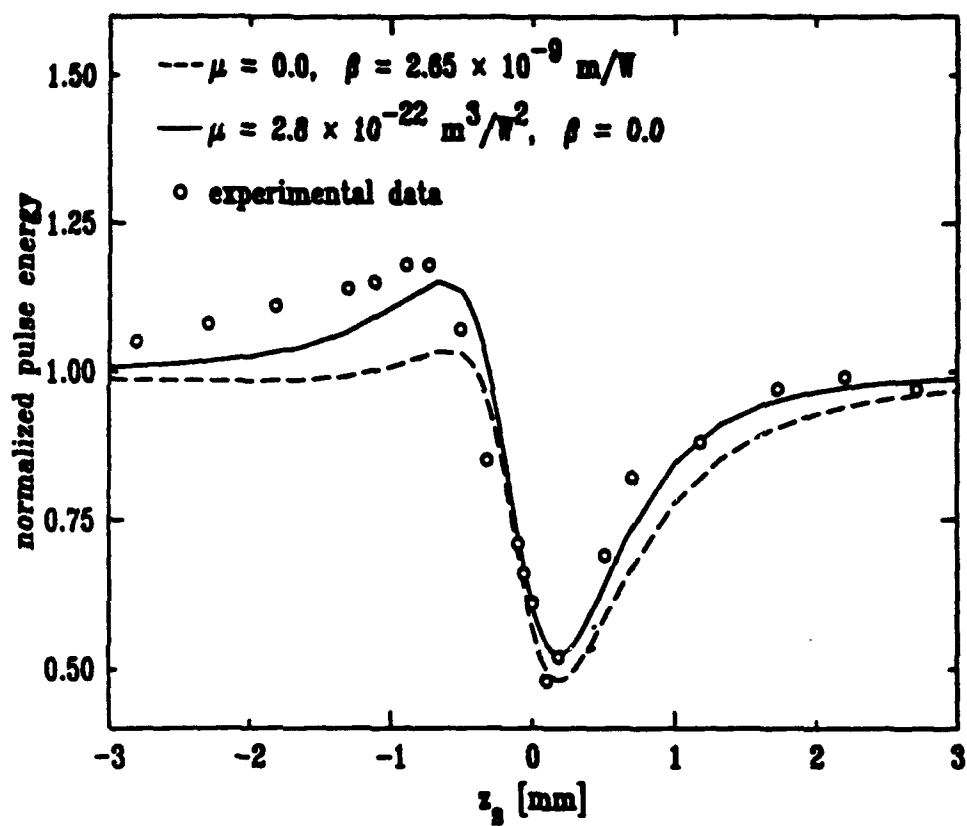


Figure 32: Small Aperture Z-scan.

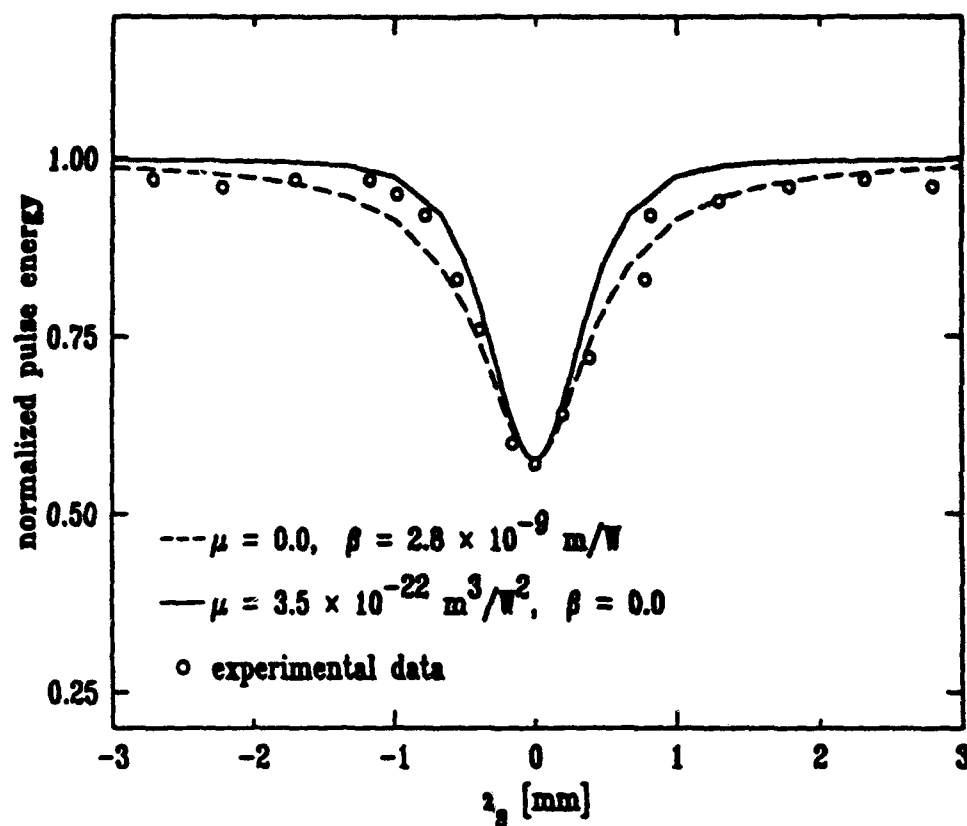


Figure 33: Large Aperture Z-scan.

Using $f_\alpha = 1.0, f_\beta = f_\mu = 0$, means that all of the energy absorbed through linear absorption is converted into heat, but none of the higher order absorption processes result in heating of the sample within the duration of the pulse. This results in a third order refractive process, that is, $\Delta n \propto I$. The linear absorption, α , was adjusted to match the peak to peak variation of the experimental z -scan. Taking $\gamma = 0.0$ means that, in the calculations, all of the nonlinear refraction comes from heating. This is done for illustrative purposes here, in order to show that the resultant magnitude of the nonlinear refraction is in reasonable agreement with the measurements. However, if we take for γ the value measured with 33 ps pulses, where instantaneous effects presumably dominate, the resulting contribution to the phase shift, Eq. 56, is negligible.

The solid curves in Figs. 32 and 33 are for a purely fifth order absorptive process, where we put in Eq. 55 $\beta = 0, \mu = 3.5 \times 10^{-22} \text{ m}^3/\text{W}^2$. Our consideration of fifth order absorption here is motivated by the experimental observation that the β obtained by fitting the data assuming a third order absorption in fact has a substantial linear dependence on the incident intensity. The dashed curves in Figs. 32 and 33 correspond to a purely third order absorption with $\mu = 0, \beta = 2.8 \times 10^{-9} \text{ m/W}$. These values of β and μ were chosen to match the minimum of the large aperture scan. Some understanding of the relation between the shape of the calculated curve and the order of the underlying effect can be gained by recalling that one of the results in the literature[10, 11] is that one can approximately think of nonlinear absorption and nonlinear refraction as operating independently. Then the small aperture scan curve can be thought of as the product of a refractive part, which has the peak-valley behavior, with the nonlinear absorption, which has a minimum at $z_s = 0$. In general, a higher order effect tends to bring these features of the curve closer to $z_s = 0$. For example, it was found by the CREOL group[11] that for a third order refraction, the maximum and minimum of the small aperture scan are separated by $1.7z_0$, while for a fifth order refraction, the separation is $1.2z_0$. The main effect of the fifth order absorption is seen in Fig. 33, which shows that the minimum of the large aperture scan is more concentrated near the origin, in contrast with the third order absorption. In the small aperture scan, Fig. 32, the refractive mechanisms for the two curves are the same. However, for the dashed curve, with the third order absorption, the peak at negative z_s which is normally associated with a defocusing medium[10, 11] ($n_2 < 0$) has been nearly swallowed by the broad absorption minimum. For the solid curve, which is calculated with a fifth order absorption, the narrower absorption minimum allows for a peak in the small aperture curve at negative z_s . We note that the experimental data do seem to show such a peak. We find that this feature is impossible to obtain with a purely third order absorption. The experimental large aperture scan also shows some sign of the narrower minimum characteristic of fifth order absorption, although this is difficult to distinguish from the scatter in the data. It is likely that more than one order of nonlinear absorption is in effect. However, mixtures of third and fifth order absorption constrained to give the same minimum of the large aperture scan simply interpolate between the

curves shown. Since this does not seem to result in any better fit to the data, particularly for the small aperture case, it does not seem to be possible to obtain definitive values for the coefficients by fitting a single z-scan curve.

Nonlinear absorption may contribute to heating of the sample. The experiments show that 40% of the incident energy is removed from the beam by these processes in the situation we consider. If all of this energy were converted to heat, the sample temperature would rise by

$$\begin{aligned}\Delta T &\approx \mu I_p^3 \tau / C \\ &\approx 4000 K,\end{aligned}\tag{60}$$

where I_p is the peak, on-axis intensity. Clearly this does not occur. It may be that the energy absorbed by these higher order processes remains in long-lived electronic excitations for the duration of the pulse, or is carried away by fluorescence. This is not known. If some fraction of the energy absorbed by higher order processes is turned into heat during the pulse, then f_β and f_μ should not be strictly zero. In Fig. 34 we illustrate this possibility by calculating a small aperture scan where the refractive mechanism is entirely heating due to fifth order absorption. This results in a seventh order refractive effect. We have taken $f_\mu = 1.6 \times 10^{-3}$. The result of this calculation is shown as the dashed line in Fig. 34 along with the solid curve of Fig. 32 and the experimental points.[19] The higher order refraction results in the peak of the curve being pulled in closer to $z_s = 0$, where it is almost completely eliminated by absorption. This leads to worse agreement with experiment, particularly in the region of negative z_s . Since it was reported experimentally[5] that the measured n_2 is independent of the input intensity, it appears that the dominant refractive effect is truly second order.

With regard to the thermal mechanism, we note that although we have adjusted the value of α used in the calculations of Figs. 32 and 33 to fit the experimental data, the resultant value of $\alpha = 35.0 \text{ m}^{-1}$ is well within what is considered reasonable, the precise value of α being difficult to measure.[2] From the comparisons of our calculations with the experimental data, we conclude that the magnitude of the observed nonlinear refraction, as measured by the peak-peak variation of the z-scan curve, is consistent with this mechanism. However, the main feature of the thermal mechanism is the way the nonlinear refraction accumulates in time, as in Eq. 57. Since the z-scan technique measures the integrated pulse energy, no information is obtained about the temporal character of the mechanism. Our z-scan curves could have been calculated by putting $f_\alpha = f_\beta = f_\mu = 0$ in Eq. 57 and using $\gamma = -2.7 \times 10^{-16} \text{ m}^2/\text{W}$ with nearly identical results. In order to gain information about the temporal behavior of the nonlinearities, we have performed experiments (Sec. 4.1 and Ref. [5]) in which we observed the temporal profile of the outgoing pulse with two closely spaced input pulses. Fig. 35 shows a simulation of just such a situation.

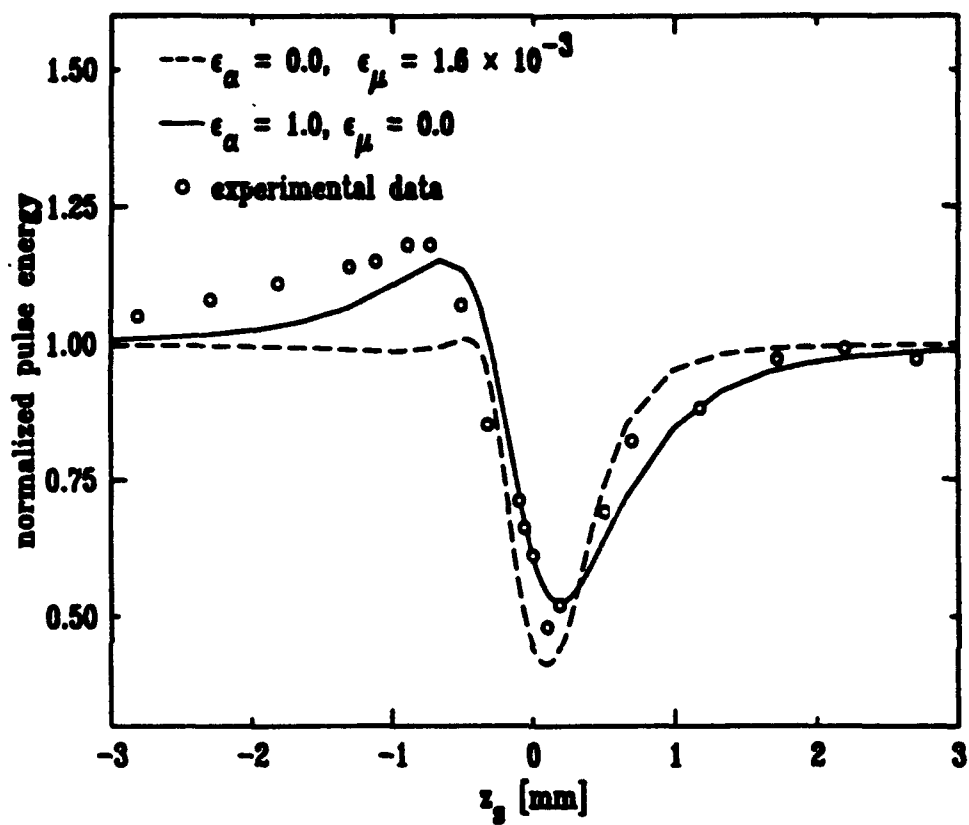


Figure 34: Z-scan resulting from purely 5th order heating.

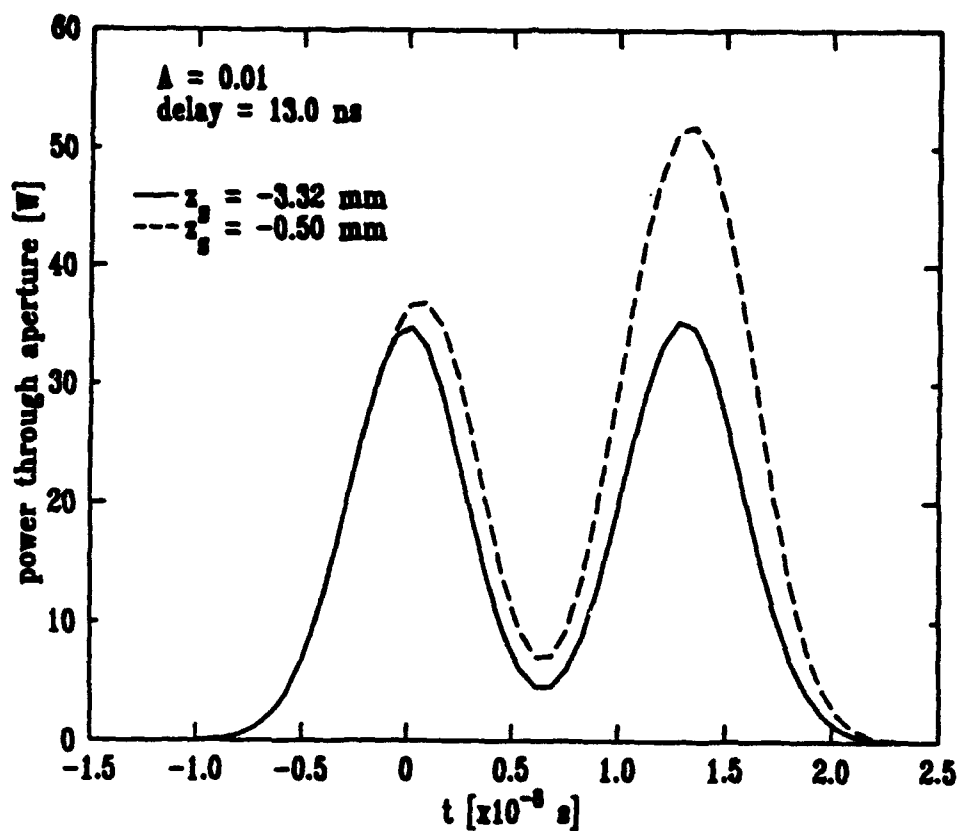


Figure 35: Two pulse Z-scan.

Temporal profile of a double pulse. The solid curve is for a sample position far from the focus. The dashed curve corresponds to a sample position near the maximum of the small aperture z-scan

The material parameters are the same as those used for the solid curve of Fig. 32, with the nonlinear refraction again being assumed to be entirely thermal. The solid curve of Fig. 35 shows the outgoing power through the small aperture for a case in which the sample is located far from the beam focus, so that nonlinear effects are not important. In this case the output power is simply proportional to the input power. The dashed curve shows the case in which the sample is positioned near the maximum of the small aperture scan, Fig. 32. In this case there is important nonlinear refraction, which tends to increase the energy flux through the aperture. This nonlinear refractive effect builds up in time according to Eq. 57 with the accumulation of heat in the sample. Since there is effectively no diffusion of heat over the time scales we are considering, the heat accumulated during the first pulse is still in place during the second pulse, leading to a strong influence of the first pulse on the second. This type of behavior has been observed experimentally.[5]

7.3.4 Interpretations

We have performed numerical simulations of *z*-scan experiments for comparison with the experimental results published [4, 5, 19] and described in Sec. 4. In particular, we have considered the *z*-scan experiments with 7 ns pulse duration and the material 5CB, which was the most extensively studied. We have shown calculations to illustrate the *z*-scan signature associated with various orders on nonlinear absorption and nonlinear refraction. Qualitative features of the experimental *z*-scan curves seem to be consistent with third order refraction and fifth order absorption. We find that the magnitude of the observed nonlinear refraction is consistent with laser heating of the sample due to linear absorption. We have also shown a calculation of the temporal profile of the detected power through a small aperture in the case where the incident beam consists of two closely spaced gaussian pulses. Due to the cumulative nature of the thermal mechanism, the presence of the first pulse has a strong influence on the second. Our calculated result is qualitatively similar to the our experimental measurements, which clearly shows such a cumulative effect.

In our calculations, we have only considered one order of nonlinear refraction or nonlinear absorption at a time. In reality, various orders of nonlinearity will be operative simultaneously. In principle, the shape of the *z*-scan curve contains information about the coefficients of various orders. In practice we find the level of disagreement between calculated and experimental curves precludes any such detailed analysis. In addition to random scatter of the experimental points, which presumably results from fluctuations in laser pulse energy, there seem to be systematic deviations between calculation and measurement. One possible source of such deviations is imprecise location of the origin, $z_0 = 0$, in the experiments. We have not attempted to correct for this in the plots shown here. Instead of trying to obtain a very refined curve shape for a single pulse energy,

it would seem to be fruitful to try to obtain the coefficients of the various processes by fitting z-scan curves measured over a range of pulse energies.

Energy dependent measurements were experimentally measured and the data were analysed to obtain pulse energy dependent "effective" values for n_2 and β . The effective n_2 was found to be independent of intensity, while β was found to depend linearly on intensity, indicating the presence of fifth order absorption. A rough estimate of the fifth order absorption coefficient can be obtained from their plot using $\mu \sim \Delta\beta/\Delta I \approx 10^{-21} \text{ m}^3/\text{W}^2$. This compares favorably with the value $3.5 \times 10^{-22} \text{ m}^3/\text{W}^2$ used in the plot of Fig. 32. More detailed fitting of energy dependent z-scans to obtain definitive values of the coefficients would seem to be very profitable.

Both the magnitude and the temporal behavior of the observed nonlinear refraction are consistent with a thermal mechanism. We have noted that the thermal mechanism has one shortcoming with respect to explaining the observed n_2 , and that is that the n_2 observed with 7 ns pulses is found to be nearly independent of temperature,[5] while on the basis of Eq. 47 one expects that n_2 will have the temperature dependence of dn/dT , which has rapid variation near the nematic-isotropic transition. However, we point out that 7 ns is actually much shorter than the characteristic relaxation time, τ_r , associated with variations in the orientational order parameter, S , for temperatures near the transition. Given that τ_r has the same dependence on the temperature as dS/dT near the phase transition, it is quite likely that the observed lack of temperature dependence of n_2 is a result of the finite response time of S . We are currently investigating molecular orientational dynamics theoretically, and should soon be able to make more definite statements regarding the dynamics of the response of the orientational order to variations of temperature and external fields, and the resulting temperature dependence of n_2 .

Further experimental data would also be very valuable in identifying the underlying mechanism of the nonlinear optical response. For example, we have noted that the cumulative temporal behavior of the nonlinear refraction is characteristic of the thermal mechanism. However, one can imagine other mechanisms which would exhibit similar behavior. Excited state refraction in which the molecular polarizability is changed through a one photon excitation would have a very similar signature. In fact, if the relaxation time of the excited state were long compared with the pulse duration, the theoretical description would be essentially identical with Eq. 57 except that the parameters would be interpreted differently. In the case of the thermal mechanism, we know that the decay time, which is essentially the diffusion time, Eq. 48, is indeed long. Therefore, if the thermal mechanism is the operative effect, one should not observe any diminution of the effect of the first pulse on the second in a double pulse experiment as the delay between pulses is increased to quite large values ($\sim 1 \text{ ms}$). This is a quite definite prediction of the thermal mechanism and any departure from this behavior would be strong evidence

against a thermal interpretation. Observations of fluorescence would help to determine the fate of the large amounts of energy removed from the beam by nonlinear absorption. Also, the observation of fluorescence at wavelengths shorter than $\lambda/2$ would confirm the presence of fifth order (three photon) absorption.

8 Materials Synthesis, Acquisition and Preparation

8.1 Materials Preparation

The initial thrust of this contract, as described in the proposed work, was the investigation of novel composite systems offering possibilities for enhanced nonlinear effects. Subsequent changes in the immediate interests of the overall DARPA OPL effort resulted in more attention to pure materials.

The primary activity in the materials program for the first portion of the project was the preparation and characterization of polymer dispersed liquid crystal (PDLC) films. PDLC films are made through one of a variety of processes. While considerable experience exists in house in PDLC preparation, the process changes for each set of new materials. In principle, any one of thousands of liquid crystal materials can be combined with a similarly large number of polymers to produce a PDLC film. Since the preparation conditions determine the properties of the final film, there is considerable experimentation and characterization necessary in order to achieve desirable characteristics in any particular polymer/liquid crystal system.

PDLC films were formed either by polymerization induced phase separation (PIPS) or by a combination of solvent induced and thermally induced phase separation (SIPS and TIPS respectively). The droplet size was controlled by either the curing temperature for PIPS or by the rate of cooling from the isotropic melt for SIPS/TIPS.

The droplet formation process was studied for the polymers PMMA, PVP and the epoxy matrix made using Epon 282, MK107 and Capcure. In the initial studies of PDLCs, the commercially available liquid crystal E7 was used as a standard test case. For PMMA and PVP the droplet size is a function of the rate of cooling from the isotropic melt. The PDLC films were formed by solvent casting a chloroform solution on a glass substrate. The resulting films were further processed by being heated above the melting point of the polymer resulting in formation of a homogeneous solution. The films were then cooled at a prescribed rate and the resulting droplet size measured using optical microscopy. The same films could be thermally cycled several times to change the droplet size. For the epoxy systems, the cure rate and concentration of liquid crystal determined the droplet size and concentration. In all cases, the thickness of a film is determined when it is sandwiched (prior to droplet formation) between two glass substrates. The glass substrates are separated by spacers to produce films of thickness typically between 10 μm and 100 μm .

The film preparation supported both the nonlinear optical measurements activities and the IR Shutter activities. For the IR shutter effort, the principle effort was at producing and evaluating a variety of PDLC systems. We had no experience with the IR properties of these materials so a very broad screen process was initiated. Further details on film preparation specific to the IR project are contained in Sec. 9. The very particular requirements related to response time and droplet morphology as well as optical properties required a more extensive investigation into PDLC formation.

The studies of nonlinear response of composites relied largely on the Epon/Capcure epoxy with the E7 liquid crystal during the first phase of the effort. This is a system with which we had experience switching in electro-optics applications, so it required less initial investment in materials preparation effort. The Active Feedback studies described in Sec. 3.1 used preparation techniques which had been tested in liquid crystal display (LCD) applications. The variable requiring adjustment was the opacity on the scattering state, since the electronic circuits could be adjusted to balance feedback with transmission.

8.2 Nonlinear Materials Selection

In the second year of the project, a change in emphasis occurred from investigating novel system to demonstrating large materials nonlinearity. This was a change in direction communicated to all contractors during the second annual review meeting.

To help separate and identify the operative mechanisms for OPL, we systemized our selection of the class of materials to be studied. The following properties and selection criteria were applied in our literature search.

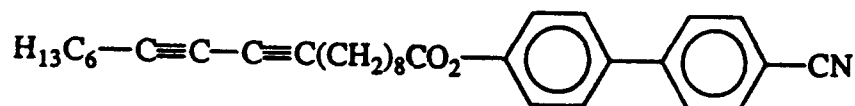
1. A solid to nematic or smectic transition should occur near or below room temperature and have a range of at least 10 degrees C or more to facilitate experimental measurement.
2. The material should be chemically stable to eliminate uncertainties about contaminants contributing to or masking nonlinear effects. Similarly, laser induced reactions would unnecessarily complicate analysis at this stage.
3. Transparency in the IR and visible range is highly desirable.
4. Chemical breadth was desired. We sought compounds with:
 - (a) Varying sizes of conjugated cores
 - (b) Varying linkages between benzene rings

- (c) Varying substituent groups
- (d) Ease of synthesis or even possible commercial availability.
- (e) Simple and small conjugation structures to facilitate theoretical calculations

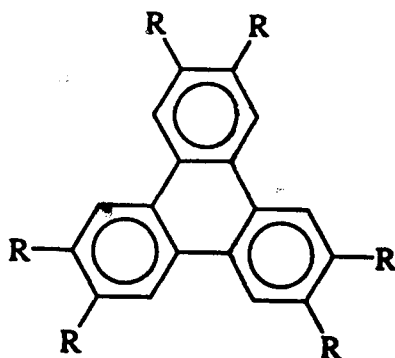
Except for requirements that a nematic or smectic exist at a temperature accessible to the laser measurement facility, none of the above criteria were deemed absolute. We compiled a list of materials which satisfy all or most of the above. The list is provided in Appendix A.

A subset of the list of potentially interesting liquid crystals was actually chosen for acquisition and study. The liquid crystal materials which were selected for study are listed below. All were acquired or synthesized. Those synthesized under this contract are indicated as KSU synthesis.

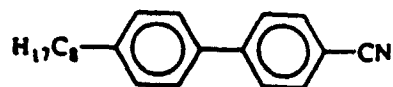
- 6DA8CB (KSU Synthesis)



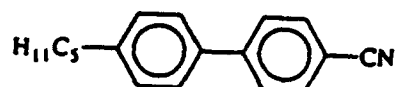
- HDAT (KSU Synthesis)



- 8CB (K24), (4-cyano-4'-n-octylbiphenyl)



- 5CB (4-cyano-4'-n-pentylbiphenyl)



- E7

Commercial Mixture, Proprietary

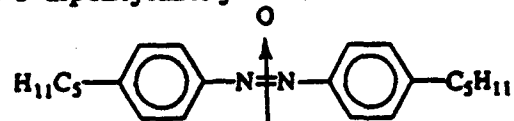
- OPL-7-1 (8YCB) (KSU Synthesis)

4-(1-octynyl)-4'-cyanobiphenyl



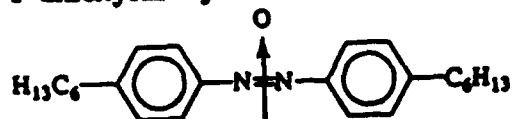
- OPL-10-1 (5AZXB) (KSU Synthesis)

4-4'-dipentylazoxybenzene

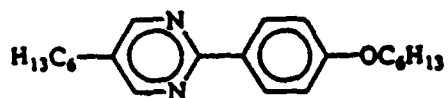


• OPL-10-2 (6AZXB) (KSU Synthesis)

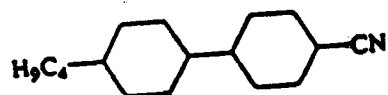
4-4'-dihexylazoxybenzene



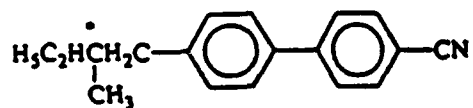
• ZLI 2303 (PYP-606) Phenylpyrimidine



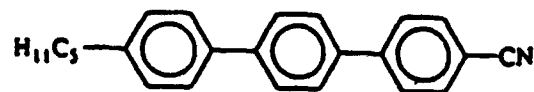
• ZLI 1538 (CCH-4) Cyclohexylcyclohexane



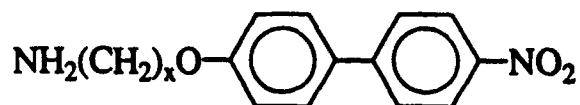
• CB15



- T15 (4-cyano-4"-n-alkyl-p-terphenyl)



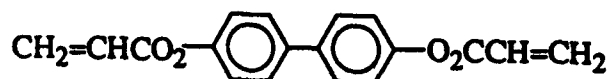
- AANB-5 4-(*omega*-aminoalkyloxy)-4'-nitrobiphenyls (KSU Synthesis)
- AANB-7 4-(*omega*-aminoalkyloxy)-4'-nitrobiphenyls (KSU Synthesis)
- AANB-10 4-(*omega*-aminoalkyloxy)-4'-nitrobiphenyls (KSU Synthesis)



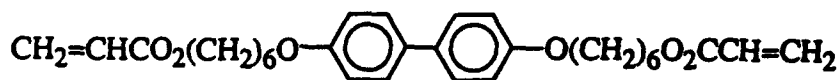
4-(ω -aminoalkyloxy)-4'-nitrobiphenyls (AANB)

X = 5,7,10

- 4,4'-bis(acryloyloxy)biphenyl (BAB) (KSU Synthesis)

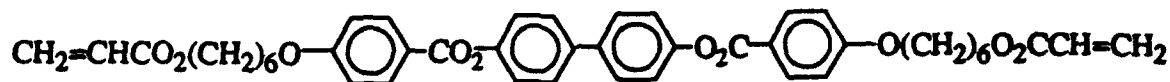


- (KSU Synthesis)
- 4,4'-bis[6-(acryloyloxy)hexyloxy]-1,1'-biphenyl (BAB-6)



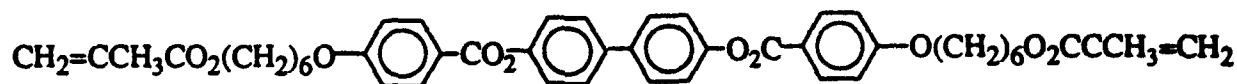
(KSU Synthesis)

4,4'-bis{4-[6-(acryloyloxy)hexyloxy]benzoate}-1,1'-biphenylene (BABB-6)



(KSU Synthesis)

4,4'-bis{4-[6-(methacryloyloxy)hexyloxy]benzoate}-1,1'-biphenylene (BMBB-6)



The specific measurements and nonlinear parameters (or IR parameters) are described elsewhere in the text of the pertinent experimental section. A tabulation of materials and nonlinear parameters are collected in Appendix A.

9 IR Shutter

Included in our original contract was a separate project to evaluate the use of liquid crystal composites in infrared shuttering applications. The particular applications were night vision devices which currently employ a mechanical shutter as a modulator of incident IR radiation. The IR detectors which form the image require modulation of the IR radiation. We were not informed of the details of operation or geometry of current devices employed by DoD. We were however given some guidelines.

The device requirements as understood at the time of the proposal were:

1. Acceptance angle of 40 degrees - full angle
2. Electrically line addressable
3. Line dimensions of 0.5 inches long and 100 μ wide
4. 0.5 inches by 0.5 inches array Size
5. Low insertion loss, less than 20%
6. > 95% of incident radiation forward scattered into an annulus of radius equivalent to 10 line widths
7. Submillisecond switching times
8. Broadband response over the 8 - 14 μm region.

The project developed through several phases.

1. Concept testing to determine if any shuttering of IR radiation was possible with existing PDLCS.
2. Materials testing for contrast enhancement.
3. Prototype shutter construction for transmission enhancement.
4. IR camera device testing
5. Materials testing for response time and scattering angles.

We will follow the above outline as a final report on the IR shutter segment of our effort and end with an evaluation discussion.

9.1 Concept Testing

In the first quarter of the effort, existing materials that are used in PDLC display application were used to form large droplet films for concept testing. Visible wavelength scattering utilized a polymer film with liquid crystal droplets in the $.5 - 1 \mu m$. The rule of thumb that effective scattering requires droplets comparable to the wavelength was applied to create PDLC films.

A PDLC film is prepared by cooling a solution of E7 in the thermoplastic PMMA melt. The size of the E7 droplets is governed by the rate of cooling and the relative concentration of PMMA and E7. We found the best results were achieved with very large droplets, $\approx 20 \mu m$ in diameter and with a ratio of E7:PMMA of 4:1. The droplets were formed by slowly cooling the solution from 75 degrees C to 21 degrees C in about 12 hours, yielding droplets of $20 - 30 \mu m$ in diameter. A $10 \mu m$ thick film of the material was sandwiched between NaCl substrates with a platinum conducting electrode. The platinum electrodes absorb about 50% of the incident IR. The IR transmission of the shutter was measured with a Sargent Welch 3 - 200 IR spectrophotometer. The resulting spectra with and without an applied voltage are shown in Fig. 36

The transmitted intensity is not quantitative for these films, however, without an applied voltage the scattering intensity in the $2.5 - 5 \mu m$ region is on the order of the strongest absorption of the film and is switched to a highly transmitting state upon application of a voltage. Optoelectronic modulation of the transmitted intensity is seen at all wavelengths where there is no significant absorption; $2.5 - 3.5 \mu m$, $4.0 - 6.0 \mu m$, $9.5 - 10.5 \mu m$ and $8 - 14 \mu m$.

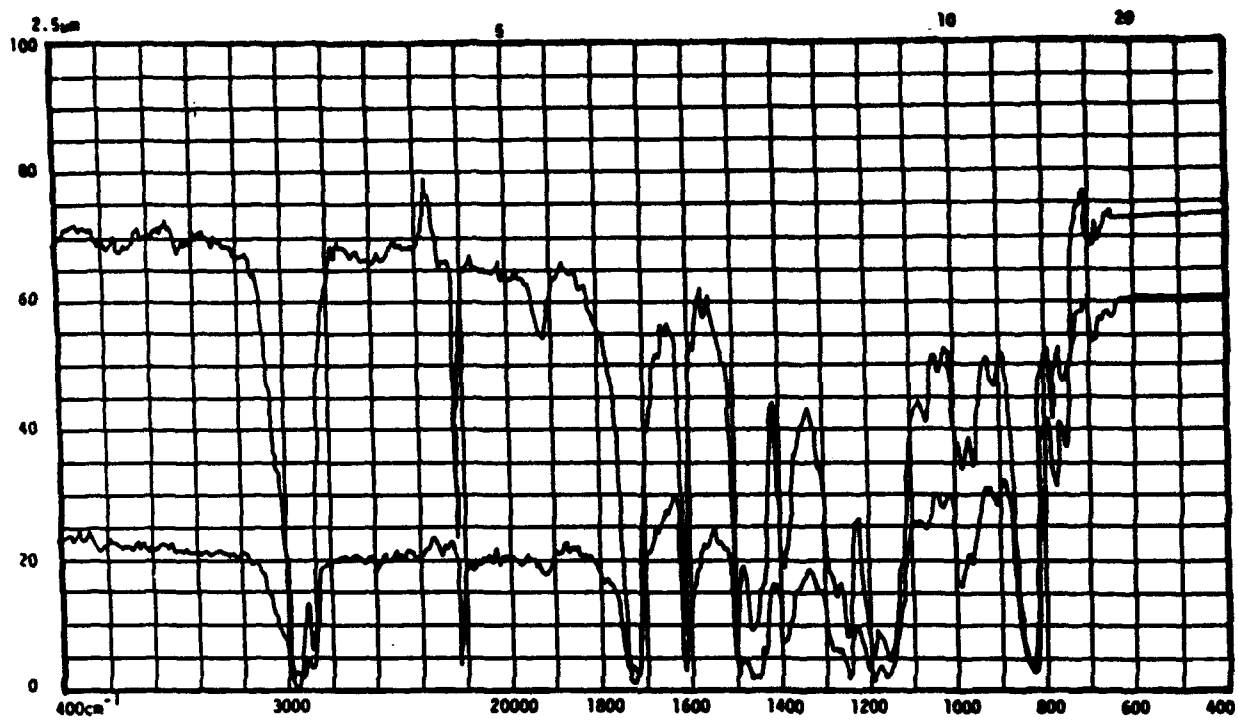


Figure 36: IR Transmission of PMMA/E7 PDLC

9.2 Contrast Enhancement

The effective modulation of IR radiation by a PDLC device is not possible if there is

1. High absorption loss,
2. High surface reflection loss,
3. Poor matching of the IR index of refraction of the polymer and the ordinary index of refraction of the liquid crystal, or
4. Poor birefringence or small differences in the IR ordinary and extraordinary indices of refraction of the liquid crystal.

While there are other parameters affecting device performance, the above were deemed important enough to address first.

The initial phase of the research involved screening of polymers and liquid crystals for large absorption windows in the 2.5 - 5 μm or 8 - 14 μm region. The polymers screened include: polymethylmethacrylate, polyvinylfluoride, polystyrene, polyvinylacetate, polycarbonate, polyvinylpyrrolidone, and polyvinylchloride. Epoxy resins and cure agents were also screened. The polymers all have absorption bands in the 8 - 14 μm region; however, several of the polymers have broad transparent regions so that total transmission is acceptable for further experimental development.

Table 7 lists the polymers and liquid crystals surveyed for use in this project. The IR transmission spectrum of each of the pure materials was obtained to determine their absorption characteristics in the 2.5 - 5 and 8 - 14 μm regions. Materials with broad transmission windows in these regions were used for formation of PDLC films.

The E7 liquid crystal mixture is representative of the IR absorption characteristics of a wide variety of commercially available eutectic liquid crystal mixtures based on cyanobiphenyls and terphenyls. The CM-1644 liquid crystal is a not conjugated liquid crystal based on cyclohexanes and has a broad transmission window. However, it has a very low dielectric anisotropy and therefore requires unacceptably high driving voltages to switch to the transparent state.

PDLC films were formed either by polymerization induced phase separation (PIPS) or by a combination of solvent induced and thermally induced phase separation (SIPS and TIPS respectively). The droplet size was controlled by either the curing temperature for PIPS or by the rate of cooling from the isotropic melt for SIPS/TIPS. The IR transmission

Polymer / liquid crystal	IR Transmission
polymethylmethacrylate (PMMA)	acceptable
polyvinylpyrrolidone (PVP)	acceptable
polystyrene	acceptable
polyvinylfluoride	unacceptable
polyvinylacetate	unacceptable
polycarbonate	unacceptable
polyvinylchloride	unacceptable
epoxies (Epon 828, Mk107, WC68 with Capcure 3-800)	unacceptable
E7	acceptable
CM-1644	acceptable

Table 7: IR Transmission characteristics of selected polymer and liquid crystals.

Cooling Rate (°C/min)	Droplet Diameter (μm)	
	E7/PVP	E7/PMMA
>>10	<<5	<<5
4	10-15	3-5
2	15-25	5-10
1	20-30	10-15
0.5	25-40	15-25

Droplet size as a function of cooling rate for E7/PVP and E7/PMMA PDLC films.

Table 8: Droplet size as a function of cooling rate for E7/PVP and E7/PMMA PDLC films.

spectra of the resulting PDLC films were measured. The E7/PVP and the E7/PMMA PDLC films had the highest contrast and broadest transmission windows in the ON state.

The droplet formation process was studied for E7/PMMA and E7/PVP PDLC systems. The droplet size is a function of the rate of cooling from the isotropic melt. The PDLC films were formed by solvent casting a chloroform solution on transparent conducting electrodes with 26 or 10 μm spacers to control thickness. The resulting films were heated to above the melting point of the polymer resulting in formation of a homogeneous solution. The films were then cooled at a prescribed rate and the resulting droplet size measured using optical microscopy. Table 8 lists the cooling rate and droplet size for 10 μm thick films of E7/PMMA and E7/PVP. The same films can be thermally cycled several times to change the droplet size. The IR transmission in the ON and OFF state was measured as a function of droplet size for both PDLC systems.

Fig. 37 shows the IR transmission in the ON and OFF state of an E7/PVP film with a) $\approx 5\mu\text{m}$ droplets and with b) 15 - 25 μm droplets. Comparison of the OFF state transmission of these two films shows that smaller droplets results in higher scattering in the 2.5 - 5 μm region while the film with the 15 - 25 μm droplets has much higher scattering in the 9 - 14 μm region. This result agrees with the general theoretical prediction that light scattering will be most efficient when the droplet size is comparable to the wavelength.

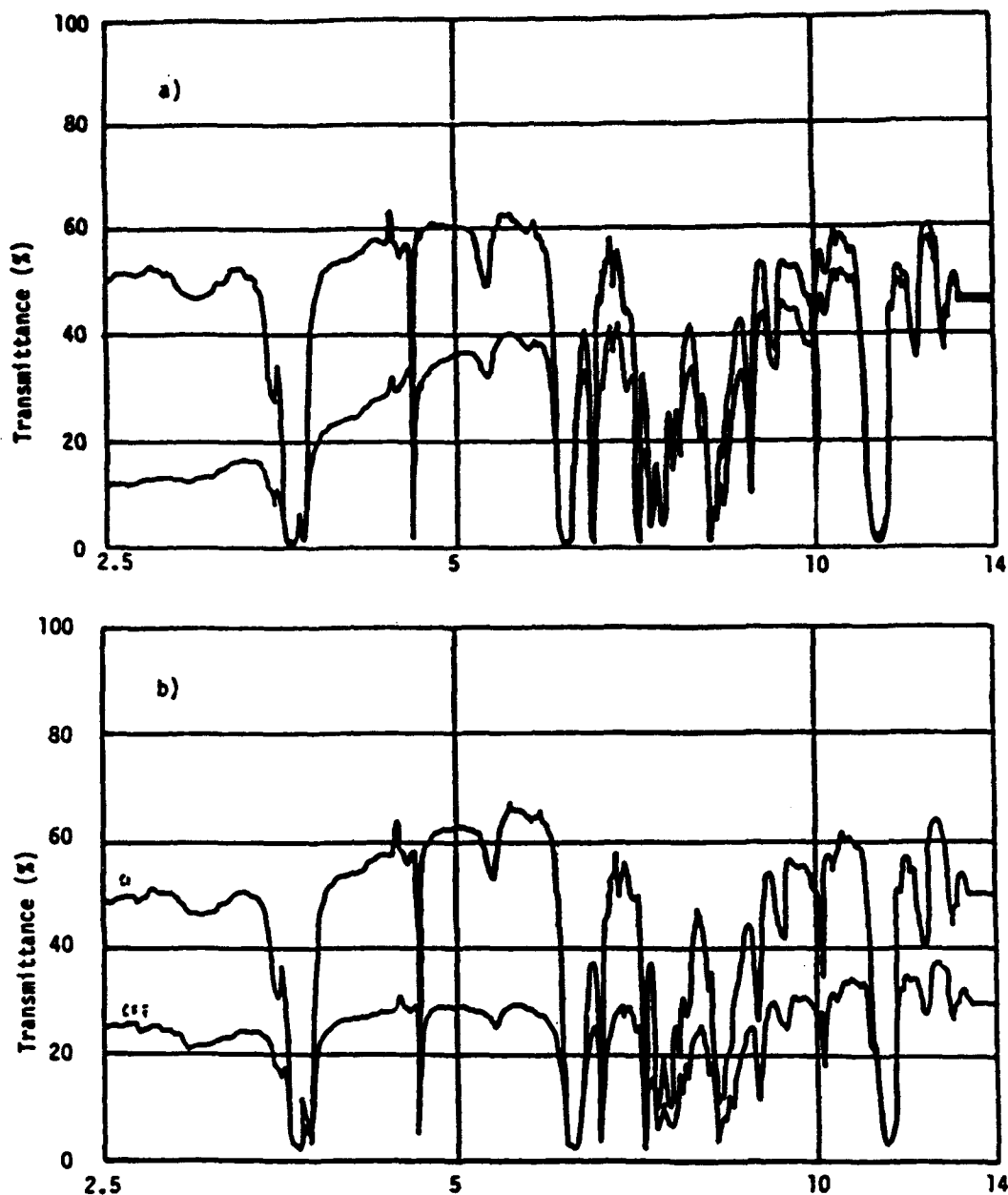


Figure 37: On and OFF transmission of small droplet ($\approx 5\mu m$) film (top) and large droplet ($15 - 20\mu m$) film (bottom). Horizontal axis wavelength μm .

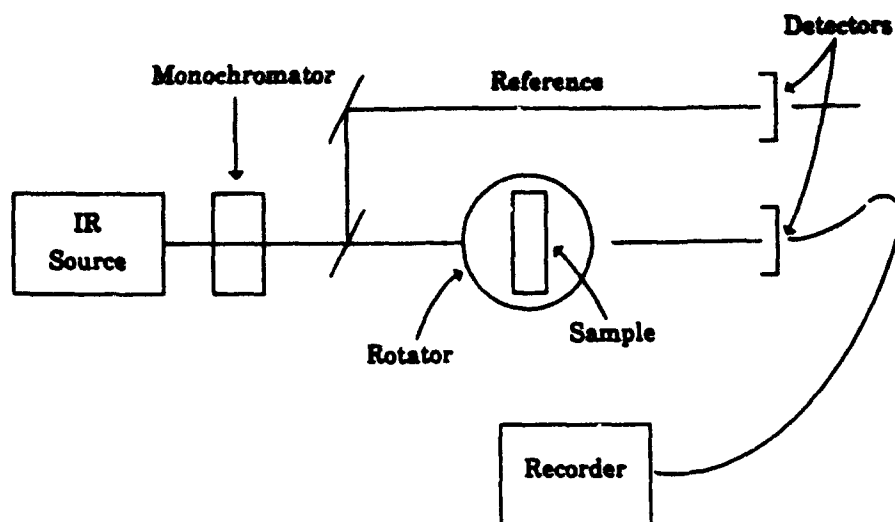


Figure 38: Experimental Set up for angular transmission measurements.

9.3 Angular Transmission

Angular transmission studies were carried out using an experimental set up shown below.

In preparing for transmission and scattering studies of PDLC films in the IR when radiation is not at normal incidence, we measured the necessary transmission characteristics of the NaCl coated substrates. These curves were fit to determine surface reflectivity and absorption coefficients.

Similar preparatory measurements were performed on a mixture of liquid crystal and polymer (E7 and polyvinylpyrrolidone) when the concentration of liquid crystal (E7) was too small to form droplets. This material mimics the polymer host with its residual liquid crystal concentration in the films where droplets have been formed. Transmission studies as a function of incident angle were performed on these films without droplets to determine their contribution to background reflection and absorption profiles.

Finally, the angle dependent transmission characteristics of the PDLC films were measured at a number of points from 2 - 18 μm (in regions with low absorption). The 5 μm is

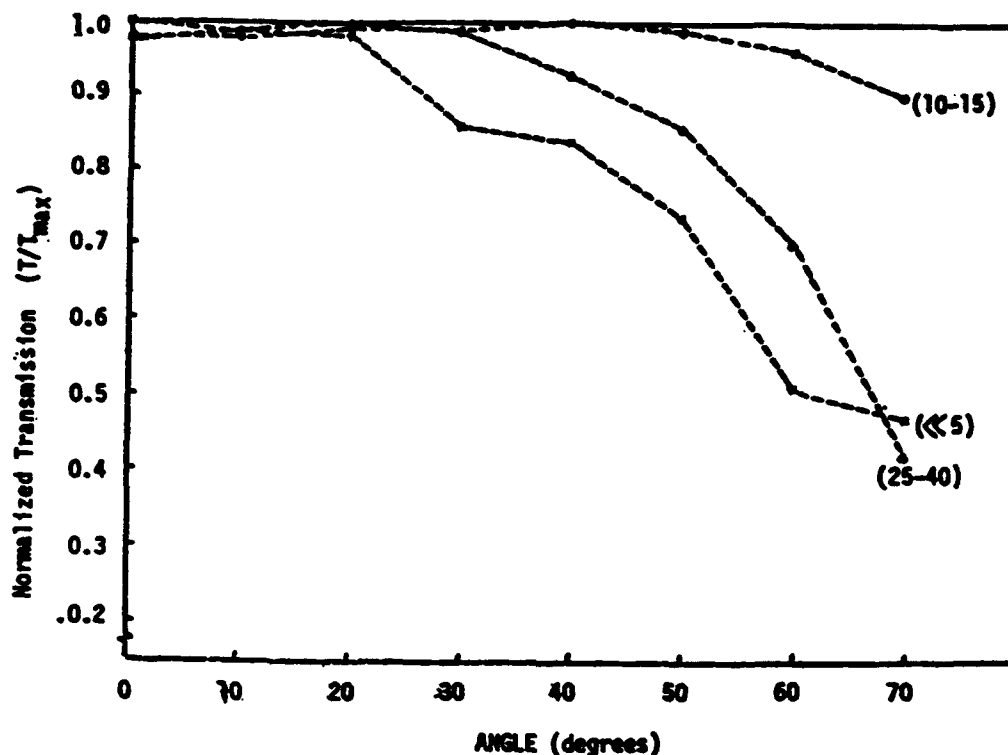


Figure 39: Normalized transmission as a function of incident angle for E7/PVP film with 5, 10-15, 25-40 μm size droplets.

shown in the figure as an illustration of the results. The results for one sample with 80% E7 in polyvinylpyrrolidone cooled at different rates are shown in the figure below.

The maximum ON transmission can be achieved if there is perfect index matching of the ordinary index of the droplet, n_o , with the host polymer. It is inherent in the birefringent optical properties of the droplet that as the direction of the light becomes off-axis, part of the extraordinary, n_e , index is encountered during propagation. The extent to which the resulting scattering decreases the amount transmitted is indicated by the difference between the substrate + polymer sample and the substrate + polymer + droplet sample. At visible wavelengths, this phenomena manifests itself as a slight haze

when a PDLC is viewed off axis. Compared to similar studies in those systems, the IR haze effect is reasonably small.

10 IR Camera

Having produced PDLC films capable of modulation in the IR, we attempted to use a liquid crystal composite as a shutter in an IR camera. The first tests showed only that it would modulate the intensity of the IR signal detected by the camera. Subsequently, it was shown that the modulation was sufficient to produce an image with the camera. Fig. 40 shows an early qualitative plot of signal intensity versus temperature of an object for both mechanical shuttering and PDLC shuttering. The difference between the brightness of the image using the two systems shows that substantial optimization of the PDLC materials and the electronics of the IR camera remains to be carried out. The mechanical shutter can produce an image of an object which is only a few degrees above background while the PDLC begins imaging only when the object is at least 20 degrees C above background.

We investigated the effect of sample thickness on the contrast of PDLC films having relatively large droplets (15 - 25 μms). PDLC shutters with a film thickness of 10, 26 or 61 μms were made and their contrast measured. The 10 μm films show little modulation of the incident radiation whereas the 26 μm thick films switch from 34% to about 52% transmission between the OFF and ON states and the 61 μm thick films switch between 7% and 21% (note that the absolute values for the percent transmission are highly dependent on the optical arrangement used to make the measurements, however, the general trends are valid). Much of the light lost when passing through the PDLC shutters results from front and back surface reflections from the germanium substrates. We used antireflection coatings on the germanium to increase the transmission through the substrates from about 22% to 60% .

We incorporated the 61 μm thick PDLC shutter with antireflection coatings in an infrared video camera. The camera with this shutter could be used to image objects in our laboratory such as computer monitors and human faces. We did not measure the sensitivity of the camera with this shutter, however, from visual observation it is clear that the sensitivity has been greatly increased.

DETECTED IMAGE BRIGHTNESS AS A FUNCTION OF TARGET
TEMPERATURE FOR MECHANICAL AND ELECTRO-OPTIC
SHUTTERING CONFIGURATIONS USING THE MODEL 86
THERMAL IMAGING SYSTEM

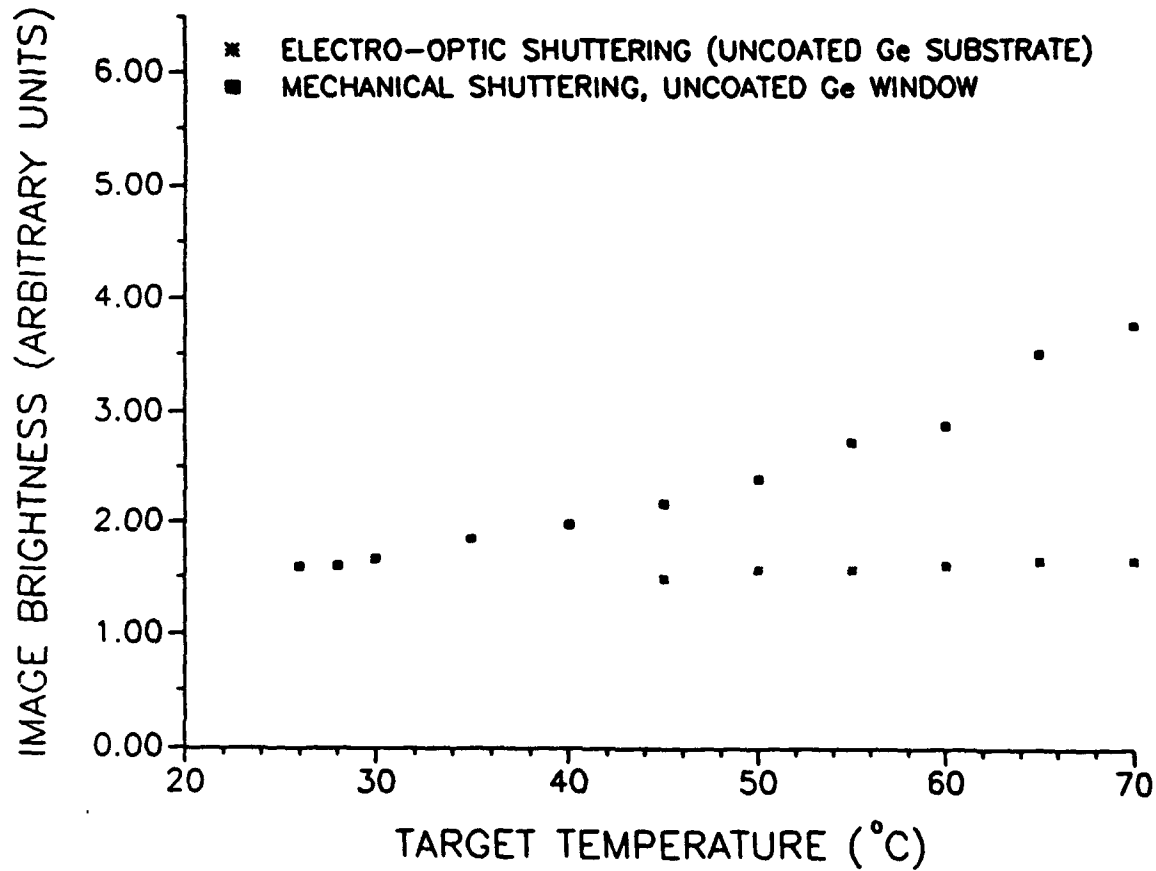


Figure 40: Measured image brightness as a function of temperature.

Substrate	film thickness d (μm)	droplet diameter (μm)	$\lambda = 2-5\mu\text{m}$			$\lambda = 8-14\mu\text{m}$				
			%T _{ON}	%T _{OFF}	C*	%T _{ON}	%T _{OFF}	C*	V ₉₀ [†] (volts)	τ_{OFF} (ms)
Ge	10	20-25	18.8	8.9	2.1	23.9	21.9	1.1	-	24
AR ctd. Ge	10	20-25	30.7	17.8	1.7	60.4	56.1	1.1	29.1	16
AR ctd. Ge	26	10-25	28.2	7.4	3.8	51.0	34.2	1.5	13.4	254
AR ctd. Ge	61	10-25	15.8	3.3	4.8	23.0	11.2	2.1	19.0	941

* C* = %T_{ON}/%T_{OFF}

† Measured for electro-optic response for $\lambda = 8-14\mu\text{m}$

Table 9: Electro-optic characteristics of several PDLC films.

10.1 Temporal Response

Since the IR detection system is sensitive to changes in intensity and not absolute intensity, the contrast capability of the IR switch is important. Furthermore, since there is a response time to the IR detector, the temporal modulation characteristics of the PDLC are important. Modulation characteristics as a function of droplet sizes were investigated.

As expected, the observed turn-off times for the PDLC devices are large (Table 9). Increasing the diameter of PDLC droplets yields longer turn-off times. The turn-off time is defined as the time for transmission to fall from 90% to 10% after removal of an rms voltage required to attain 90% of the overall device transmittance, V_{90} . It is unusual that the turn-off times measured in our experiments vary as a function of film thickness. The turn-off times presented in Table 9 vary from tens of milliseconds for the 10 μm shutters to almost a full second for the 61 μm sample. V_{90} values presented in Table 9 should increase with increasing PDLC film thickness, but instead are nearly constant for our experiments. This indicates that the droplet size or shape of the PDLC film varies with thickness.

10.2 Transmission Enhancement

Measurements were also performed on direct transmittance of the PDLC films for various voltages and film characteristics. These are shown in Fig. 41.

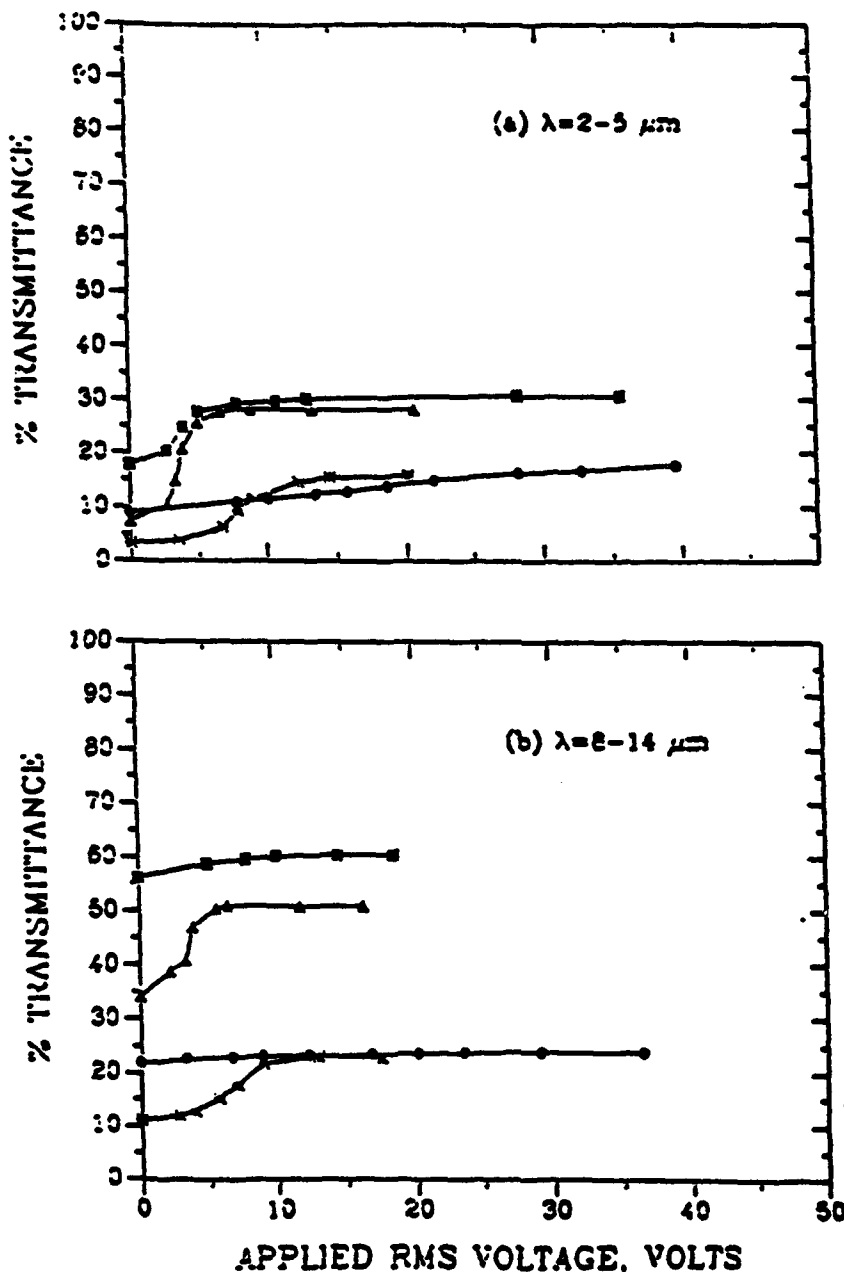


Figure 41: IR Transmission as a function of applied voltage. (o) Germanium uncoated substrate, $d=10 \mu m$ (square) AR coated Ge substrate, $d=10 \mu m$ (triangle) AR coated Ge substrate, $d=26 \mu m$ (*) AR coated Ge substrate, $d=61 \mu m$.

10.3 Angular Distribution of Scattering

Measurements of angular distribution of scattered light from PDLC films were carried out.

Below is a schematic of the experimental apparatus used for electro-optic and differential scattering measurements. The in-plane scattering plane is defined by the incident and scattered wave vectors (k and k_1 respectively) and the angle δ between the optical axis and k_1 . The black body radiator (Infrared Industries) was operated at 900 degrees C for all measurements. The black body radiation was modulated at 1 kHz and the beam collimated by a zinc-selenide lens and aperture combination on a layered InSb ($2 - 5 \mu m$)/MCT ($8 - 14 \mu m$) detector configuration contained in a dewar mount (E, G & G Judson). The detected signal was amplified by a dual preamplifier and processed by a lock-in amplifier (Stanford Research Systems Model SR510). The output of the lock-in amplifier was fed to a Zenith PC for scattering measurements and an oscilloscope (Hewlett-Packard Model 54501 A) for measuring electro-optic properties (transmittance in the ON and OFF states, driving voltage and turn-off time). Infrared PDLC shutters were modulated with a gated AC pulse of varying amplitude and duration. FTIR spectra were recorded with a Perkin-Elmer Model 1310 IR spectrophotometer.

The following figure illustrates the effect of droplet size on angular scattering. The PDLC was $26 \mu m$ thick with anti-reflective coated Ge substrates. The incident radiation was polychromatic and unpolarized. As can be seen from the figure, the effect of droplet size on the scattering profiles is pronounced. For $2 - 5 \mu m$ and $8 - 14 \mu m$ incident radiation, there is an increase in the angular scattering with droplet size, as expected. Very little scattered radiation is detected for $8 - 14 \mu m$ radiation when the droplet size is $\approx 2 \mu m$. It should be noted that in both cases, only the detected intensity at $\delta > 13$ degrees is truly scattered and transmitted radiation, evidenced by comparing the background curves to those for the PDLC. At $\delta = 0$ degrees (normal incidence), only transmitted radiation is detected. Differences in the off-state transmission at normal incidence may be due to back-scattering. No back scattering was evident between $\delta = 90$ degrees and $\delta = 150$ degrees. Angles beyond 150 degrees were inaccessible due to geometric constraints of the experimental set-up.

These figures show that there is very strong forward scattering. Beyond $8 - 10$ degrees intensity has dropped by over two orders of magnitude in all cases.

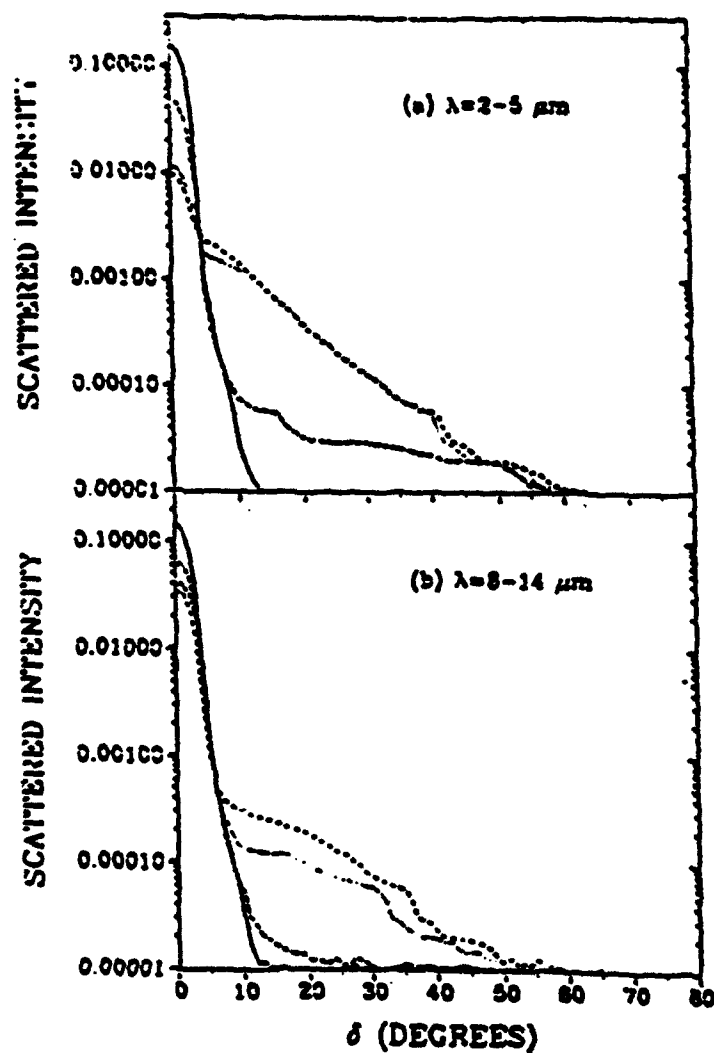


Figure 42: Angle dependence of scattering from a $26 \mu\text{m}$ thick AR coated Ge substrate PDLC with (a) $2-5 \mu\text{m}$ and (b) $8-14 \mu\text{m}$ incident radiation. Droplet sizes are $\approx 2 \mu\text{m}$ (dash-dot), $10 - 25 \mu\text{m}$ (dots), $15 - 30 \mu\text{m}$ (solid) and background (dashes).

11 Summary, Conclusions and Recommendations

11.1 Summary

This investigation has concluded that there are a number of large optical nonlinearities in liquid crystals which have potential application in Optical Power Limiting devices. They cover the temporal range of CW to approximately one nanosecond. We are less certain of the applicability of liquid crystals in the picosecond domain, but there is reason to expect that the useful nonlinearities extend to subnanoseconds. We are not, however, ruling out the usefulness in the picosecond regime.

In the scientific literature, both before and during the course of this investigation, there were reports of various large optical nonlinearities in liquid crystals over this whole temporal domain. A fundamental element of our investigation was the measurement of a variety of liquid crystals to determine whether the reported nonlinearities were peculiar to a one or a few liquid crystal species and whether larger nonlinearities were available through a simple process of searching. A second fundamental element of our research was to clarify the mechanisms responsible for the observed nonlinearities. Finally, we also participated in analysis of potential applications and device prototype development.

11.2 Conclusions

The technical data presented in this report and the Quarterly Scientific and Technical Reports as well as the information obtained from other contractors during this period lead us to the following conclusions.

- In the CW regime, there is certainly sufficiently effective OPL behavior of a variety of liquid crystals for device development. The active feedback prototype delivered under this contract clearly demonstrated one particular design. This design is robust, capable of being fitted to a variety of devices needed in the field and capable of offering protection on a wide range of time scales.

The passive OPL behavior that we investigated in this contract is much less developed than the active form. There is need for a fundamental alteration of the manner in which a passive OPL device is designed if it is to have the effectiveness of the active device. There is reason to believe that such alterations are possible, but they will at present have to be tailored to the specific environment and specifications of field devices. If certain device specifications allow compromise, such as response

time, temperature range or insertion loss, then variations such as dyed liquid crystals or temperature controlled liquid crystals may be acceptable in passive devices. In any case, since passive functionality necessitates that the active characteristic for power limiting be inherent to the material, more research on the mechanisms of alternative liquid crystal materials, such as mixtures and composites, will be needed to move this form of OPL action towards field applications.

- The regime of nanosecond OPL was one of the other successes of this investigation. Our group was the first to offer 5CB as an effective OPL material. This initiated the discovery of several materials with large nonlinear optical parameters. (Other contractors discovered other liquid crystal materials with similarly encouraging properties.) This made it clear that there was device potential in this time regime as well. A major effort was undertaken to determine the mechanism for the observed nonlinearity. This effort was undertaken to avoid random searching for nonlinear enhancement as well as a way to obtain a theoretical understanding that could be used in device modeling.

Our investigations into mechanism were successful, but left several questions incompletely resolved. The positive aspect of our results is that we now know that effective OPL is accompanied by more than simply a large nonlinear refractive index. We found strong nonlinear absorption and the presence of higher-order nonlinearities. The two photon absorption, which we and others observed, seems to be an important mechanism for removing beam intensity in the OPL process. While this is reasonable in and of itself, two other questions are raised. First, why is the nonlinear absorption increased by the presence of dyes (linear absorption) in the liquid crystal. Second, where does the energy go which has been absorbed. Simple conversion of electromagnetic energy to thermal energy (by whatever relaxation mechanism) can not be effective in the nanosecond time scale. The energy blocked by the OPL is enough to vaporize the sample. This is both a positive and negative. It is positive because other competing materials which rely on absorption as the OPL mechanism will suffer heating and thus have a restricted dynamic range. Our damage studies showed that the liquid crystal could not be damaged (instead the sample cell or surface alignment layer was damaged). Such is not the case for some proposed semiconductor based OPLs. The negative aspect of the role of nonlinear and linear absorption is that we do not finally know what the operative absorption mechanism is or how it enhances the overall nonlinear activity of the OPL.

- The effectiveness of liquid crystals as optical power limiters in the picosecond regime is still an open question. It is clear that new mechanisms become operative on this time scale, and it was one of the successes of these investigations that we discovered that the nonlinear activity of the liquid crystal continues to function when the pulse duration is reduced by a factor of a thousand. The reason for the nonlinear behavior of the liquid crystal in this regime is almost certainly contains a contribution from

purely electronic hyperpolarizability of the molecules. If this is indeed the primary effect, then it is likely that nonliquid crystalline organic materials (e.g. highly conjugated polymers) will be found to be superior in OPL applications.

Still, liquid crystals offer potential in the picosecond regime. First, it is possible that mechanisms in addition to the electronic mechanism are operative. Such would not be expected in the case of conjugated polymers. The other mechanisms, such as long axis rotation, go hand in hand with other normal physical properties such as the fluidity of the liquid crystals. Fluidity, for example, also conveys another desirable effects, that of self healing in the event of damage. (If a OPL medium is fluid, then a damaged area will disperse.)

- The IR Shutter project was funded as part of this contract even though it had nothing to do with nonlinear optics. It was however based on liquid crystal composites and it was relevant to the mission of the funding agency.

While this research project established the shuttering capability of liquid crystal composites in the IR, it fell short of establishing the materials as a potential replacement of mechanical shutters presently in use. This project did not conclude that liquid crystals were unsuitable for shuttering applications, it simply did not establish that they were suitable.

When the project ended, the use of a liquid crystal shutter in an IR imaging system had been demonstrated. We were not able to show the potential use for in night vision applications and did not find materials that *fully met the specifications* we were given for night vision applications.

11.3 Recommendations

In all the areas described above, considerable experimental and theoretical understanding of the systems was achieved. The value of this data would have been greater had a better understanding of the interface of the contract work and the system applications been achieved earlier in the project. For example, we were three years into the project before written criteria for measurement of OPL performance were provided to the contractors, and it was a year after that before the first independent measurements in an actual device were performed by the contracting agency. Even then, we did not receive feedback on the performance of the device prototype that we provided.

The continuation of work in this area, the use of liquid crystals in optical power limiting applications, is strongly advised. As a result of the past research, enormous advances toward that application, as well as scientific advances, have been made. Our recommendation is that future efforts involve a more informed cooperative

venture, where the researcher does research and the device developer addresses engineering issues while communicating with each other.

There are really two avenues that are separately identifiable as needed for advancements that are not just hit or miss. These are further measurement and mechanism study. First, having identified the dozens of other compounds that maybe useful, they should be measured for the various nonlinear parameters and tested for optical power limiting. This is more than just putting it in a sample holder and seeing the power limiting curves. There is clearly more going on than just a bigger and better nonlinear index of refraction, so both power limiting properties and nonlinear parameters need to be measured for about 30 or 40 other compounds. Secondly, the mechanism for the power limiting is still obscure and needs more study. We have managed to eliminate more wrong guesses than we have been able to identify mechanisms. No device is optimized during its development and the devices under consideration here can benefit greatly from a well defined program that builds on what we learned already in materials and device physics.

References

- [1] Y. R. Shen, Personal communication.
- [2] P. Palffy-Muhoray in *Liquid Crystals, Applications and Uses*, Vol. 1, ed. Birendra Bahadur (World Scientific, Singapore, 1990).
- [3] I. C. Koo, in *Progress in Optics XXVI*, ed. E. Wolf (North Holland, New York, 1988).
- [4] P. Palffy-Muhoray *et. al.*, *Mol. Cryst. Liq. Cryst.* **207**, 291 (1991).
- [5] L. Li, P. Palffy-Muhoray, M. A. Lee and H. J. Yuan in *Symposium on Optical Engineering and Photonics in Aerospace Sensing*, SPIE Proc., Orlando, FL, 1992; L. Li, H.J. Yuan, G. Hu, and P. Palffy-Muhoray, *Liq. Cryst.*
- [6] G. K. L. Wong and Y. R. Shen, *Phys. Rev. Lett.* **30**, 895 (1973).
- [7] J. Prost and J. R. Lalanne, *Phys. Rev. A* **8**, 2090 (1973).
- [8] D. Armitage and S. M. Delwart, *Mol. Cryst. Liq. Cryst.* **122**, 59 (1985).
- [9] H. J. Coles, *Mol. Cryst. Liq. Cryst.* **49**, 67 (1978).
- [10] M. Sheik-bahae, A. A. Said and E. W. Van Stryland, *Optics Lett.* **14**, 955 (1989).
- [11] Mansoor Sheik-bahae, Ali A. Said, Tai-Huei Wei, David J. Hagan and E. W. Van Stryland, *IEEE Journal*
- [12] P. G. de Gennes, *Mol. Cryst. Liquid Cryst.* **12**, 193 (1971).
- [13] K. C. Chu, C. K. Chen and Y. R. Shen, *Mol. Cryst. Liq. Cryst.* **59**, 97 (1980).
- [14] J. W. Emsley, G. R. Lockhurst and C. P. Stockley, *Mol. Phys.* **44**, 565 (1981).
- [15] P. G. de Gennes, *The Physics of Liquid Crystals*, Oxford University Press (Oxford 1974).
- [16] G. S. Iannacchione and D. Finotello, *Phys. Rev. Lett.* **69**, 2094 (1992).
- [17] S-T Wu and K-C Lim, *Appl. Opt.* **26**, 1722 (1987).
- [18] C. W. Greeff, J. Lu and M. A. Lee, *Liq. Cryst.*
- [19] Haiji Yuan, Doctoral Dissertation, Kent State University (1991).
- [20] S. Risser, D. W. Allender, Michael A. Lee and K. E. Schmidt, *Mol Cryst. Liq. Cryst.* **179**, 335 (1990).

- [21] J. Prost and J. R. Lalanne, *Phys. Rev. A* **8**, 2090 (1973).
- [22] H. Kogelnik and T. Li, *Applied Optics* **5**, 1550 (1966).
- [23] J. D. Jackson, *Classical Electrodynamics*, Second Edition (Wiley, New York 1975).
- [24] D. Weaire, B. S. Wherrett, D. A. B. Miller and S. D. Smith, *Opt. Lett.* **4**, 331 (1974).

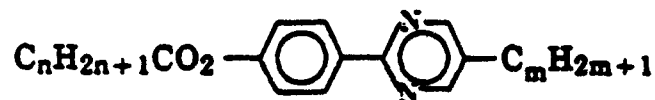
A Appendix: Materials Survey

To help separate and identify the operative mechanisms for OPL, we systemized our selection of the class of materials to be studied. The following properties and selection criteria were applied in our literature search.

1. A solid to nematic or smectic transition should occur near or below room temperature and have a range of at least 10 degrees C or more to facilitate experimental measurement.
2. The material should be chemically stable to eliminate uncertainties about contaminants contributing to or masking nonlinear effects. Similarly, laser induced reactions would unnecessarily complicate analysis at this stage.
3. Transparency in the IR and visible range is highly desirable.
4. Chemical breadth was desired. We sought compounds with:
 - (a) Varying sizes of conjugated cores
 - (b) Varying linkages between benzene rings
 - (c) Varying substituent groups
 - (d) Ease of synthesis or even possible commercial availability.
 - (e) Simple and small conjugation structures to facilitate theoretical calculations

Except for requirements that a nematic or smectic exist at a temperature accessible to the laser measurement facility, none of the above criteria were deemed absolute. We compiled a list of materials which satisfy all or most of the above. This list was used by us in the selection of nonlinear materials. Those selected were purchased or synthesized and are listed in Sec. 8.2 along with additional materials used in the study. This list is provided as part of our recommendations for further materials evaluation. Appendix A and the tables in Sec. 5.1 contain the measurement results.

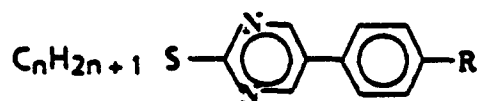
1.



n	m	K →	N →	I
5	6	36	37.5	
7	6	38.5	44	

Z. Chem 15, 441 (1975), Zaskkett, H., Stolle, R.

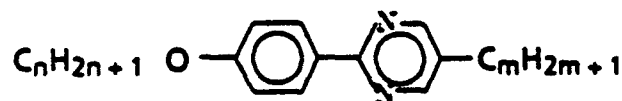
2.



R = alkyl, alkoxy	n	K →	S _A →	I
	4-6	~25	~76	

Z. Chem. 17, 293 (1977).

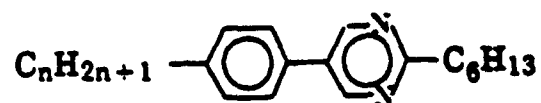
3.



n	m	K →	N →	I
5	4	36	(.32)	
4	8	35	60	

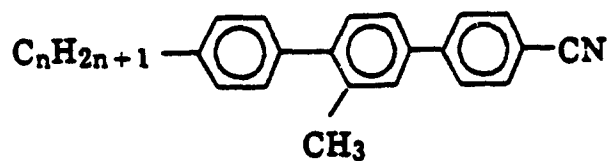
J. Prakt. Chem. 317, 617 (1975), Zaskkett, H.

4.



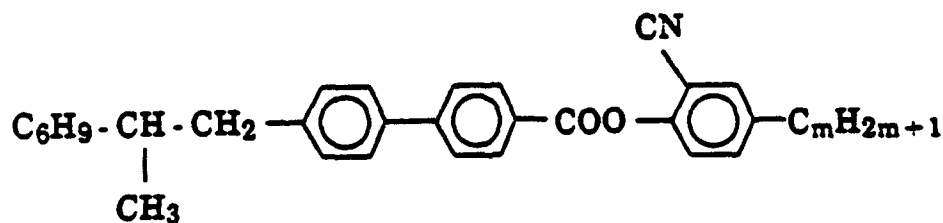
n	K →	S _A →	I
2	30	(.28)	
3	23	32	
4	24.5	44	

5.



n=8	K →	S _A →	N →	I
	37.4	47.8	86.9	

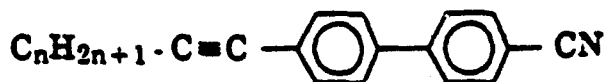
6.



m	K →	N →	I
8	29	71	
5	37	49.5	

CA 88, 137448
 Erdmann D., DZ-OS 2613293 (1977)

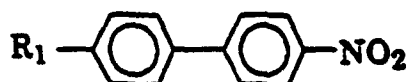
7.



n	K	→	S _A	→	N	→	I
7	32.4		50.1		53.8		
8	35				50.3		

Adomens, P., et al., *Adv. in Liquid Crystal Research and Application* (ed. by L. Bata) Oxford: Pergamon Press; Budapest: Akademiai Kiado 1980, S. 1029.

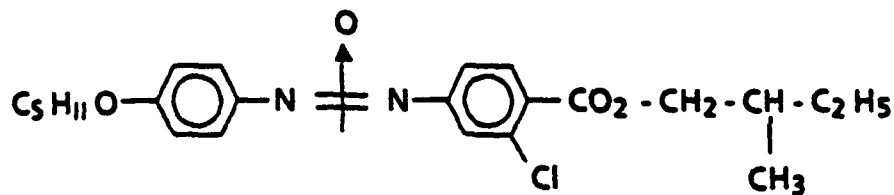
8.



R ₁	K	→	S _E	→	N	→	I
C ₅ H ₁₁ O	56.5						
C ₆ H ₁₃ O	67						
C ₇ H ₁₅ O	36.5				38.5		

J. Phys. (Paris) Coll. C1, 36, 337 (1975).
Gray, G.W.

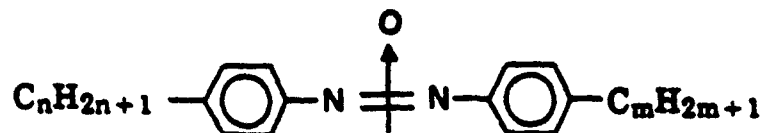
9.



K	→	N	→	I
37		44.5		

Zh. Org. Khim. 16, 138 (1980).
Bezborodov, V.S.

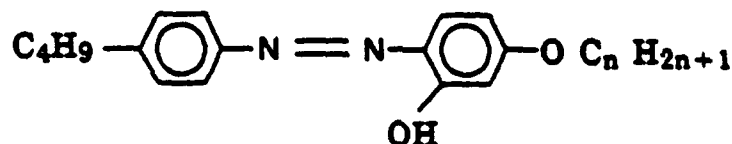
10.



n	m	K	N	I
2	3	14	33	
2	5	5	40.5	

MCLC 61, 61 (1980).

11.



n	K	N	I
7	23	79	
8	27	81.5	
9	36	80	

Angew. Chem. 86, 378 (1976).
Van Der Veen, J.

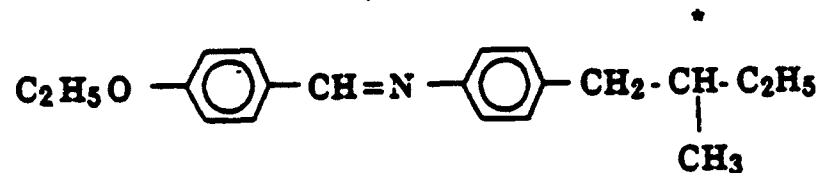
12.



n	m	K	N	I
3	6	23	92	
3	8	28	89	

Mailer, H., DE-OS 2852881 (1979).
MCLC 35, 155 (1976), MCLC 41, 141 (1978).

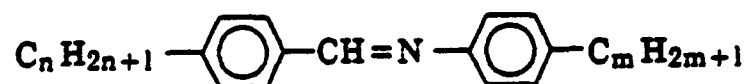
13.



K → N → I
29 60.1

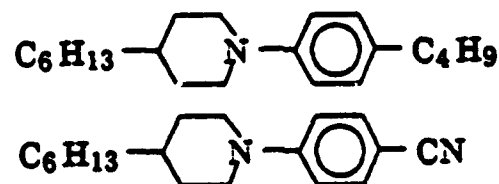
J. Chem. Phys. 58, 413 (1973)

14.



n m K → S_B → I
3 5 27.1 37.1

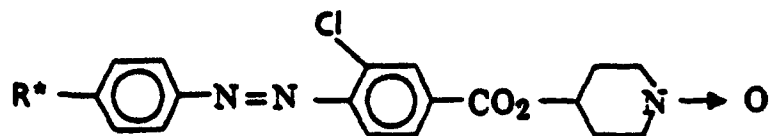
15.



K → S_B → N → I
20 44
R = CN K → N → I CN
30

MCLC 67, 241 (1981).

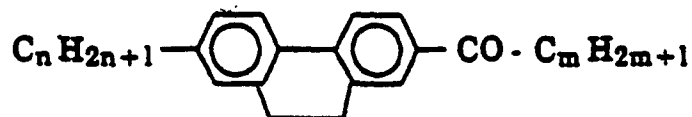
16.



K → N → I
35

ABS 4, LCCSL 1981 (C11)

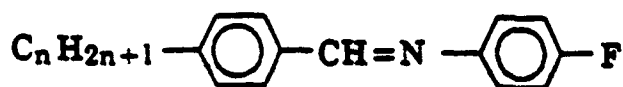
17.



n m K → S_A → N → I
8 4 22.5 31.5 33

International Liquid Crystal Conference, 397, (1973)
Am. Phys. (Paris) 3, 131 (1978).

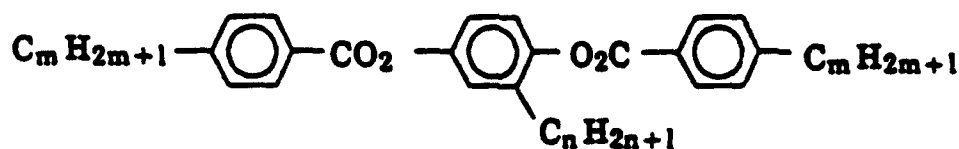
18.



n K → N → I
6 26 --
7 25 (8.5)

Billard, J., Dubois, J.C., *J. Phys. (Paris) Coll. C1* 36, C1-355 (1975).

19.



m	n	K →	N →	I
7	6	19	41	
5	6	33.5	41	
6	6	29		

Crys. Res. Technol. 19, 55 (1984), Weissflog, W., Demus, D.

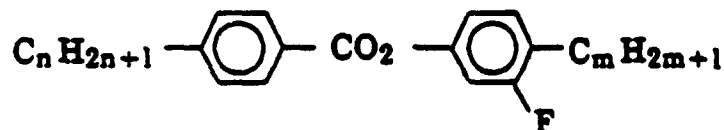
20.



n	m	K →	N →	I
5	4	28	34.7	
4	4	13.9	22.5	

Reynolds, R., et al., MCLC 36, 41 (1976).

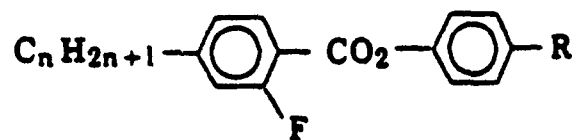
21.



n	m	K →	N →	I
Several		~room temp.	~R.T.	

MCLC 67 1 (1981).

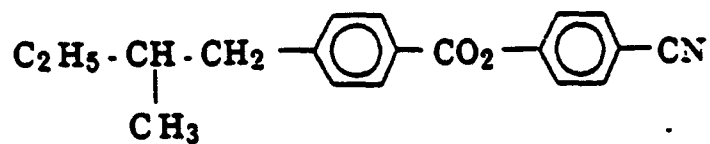
22.



n	R	N	I
1	CH ₃	2.0	r.t.
to	F	50	
18			

MCLC 67, 1 (1981).

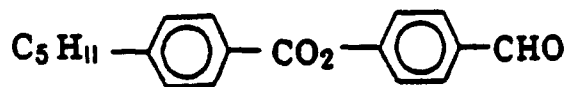
23.



K	N	I
37		

JACS 90, 1585 (1985).

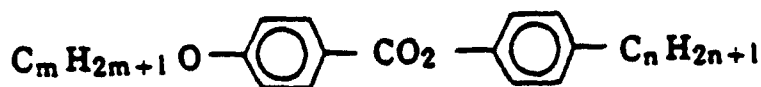
24.



K	N	I
33.8	(.24)	

Osman, M.A., DE--OS2716610 (1978).

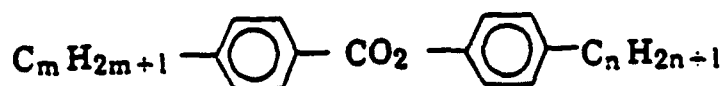
25.



m	n	K	N	I
1	5	29	42	

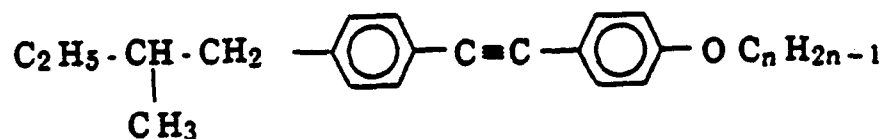
Z. Naturforsch 27b, 774 (1972), Steintraser, R.
Arora, S., U.S. - Pat 4086002 (1978).

26.



n	m	K	N	I
vary		15°-50°	15°-50°	

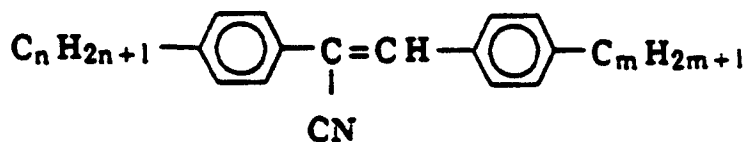
27.



n	K	N	I
5	26	42	
6	30.5	51.8	

CA 95, 124545 (1981)

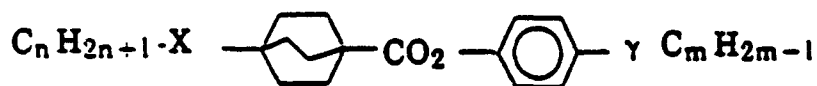
28.



$\begin{matrix} n & m & K \rightarrow & N \rightarrow & I \\ 6 & 5 & 29 & 48.3 \end{matrix}$

Zh. ObsLch. Khim. 46, 2125 (1976), Daugvila, J.

29.



$\begin{matrix} n & m & K \rightarrow & N \rightarrow & I \\ & & & 50-60 \end{matrix}$

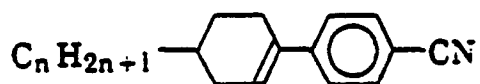
$X=\gamma=-, O, \text{CO}_2^-$

vary

RT

MCLC 75, 95 (1981); 67, 109 (1981).

30.



$\begin{matrix} n & K \rightarrow & N \rightarrow & I \\ 4 & 31 & 44 \end{matrix}$

CA 92, 6287 (1978)

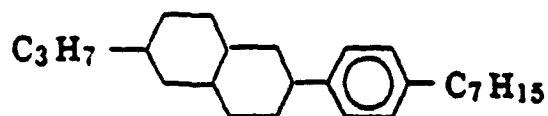
31.



K \rightarrow N \rightarrow I
~20 37~40

Sato, H., et al., CA 91, 210978 (1979).

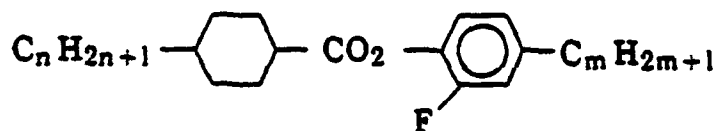
32.



K \rightarrow N \rightarrow I
22.6 38.7

Helv. Chim. Acta 65, 1242 (1982), Petrzilka, M.

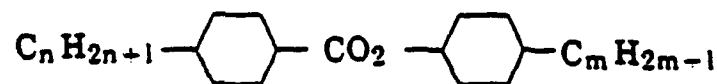
33.



K \rightarrow N \rightarrow I
R.T. R.T. or ~50°

Gray, G., et al., MCLC 67, 1 (1981).

34.



K \rightarrow N \rightarrow I
R.T. 35~50°

Adv. in LC Research (1980), S1075, Deutscher, H. J.

A Appendix: Data Sheets and Results Tabulation

The attached data sheets and tabulation of properties, including χ^3 values and nonlinear parameters were provided as part of the Scientific and Technical Reports during the course of the contract and are reproduced here for completeness.

Name of Organization: LIQUID CRYSTAL INSTITUTE, KENT STATE UNIVERSITY

Principal Investigator: Michael A. Lee (Co-PIs: Peter Palfy-Muhoray, John L. West, Liang-Chy Chien, J. William Doane)

Material: 21.1-2303 phenylpyrimidine Measurement: resonant _____; nonresonant _____ x

$\chi_{ R_e}^{(j)}$ (esu)	n_i (esu)	$\tau_{ }$ (sec)	τ_{\perp} (sec)	$\Delta\lambda$ (nm)	α (cm ⁻¹)	$\chi_{\perp}^{(j)}$ (esu)	d_o (micron)	ℓ_o (micron)	ℓ_o (ℓ_o)
-------------------------------	----------------	----------------------	-------------------------	-------------------------	---------------------------------	-------------------------------	-------------------	----------------------	--------------------------

Present Value $\chi_{||R_e}^{(j)} = -0.26 \times 10^{-4}$; $n_2 = -0.97 \times 10^{-4}$

Present Best

Estimated Max.
Attainable

What must be done to attain this maximum value?



PYP-606

32°C 61°C

C → N → I

Measured at $\lambda = 514.5\text{nm}$, $\tau = 10 \times 10^{-9}\text{ sec}$

T = 45°C for nematic phase

T = 85°C for isotropic phase

$n_{2\perp} = +0.082 \times 10^{-4}(\text{esu})$

$n_{2i} = -0.30 \times 10^{-4}(\text{esu})$

β — not observed under the same intensity used to measure n_2

$\chi_{\perp R_e}^{(j)} = +0.019 \times 10^{-4}(\text{esu})$

$\chi_{\perp R_e}^{(j)} = -0.075 \times 10^{-4}(\text{esu})$

Name of Organization: LIQUID CRYSTAL INSTITUTE, KENT STATE UNIVERSITY

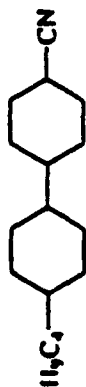
Principal Investigator: Michael A. Lee (Co-PIs: Peter Palffy-Muhoray, John L. West, Liang-Chy Chien, J. William Doane)

Material: 21.1-1538 cyclohexylcyclohexane Measurement: resonant; nonresonant \times

	$\chi^{(2)}$ (esu)	n_o (esu)	τ_{ω} (sec)	τ_{ω} (sec)	$\Delta\lambda$ (nm)	α (cm ⁻¹)	$\chi^{(2)}$ (esu)	d_o (mksa)	f_o (mksa)	f_o (eJ)
Present Usual	$\chi_{ Re}^{(2)} = -0.11 \times 10^{-4}$; $n_{2H} = -0.43 \times 10^{-4}$									
Present Best										
Estimated Max. Attainable										

What must be done to attain this maximum value?

Comments



XC11-4

$$n_{2L} = -0.13 \times 10^{-4}(\text{esu})$$

$$n_{2H} = -0.35 \times 10^{-4}(\text{esu})$$

β — not observed under the same intensity used to measure n_2

$$\chi_{\perp Re}^{(2)} = -0.031 \times 10^{-4}(\text{esu})$$

$$\chi_{\perp Re}^{(2)} = -0.088 \times 10^{-4}(\text{esu})$$

28°C 54°C 79°C



Measured at $\lambda = 514.5\text{nm}$, $\tau = 10 \times 10^{-9} \text{ sec}$.

T=70°C for nematic phase

T=97°C for isotropic phase

MATERIALS PROPERTIES QUESTIONNAIRE

(See instruction sheet)

Name of Organization: LIQUID CRYSTAL INSTITUTE, KENT STATE UNIVERSITY

Principal Investigator: Michael A. Lee (Co-PIs: Peter Palffy-Muhoray, John L. West, Liang-Chy Chien, J. William Doane)

Material: CH15 Measurement: resonant; concentration: x

	X^{90} (esu)	n_i (esu)	τ_{90} (sec)	τ_{90} (sec)	$\Delta\lambda$ (nm)	α (cm ⁻¹)	X^{90} (esu)	d_p (mksc)	Γ_p (mksc)	ϵ_p (ϵ)
Present Value										
Present Best										
Estimated Max. Attainable										

$\chi_{111}^{(3)} = -0.063 \times 10^{-4}$; $n_2 = -0.25 \times 10^{-4}$ 0.1

What must be done to attain this maximum value?



n_{21} not measured because our temperature cannot be cooled below 22°C
 n_{21} not measured because our temperature cannot be cooled below 22°C
 β — not observed under the same intensity used to measure n_2

CH15

14°C -30°C

C → I; Ch → I

Measured at $\lambda = 514.5\text{nm}$, $\tau = 10 \times 10^{-3}$ sec

T=22°C for isotropic phase

Name of Organization: LIQUID CRYSTAL INSTITUTE, KENI STATE UNIVERSITY

Principal Investigator: Michael A. Lee (Co-PIs: Peter Palfy-Muhoray, John L. West, Liang-Chy Chien, J. William Doane)

Material: T15 4-cyano-4'-n-alkyl-p-terphenyl Measurement: resonant _____; nonresonant _____ x

$X_{ Re}^{(3)}$ (esu)	n_i (esu)	$\tau_{ }$ (sec)	τ_{\perp} (sec)	$\Delta\lambda$ (nm)	α (cm ⁻¹)	$X_{\perp}^{(3)}$ (esu)	d_e (mksa)	ϵ_e (mksa)	ϵ_o (CJ)
---------------------------	----------------	----------------------	-------------------------	-------------------------	---------------------------------	----------------------------	-----------------	------------------------	----------------------

Present Value $X_{||Re}^{(3)} = -0.19 \times 10^{-4}$; $n_2 = -0.68 \times 10^{-4}$

Present Best

Estimated Max.
Attainable

What must be done to attain this maximum value?



$n_{2\perp} = -0.092 \times 10^{-4}$ (esu)

$n_{2i} =$ not measured

T15

β — not observed under the same intensity used to measure n_2

131°C 240°C

C \rightarrow N \rightarrow I

$X_{\perp Re}^{(3)} = -0.022 \times 10^{-4}$ (esu)

$X_{i Re}^{(3)} =$ not measured

Measured at $\lambda = 514.5$ nm, $\tau = 10 \times 10^{-3}$ sec

T = 180°C for nematic phase

(See instruction sheet)

Name of Organization: LIQUID CRYSTAL INSTITUTE, KENT STATE UNIVERSITY

Principal Investigator: Michael A. Lee (Co-PIs: Peter Palffy-Muhoray, John L. West, Liang-Chy Chien, J. William Doane)

Material: T15 4-cyano-4'-n-alkyl-p-terphenyl Measurement: resonant _____; nonresonant _____

$\chi^{(2)}$ (esu)	n_1 (esu)	τ_m (sec)	$\Delta\lambda$ (nm)	α (cm ⁻¹)	$\chi^{(2)}$ (esu)	d_{ij} (mksa)	f_c (mksa)	ϵ_c (eJ)
-----------------------	----------------	-------------------	-------------------------	---------------------------------	-----------------------	--------------------	-----------------	----------------------

Present Usual $\chi_{||Re}^{(2)} = -14 \times 10^{-11}$; $n_{2||} = -52 \times 10^{-11}$

Present Best

Estimated Max.
Attainable

What must be done to attain this maximum value?

$$n_{2\perp} = +21 \times 10^{-11} \text{ (esu)} \quad \chi_{||lm}^{(2)} = 12.6 \times 10^{-11} \text{ (esu)}$$



$$n_{2i} = \text{not measured} \quad \chi_{\perp lm}^{(2)} = 0.64 \times 10^{-11} \text{ (esu)}$$

$$\chi_{\perp Re}^{(2)} = +5.0 \times 10^{-11} \text{ (esu)} \quad \chi_{ilm}^{(2)} = \text{not measured}$$

$$\chi_{iRe}^{(2)} = \text{not measured (esu)}$$

131°C 240°C



$$\beta_{||} = 270 \left(\frac{\text{cm}}{\text{Å}} \right)$$

Measured at $\lambda = 532 \text{ nm}$, $\tau = 7 \times 10^{-9} \text{ sec}$

$$\beta_{\perp} = 18 \left(\frac{\text{cm}}{\text{Å}} \right)$$

T = 180°C for nematic phase

$$\beta_i = \text{not measured}$$

Name of Organization: LIQUID CRYSTAL INSTITUTE, KENT STATE UNIVERSITY

Principal Investigator: Michael A. Lee (Co-PIs: Peter Palffy-Muhoray, John L. West, Liang-Chy Chien, J. William Doane)

Material: ZLI-2303, Phenylpyrimidine

Measurement: resonant; nonresonant x

$\chi^{(2)}$ (esu)	n_o (esu)	τ_m (sec)	$\Delta\lambda$ (nm)	α (cm ⁻¹)	$\chi^{(2)}$ (esu)	d_o (mksa)	f_o (mksa)	ϵ_o (ϵ)
Present Usual	$\chi_{ lc}^{(2)} = -5.4 \times 10^{-11}$; $n_{2 } = -20 \times 10^{-11}$			0.1				10

Present Best

Estimated Max.
Attainable

When must be done to attain this maximum value?



PYP-606

32°C 61°C

C → N → I

Measured at $\lambda = 532\text{nm}$, $\tau = 7 \times 10^{-9}\text{ sec}$

T = 45°C for nematic phase

T = 85°C for isotropic phase

$$n_{2\perp} = +3.0 \times 10^{-11}(\text{esu})$$

$$\chi_{||lm}^{(2)} = 3.1 \times 10^{-11}(\text{esu})$$

$$n_{2i} = -3.8 \times 10^{-11}(\text{esu})$$

$$\chi_{\perp lm}^{(2)} = 0.29 \times 10^{-11}(\text{esu})$$

$$\chi_{\perp R_e}^{(2)} = +0.71 \times 10^{-11}(\text{esu})$$

$$\chi_{i lm}^{(2)} = 0.75 \times 10^{-11}(\text{esu})$$

$$\chi_{i R_e}^{(2)} = -0.95 \times 10^{-11}(\text{esu})$$

$$\beta_{||} = 67 \left(\frac{\text{esu}}{\text{cm}} \right)$$

$$\beta_{\perp} = 8.2 \left(\frac{\text{esu}}{\text{cm}} \right)$$

$$\beta_i = 19 \left(\frac{\text{esu}}{\text{cm}} \right)$$

(See instruction sheet)

Name of Organization: LIQUID CRYSTAL INSTITUTE, KENT STATE UNIVERSITY

Principal Investigator: Michael A. Lee (Co-PIs: Peter Palffy-Muhoray, John L. West, Liang-Chy Chien, J. William Doane)

Material: 211-1538, Cyclohexylcyclohexane

Measurement: resonant scattering

$X_{||}^{(2)}$ (esu) n_i (esu) λ (nm) α (cm⁻¹) $X_{||}^{(2)}$ (esu) d_o (micron) t_o (micron) ϵ_o (2J)

$\chi_{||}^{(2)}$ He = ; $n_{2||}$ = $\times 10^{-11}$

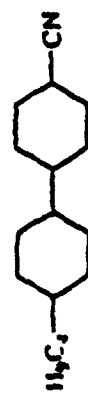
Percent Used

Percent Rest

Estimated Max. Available

What must be done to attain this maximum value?

$n_{2\perp}$ = $\times 10^{-11}$ (esu) $\chi_{||}^{(2)}$ = $\times 10^{-11}$ (esu)



n_{2i} = $\chi_{\perp}^{(2)}$ He = $\times 10^{-11}$ (esu)

$\chi_{\perp}^{(2)}$ He = $\times 10^{-11}$ (esu) $\chi_{||}^{(2)}$ =

$\chi_{||}^{(2)}$ He = (esu) $\beta_{||}$ = (esu)



Measured at $\lambda = 532$ nm, $\tau = 7 \times 10^{-9}$ sec

T = 70°C for nematic phase

No measurable nonlinearity was observed within our experimental error!

Name of Organization: LIQUID CRYSTAL INSTITUTE, KENT STATE UNIVERSITY
 Principal Investigator: Michael A. Lee (Co-PIs: Peter Palffy-Muhoray, John L. West, Liang-Chy Chien, J. William Doane)

Material: CN15 Measurement: resonant _____; nonresonant _____ x

$X_{ }^{(2)}$ (esu)	n_o (esu)	$\tau_{ }$ (sec)	τ_{\perp} (sec)	$\Delta\lambda$ (nm)	α (cm ⁻¹)	$X_{\perp}^{(2)}$ (esu)	d_o (micron)	f_o (micron)	E_c (eV)
$\chi_{ }^{(2)} = +2.0 \times 10^{-11}$; $n_2 = +7.4 \times 10^{-11}$ (esu)					~ 0.1				10

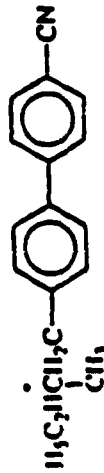
Present Best

Estimated Max.
Attainable

Which must be done to attain this maximum value?

 $n_{2||}$ not measured because our temperature cannot go below 22°C $n_{2\perp}$ not measured because our temperature cannot go below 22°C

Comments



CN15

14°C

-30°C

C \rightarrow I; Ch \rightarrow I $\chi_{\perp R_c}^{(2)}$ = not measured because our temperature cannot go below 22°C $\beta_{||}$ = not measured because our temperature cannot go below 22°C β_{\perp} = not measured because our temperature cannot go below 22°CMeasured at $\lambda = 532\text{nm}$, $\tau = 7 \times 10^{-9}$ sec

T = 24°C for isotropic phase

 $\chi_{||lm}^{(2)}$ = not measured because our temperature cannot go below 22°C $\chi_{\perp lm}^{(2)}$ = not measured because our temperature cannot go below 22°C $\chi_{||lm}^{(2)}$ = 1.5×10^{-11} (esu)

MATERIALS PROPERTIES QUESTIONNAIRE

(See instruction sheet)

KENT STATE UNIVERSITY

Name of Organization: LIQUID CRYSTAL INSTITUTE, KENT STATE UNIVERSITY

Principal Investigator: Michael A. Lee (Co-PIs: Peter Palffy-Muhoray, John L. West, Liang-Chy Chien, J. William Doane)

Material: 8CB 4-cyano-4'-n-octylbiphenyl Measurement: not used; not measured

$X_{ }^{(1)}$ (esu)	n_1 (esu)	$\tau_{ }$ (sec)	$\Delta\lambda$ (nm)	α (cm ⁻¹)	$X_{ }^{(2)}$ (esu)	d_p (micron)	r_p (micron)	ϵ_p (esu)
$X_{ }^{(1)} = -7.1 \times 10^{-11}$; $n_{2 } = -26 \times 10^{-11}$				0.1				10

Present Best

Estimated Max. Available

What must be done to attain this maximum value?



8CB (K24)

21.5°C

40.5°C



Measured at $\lambda = 532\text{nm}$, $\tau = 7 \times 10^{-9}$ sec

$T = 22^\circ\text{C}$ for smectic phase

$$n_{2\perp} = 3.7 \times 10^{-11} \text{ (esu)} \quad X_{||}^{(2)} = 11.4 \times 10^{-11} \text{ (esu)}$$

$$n_{2i} = \text{not measured} \quad X_{\perp}^{(2)} = 0.72 \times 10^{-11} \text{ (esu)}$$

$$X_{\perp}^{(2)} = +0.87 \times 10^{-11} \text{ (esu)} \quad X_{||}^{(2)} = \text{not measured}$$

$$X_{||}^{(2)} = \text{not measured}$$

$$\beta_{||} = 246 \left(\frac{\text{esu}}{\text{cm}^2} \right)$$

$$\beta_{\perp} = 20 \left(\frac{\text{esu}}{\text{cm}^2} \right)$$

$$\beta_i = \text{not measured}$$

(See instruction sheet)

Name of Organization: LIQUID CRYSTAL INSTITUTE, KENT STATE UNIVERSITY

Principal Investigator: Michael A. Lee (Co-Prs: Peter Palffy-Muhoray, John L. West, Liang-Chy Chien, J. William Boane)

Material: d_{22} doped (<0.2%) 8CB

Measurement: resonant ; observation x

$\chi_{ee}^{(2)}$ (esu)	n_e (esu)	τ_e (sec)	τ_e (sec)	$\Delta\lambda$ (nm)	u (cm ⁻¹)	$\chi_{ee}^{(2)}$ (esu)	d_e (mkSa)	ϵ_e (mkSa)	ϵ_e (C)
Present Usual	$\chi_{ee}^{(2)} = -41.3 \times 10^{-11}$	$n_{2H} = -152 \times 10^{-11}$							10

Present Best

Estimated Max.
Attainable

What must be done to attain this maximum value?

Comments

$$n_{2L} = +10.5 \times 10^{-11} (\text{esu}) \quad \chi_{ee}^{(2)} = 17.7 \times 10^{-11} (\text{esu})$$

$$n_{2i} = -48 \times 10^{-11} (\text{esu}) \quad \chi_{ee}^{(2)} = 1.1 \times 10^{-11} (\text{esu})$$

$$\chi_{ee}^{(2)} = +2.5 \times 10^{-11} (\text{esu}) \quad \chi_{ee}^{(2)} = 7.6 \times 10^{-11} (\text{esu})$$

Measured at $\lambda = 532\text{nm}$, $\tau = 7 \times 10^{-9} \text{ sec}$

$$\chi_{ee}^{(2)} = -12 \times 10^{-11} (\text{esu})$$

$T = 22^\circ\text{C}$ for smectic phase

$$\beta_1 = 380 \left(\frac{\text{cm}}{\text{V}^2} \right)$$

$T = 42^\circ\text{C}$ for isotropic phase

$$\beta_1 = 30 \left(\frac{\text{cm}}{\text{V}^2} \right)$$

$$\beta_1 = 193 \left(\frac{\text{cm}}{\text{V}^2} \right)$$

MATERIALS PROPERTIES QUESTIONNAIRE (See instruction sheet)

Name of Organization: LIQUID CRYSTAL INSTITUTE, KENT STATE UNIVERSITY

Principal Investigator: Michael A. Lee (Co-PIs: Peter Palfy-Muhoray, John L. West, Liang-Chy Chien, J. William Iwanke)

Material: OPL-7-1 4-(1-octynyl)-4'-cyanobiphenyl Measurement returned _____; submitted _____

$\chi_{ Re}^{(2)}$ (esu)	n_o (esu)	T_m (sec)	T_m (sec)	$\Delta\lambda$ (nm)	α (cm ⁻¹)	$\chi_{ m}^{(2)}$ (esu)	d_p (mksa)	r_p (mksa)	ϵ_o (ϵ_o)
Present Usual $\chi_{ Re}^{(2)} = -7.3 \times 10^{-11}$; $n_{2 } = -27 \times 10^{-11}$					0.1				

Present Best

Estimated Max.
Achievable

What must be done to attain this maximum value?



SYCB

32.7°C 49.5°C

C → N → I

Measured at $\lambda = 532\text{nm}$, $\tau = 7 \times 10^{-9}$ sec

T = 37°C for nematic phase

T = 60°C for isotropic phase

$$n_{2\perp} = +7.0 \times 10^{-11}(\text{esu}) \quad \chi_{||m}^{(2)} = 5.2 \times 10^{-11}(\text{esu})$$

$$n_{2i} = -5.5 \times 10^{-11}(\text{esu}) \quad \chi_{\perp lm}^{(2)} = 0.68 \times 10^{-11}(\text{esu})$$

$$\chi_{\perp Re}^{(2)} = +1.7 \times 10^{-11}(\text{esu}) \quad \chi_{\perp lm}^{(2)} = 1.3 \times 10^{-11}(\text{esu})$$

$$\chi_{iRe}^{(2)} = -1.4 \times 10^{-11}(\text{esu})$$

$$\beta_{||} = 112 \left(\frac{\text{esu}}{\text{W}} \right)$$

$$\beta_{\perp} = 19 \left(\frac{\text{esu}}{\text{W}} \right)$$

$$\beta_i = 33 \left(\frac{\text{esu}}{\text{W}} \right)$$

THE UNIVERSITY

James C. Thompson, William Dwyer

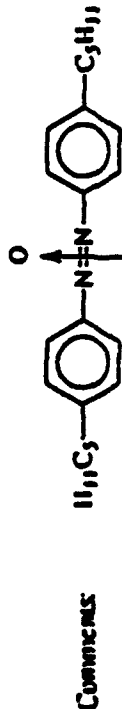
1. **Introduction**
 2. **Background**
 3. **Methodology**
 4. **Results**
 5. **Discussion**
 6. **Conclusion**
 7. **References**
 8. **Appendix**
 9. **Figure 1**
 10. **Figure 2**
 11. **Figure 3**
 12. **Figure 4**
 13. **Figure 5**
 14. **Figure 6**
 15. **Figure 7**
 16. **Figure 8**
 17. **Figure 9**
 18. **Figure 10**
 19. **Figure 11**
 20. **Figure 12**
 21. **Figure 13**
 22. **Figure 14**
 23. **Figure 15**
 24. **Figure 16**
 25. **Figure 17**
 26. **Figure 18**
 27. **Figure 19**
 28. **Figure 20**
 29. **Figure 21**
 30. **Figure 22**
 31. **Figure 23**
 32. **Figure 24**
 33. **Figure 25**
 34. **Figure 26**
 35. **Figure 27**
 36. **Figure 28**
 37. **Figure 29**
 38. **Figure 30**
 39. **Figure 31**
 40. **Figure 32**
 41. **Figure 33**
 42. **Figure 34**
 43. **Figure 35**
 44. **Figure 36**
 45. **Figure 37**
 46. **Figure 38**
 47. **Figure 39**
 48. **Figure 40**
 49. **Figure 41**
 50. **Figure 42**
 51. **Figure 43**
 52. **Figure 44**
 53. **Figure 45**
 54. **Figure 46**
 55. **Figure 47**
 56. **Figure 48**
 57. **Figure 49**
 58. **Figure 50**
 59. **Figure 51**
 60. **Figure 52**
 61. **Figure 53**
 62. **Figure 54**
 63. **Figure 55**
 64. **Figure 56**
 65. **Figure 57**
 66. **Figure 58**
 67. **Figure 59**
 68. **Figure 60**
 69. **Figure 61**
 70. **Figure 62**
 71. **Figure 63**
 72. **Figure 64**
 73. **Figure 65**
 74. **Figure 66**
 75. **Figure 67**
 76. **Figure 68**
 77. **Figure 69**
 78. **Figure 70**
 79. **Figure 71**
 80. **Figure 72**
 81. **Figure 73**
 82. **Figure 74**
 83. **Figure 75**
 84. **Figure 76**
 85. **Figure 77**
 86. **Figure 78**
 87. **Figure 79**
 88. **Figure 80**
 89. **Figure 81**
 90. **Figure 82**
 91. **Figure 83**
 92. **Figure 84**
 93. **Figure 85**
 94. **Figure 86**
 95. **Figure 87**
 96. **Figure 88**
 97. **Figure 89**
 98. **Figure 90**
 99. **Figure 91**
 100. **Figure 92**
 101. **Figure 93**
 102. **Figure 94**
 103. **Figure 95**
 104. **Figure 96**
 105. **Figure 97**
 106. **Figure 98**
 107. **Figure 99**
 108. **Figure 100**
 109. **Figure 101**
 110. **Figure 102**
 111. **Figure 103**
 112. **Figure 104**
 113. **Figure 105**
 114. **Figure 106**
 115. **Figure 107**
 116. **Figure 108**
 117. **Figure 109**
 118. **Figure 110**
 119. **Figure 111**
 120. **Figure 112**
 121. **Figure 113**
 122. **Figure 114**
 123. **Figure 115**
 124. **Figure 116**
 125. **Figure 117**
 126. **Figure 118**
 127. **Figure 119**
 128. **Figure 120**
 129. **Figure 121**
 130. **Figure 122**
 131. **Figure 123**
 132. **Figure 124**
 133. **Figure 125**
 134. **Figure 126**
 135. **Figure 127**
 136. **Figure 128**
 137. **Figure 129**
 138. **Figure 130**
 139. **Figure 131**
 140. **Figure 132**
 141. **Figure 133**
 142. **Figure 134**
 143. **Figure 135**
 144. **Figure 136**
 145. **Figure 137**
 146. **Figure 138**
 147. **Figure 139**
 148. **Figure 140**
 149. **Figure 141**
 150. **Figure 142**
 151. **Figure 143**
 152. **Figure 144**
 153. **Figure 145**
 154. **Figure 146**
 155. **Figure 147**
 156. **Figure 148**
 157. **Figure 149**
 158. **Figure 150**
 159. **Figure 151**
 160. **Figure 152**
 161. **Figure 153**
 162. **Figure 154**
 163. **Figure 155**
 164. **Figure 156**
 165. **Figure 157**
 166. **Figure 158**
 167. **Figure 159**
 168. **Figure 160**
 169. **Figure 161**
 170. **Figure 162**
 171. **Figure 163**
 172. **Figure 164**
 173. **Figure 165**
 174. **Figure 166**
 175. **Figure 167**
 176. **Figure 168**
 177. **Figure 169**
 178. **Figure 170**
 179. **Figure 171**
 180. **Figure 172**
 181. **Figure 173**
 182. **Figure 174**
 183. **Figure 175**
 184. **Figure 176**
 185. **Figure 177**
 186. **Figure 178**
 187. **Figure 179**
 188. **Figure 180**
 189. **Figure 181**
 190. **Figure 182**
 191. **Figure 183**
 192. **Figure 184**
 193. **Figure 185**
 194. **Figure 186**
 195. **Figure 187**
 196. **Figure 188**
 197. **Figure 189**
 198. **Figure 190**
 199. **Figure 191**
 200. **Figure 192**
 201. **Figure 193**
 202. **Figure 194**
 203. **Figure 195**
 204. **Figure 196**
 205. **Figure 197**
 206. **Figure 198**
 207. **Figure 199**
 208. **Figure 200**
 209. **Figure 201**
 210. **Figure 202**
 211. **Figure 203**
 212. **Figure 204**
 213. **Figure 205**
 214. **Figure 206**
 215. **Figure 207**
 216. **Figure 208**
 217. **Figure 209**

(1) 00×10^{-11}

Present Day

Estimated Mar.

What must be done to attain this maximum value?



FIXES

2552600C 6550C

一
↑
Z
↑
C

Measured: $1 - 232 \times 10^{-9}$ sec

T = 40°C for nematic phase

T = 80°C for isotropic phase:

$$(c) \quad \frac{1}{1-\alpha} = \frac{1}{1-\alpha} \quad (c)$$
$$(3) \quad \frac{1}{2} = 0.5 = 10^{-1} \text{ (unit)}$$
$$(2) \quad 0.42 \times 10^{-11} \text{ sec}^{-1}$$

(3) CO_2 10-11%

$$- \frac{55}{143} \left(\frac{5m}{5m} \right)$$

g. - 27 (cm)

2. - 11 (5m)

(See instruction sheet)

Name of Organization: LIQUID CRYSTAL INSTITUTE, KENT STATE UNIVERSITY

Principal Investigator: Michael A. Lee (Co-PIs: Peter Palffy-Muhoray, John L. West, Liang-Chy Chien, J. William Doane)

Material: OPL-10-2 4-4'-dihexyloxybenzene Measurement: none

$X_{ }^{(2)}$ (esu)	n_o (esu)	τ_m (sec)	τ_m (sec)	$\Delta\lambda$ (nm)	u (cm ⁻¹)	$X_{ }^{(2)}$ (esu)	d_p (mksa)	r_p (mksa)	ζ (ζ)
-------------------------	----------------	-------------------	-------------------	-------------------------	----------------------------	-------------------------	-----------------	-----------------	------------------------

Present Usual $X_{||}^{(2)} = -4.1 \times 10^{-11}$; $n_{2||} = -15 \times 10^{-11}$

0.1

Present Best

Estimated Max.
Ausable

What must be done to attain this maximum value?



6A2XB

27.1-27.6°C 55.7°C

$C \rightarrow N \rightarrow I$

$n_{2\perp} = +2.0 \times 10^{-11}$ (esu) $X_{||}^{(2)} = 1.77 \times 10^{-11}$ (esu)

$n_{2i} = +5.0 \times 10^{-11}$ (esu) $X_{\perp}^{(2)} = 0.15 \times 10^{-11}$ (esu)

$X_{\perp}^{(2)} = +0.47 \times 10^{-11}$ (esu) $X_{||}^{(2)} = 0.82 \times 10^{-11}$ (esu)

$X_{||}^{(2)} = +1.3 \times 10^{-11}$ (esu)

$\beta_{||} = 38 \left(\frac{esu}{W} \right)$

$\beta_{\perp} = 4.2 \left(\frac{esu}{W} \right)$

$\beta_i = 21 \left(\frac{esu}{W} \right)$

Measured at $\lambda = 532$ nm, $\tau = 7 \times 10^{-9}$ sec

T = 50°C for nematic phase

T = 66°C for isotropic phase

Name of Organization: LIQUID CRYSTAL INSTITUTE, KENT STATE UNIVERSITY

Principal Investigator: Michael A. Lee (Co-PIs: Peter Palffy-Muhoray, John L. West, Liang-Chy Chien, J. William Doane)

Material: E7 Measurement: resonant; nonresonant x

Present Usual $\chi_{||Rc}^{(3)} = -10.3 \times 10^{-11}$; $n_{2H} = -38 \times 10^{-11}$

Present Best

Estimated Max. Attainable

What must be done to attain this maximum value?

Comments

-10°C 60.5°C

C → N → I

$$n_{2L} = +3.3 \times 10^{-11}(\text{esu}) \quad \chi_{||lm}^{(3)} = 13.2 \times 10^{-11}(\text{esu})$$

$$n_{2i} = \text{not measured} \quad \chi_{\perp lm}^{(3)} = 1.4 \times 10^{-11}(\text{esu})$$

$$\chi_{\perp Rc}^{(3)} = +0.78 \times 10^{-11}(\text{esu}) \quad \chi_{ilm}^{(3)} = \text{not measured}$$

$$\chi_{iRc}^{(3)} = \text{not measured (esu)}$$

Measured at $\lambda = 532\text{nm}$, $\tau = 7 \times 10^{-9} \text{ sec}$

T = 24°C for nematic phase

$$\beta_H = 284 \left(\frac{\text{esu}}{\text{Å}^2} \right)$$

$$\beta_L = 40 \left(\frac{\text{esu}}{\text{Å}^2} \right)$$

$$\beta_i = \text{not measured}$$